THE
SCIENCE REPORTS

OF
ECONOMIC GEOLOGY RESEARCH PROJECT
UNIVERSITY OF CONCEPCION

No. 4

JAPAN INTERNATIONAL COOPERATION AGENCY
(1994)

THE
SCIENCE REPORTS
OF
ECONOMIC GEOLOGY RESEARCH PROJECT
UNIVERSITY OF CONCEPCION

No. 4

PROGRAMA DE GEOLOGIA ECONOMICA APLICADA (GEA)
Universidad de Concepción
Casilla 4107, Concepción 3, Chile

JAPAN INTERNATIONAL COOPERATION AGENCY (JICA)
P. O. Box 216, 48th Floor, Shinjuku Mitsui Building
Nishi-Shinjuku 2-1-1, Shinjuku-ku, Tokyo 163, Japan

(All announcements related with this report should be
addressed to Japan International Cooperation Agency.)

Contents

PETROGRAPHY AND PETROCHEMISTRY OF VOLCANIC ROCKS OF ANTUCO VOLCANO, CHILE

Masahiko Yamamoto*, Hirotsugu Nishido** and Sonia Helle***
*Institute of Earth Sciences, Faculty of Science, Kagoshima University,
Kagoshima 890, Japan. **Hiruzen Research Institute, Okayama
University of Science, Kawakami, Okayama 717-06, Japan. ***Programa
de Geología Económica Aplicada, Universidad de Concepción,
Concepción 3, Chile.

Abstract

Lavas from the Quaternary Antuco volcano in southern Chile were petrographically and petrochemically studied. They are petrographically composed of an olivine basalt to a basaltic andesite, and are petrochemically composed of mainly a quartz-normative metaluminous calc-alkaline rock. During the volcanic activity, the composition of lavas changes toward basic in stratigraphically ascending order.

It is indicated that the basaltic andesites of earlier and middle stages were formed by fractionation of magnesian olivine and calcic plagioclase in a basaltic magma. The olivine basalts of later stage include both an olivine accumulated rock and a plagioclase accumulated rock, and it is indicated that they were formed by fractionation of olivine in a basaltic magma.

Introduction

The Antuco volcano is located in the Meridional Andes in southern Chile. Petrological studies of volcanic rocks have been reported by Vergara and Katsui (1969) and Deruelle (1982). However, there are little petrochemical data of volcanic rocks. In the present study, detailed petrographical and petrochemical data were obtained for twelve rock samples of lavas collected from the northwestern mountainside of volcano.

Geology

The Antuco volcano is a Quaternary stratovolcano located in the Meridional Andes in southern Chile. A geologic map compiled from the field work and the aerial photographs is shown in Fig. 1. The volcano is composed of lava flows and pyroclastic rocks. They cover the Miocene to Pliocene volcanic and volcani-sedimentary rocks Nishido *et al.*, in preparation and the Miocene granitic intrusive rocks (Nishido *et al.*, in press).
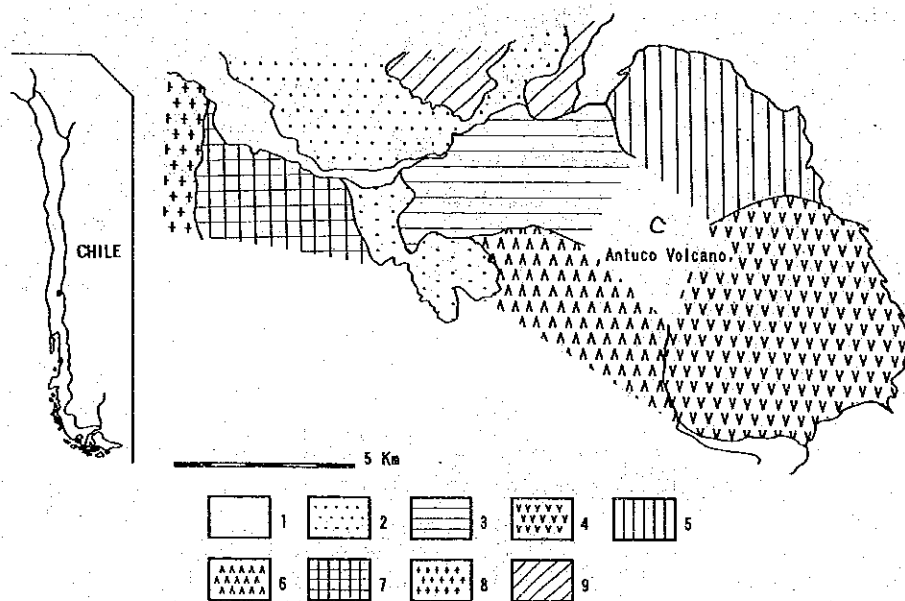
Fig 1.   Index and geologic maps of the Antuco volcanic area.
Stratigraphic sequences: 1. Alluvial deposits; 2. Pyroclastic flows; 3-7. Antuco lavas (3. Lava-1, 4. Lava-2, 5. Lava-3, 6. Lava-4, 7. Lava-5); 8. Miocene granitic rocks; 9. Neogene volcanics.

Twelve rock samples of lavas collected from the northwestern mountainside of Antuco volcano are listed in Table 1. They can be stratigraphically included into three groups in Fig. 1: Lava-1, Lava-3 and Lava-5 in ascending order. The Lava-1 of earlier stage is distributed in the westernmost of volcano. The Lava-3 of middle stage is distributed in the northern mountainside of volcano. The Lava-5 of later stage is distributed in the northwestern mountainside of volcano.

K-Ar age determinations of two specimens, Nos. 9210705 and 91B2404, in the Lava-1 were carried out. However, the age could not be obtained, because the amount of ^{40}Ar was too low.

2

Petrography

The rock samples collected from the Antuco volcano were petrographically studied under a petrographic microscope.

1. Olivine Basalt in Lava-5: (Specimen Nos. 91B2401, 91B2402, 91B2403, 9210604, 9210610)

Table 1. Rock samples collected from the Antuco volcano

No.	Sp. No.	Latitude (S)	Longitude (W)	Altitude (m)	Rock	Remarks
			(a) Lava-5			
1	91B2401	37°22'57"	71°23'03"	1375	Ol Basalt	
2	91B2402	37°22'54"	71°23'30"	1255	Ol Basalt	
3	91B2403	37°23'35"	71°25'24"	1070	Ol Basalt	
4	9210604	37°22'36"	71°21'50"	1410	Ol Basalt	
5	9210610	37°22'37"	71°22'28"	1410	Ol Basalt	
6	9210603	37°22'32"	71°21'46"	1400	Basalt	
			(b) Lava-3			
7	9210601	37°22'00"	71°20'36"	1410	Basaltic Andesite	
8	9210602A	37°22'02"	71°21'04"	1390	Basaltic Andesite	
9	9210602B	37°22'02"	71°21'04"	1390	Basaltic Andesite	
			(c) Lava-1			
10	91B2404	37°23'34"	71°27'02"	940	Basaltic Andesite	Rich in Xenoliths
11	9210705	37°23'34"	71°27'14"	940	Basaltic Andesite	Rich in Xenoliths
12	9210706	37°23'34"	71°27'14"	940	Basaltic Andesite	

All specimens of olivine basalts in the Lava-5 have the same petrographic feature. The olivine basalt occurs as a dark-colored porous block lava. It is composed of large amounts of phenocrysts of plagioclase and olivine and an intersertal textured groundmass. Plagioclase occurs as an euhedral crystal up to 5 mm in size, and the plagioclase phenocrysts consist of both fresh grains and sieve textured ones. Olivine occurs as an euhedral to subhedral unzoned crystal up to 4 mm in size. A small amount of euhedral orthopyroxene grain up to 0.7 mm in size is commonly found as a microphenocryst. Clinopyroxene can be scarcely found in almost all specimens as a phenocryst and a microphenocryst, but a clinopyroxene microphenocryst up to 0.3 mm in size is rarely found in the specimen No. 9210604. The groundmass is composed of microlites of plagioclase, clinopyroxene and orthopyroxene and a subordinate to relative amount of volcanic glass. The volcanic glass is slightly devitrified. Apatite, titaniferrous magnetite and ilmenite are contained as accessories.

2. Basalt in Lava-5: (Specimen No. 9210603)

The basalt occurs as a dark-colored porous block lava. It is composed of small amounts of phenocrysts of plagioclase and olivine and a hyalopilitic textured groundmass. Plagioclase occurs as an euhedral crystal up to 1.5 mm in size, and cloudy plagioclase phenocrysts are rarely found. Olivine occurs as an euhedral to subhedral unzoned crystal up to 1.5 mm in size. Small amounts of euhedral orthopyroxene grains up to 0.5 mm in size and of euhedral clinopyroxene grains up to 0.3 mm in size are commonly found as microphenocrysts. The groundmass is composed of microlites of plagioclase, clinopyroxene and orthopyroxene and a large amount of volcanic glass. The volcanic glass is slightly devitrified. Apatite, titaniferrous magnetite and ilmenite are contained as accessories.

3. Basaltic Andesite in Lava-3: (Specimen Nos. 9210601, 9210602A, 9210602B)

Each specimen of basaltic andesites in the Lava-3 has a different petrographic feature.

The basaltic andesite of specimen No. 9210601 occurs as a dark-colored dense lava. It is composed of large amounts of phenocrysts of plagioclase, olivine and clinopyroxene and an intersertal and seriate textured groundmass. Plagioclase occurs as an euhedral crystal up to 6 mm in size, olivine occurs as an euhedral to subhedral crystal up to 2 mm in size, and clinopyroxene occurs as an euhedral crystal up to 2 mm in size. A glomeroporhyritic aggregate of plagioclase and olivine is sometimes found. Olivine exceeds clinopyroxene in amount. A small amount of euhedral orthopyroxene grain up to 0.3 mm in size is commonly found as a microphenocryst. The groundmass is composed of microlites of plagioclase, clinopyroxene and orthopyroxene and a small amount of volcanic glass. Apatite, titaniferrous magnetite and ilmenite are contained as accessories.

The basaltic andesite of specimen No. 9210602A occurs as a dark-colored dense lava. It is composed of large amounts of phenocrysts of plagioclase and of microphenocrysts of olivine and a trachytic textured groundmass. Plagioclase occurs as an euhedral crystal up to 4 mm in size. Olivine occurs as euhedral to subhedral grains up to 0.5 mm in size. A glomeroporphyritic aggregate of plagioclase and olivine is sometimes found. Small amounts of euhedral orthopyroxene grains up to 0.3 mm in size and of euhedral clinopyroxene grains up to 0.5 mm in size are commonly found as microphenocrysts. The groundmass is composed of microlites of plagioclase, clinopyroxene and orthopyroxene and a small amount of volcanic glass. The volcanic glass is slightly devitrified. Apatite, titaniferrous magnetite and ilmenite are contained as accessories.

The basaltic andesite of specimen No. 9210602B occurs as a dark-colored dense lava. It is composed of large amounts of phenocrysts of olivine and clinopyroxene and of microphenocrysts of plagioclase and clinopyroxene and a

4

trachytic textured groundmass. Olivine occurs as euhedral to subhedral grains up to 2 mm in size, but is strongly altered to an assemblage of serpentine, chlorite, green mica and iddingsite. Clinopyroxene occurs as an euhedral crystal up to 1 mm in size, and is commonly crystallized around the olivine phenocrysts. A glomeroporphyritic aggregate of clinopyroxene grains is sometimes found. Plagioclase occurs as an euhedral crystal up to 0.5 mm in size. A glomeroporphyritic aggregate of plagioclase and olivine is sometimes found. A small amount of euhedral orthopyroxene grain up to 0.8 mm in size is commonly found as a microphenocryst. The groundmass is composed of microlites of plagioclase, clinopyroxene and orthopyroxene and a small amount of volcanic glass. The volcanic glass is slightly devitrified. Apatite, titaniferrous magnetite and ilmenite are contained as accessories.

4. Basaltic Andesite in Lava-1: (Specimen Nos. 91B2404, 9210705, 9210706)

Each specimen of basaltic andesites in the Lava-1 has also a different petrographic feature.

The basaltic andesite of specimen No. 91B2404 occurs as a dark-colored dense lava. It is composed of small amounts of phenocrysts of plagioclase and a hyalopilitic textured groundmass. Plagioclase occurs as an euhedral crystal up to 3 mm in size. Minor amounts of subhedral to anhedral pseudomorphic olivine grains up to 0.3 mm in size, euhedral orthopyroxene grains up to 0.3 mm in size and euhedral clinopyroxene grains up to 0.2 mm in size are commonly found as microphenocrysts. The groundmass is composed of microlites of plagioclase, clinopyroxene and orthopyroxene and a large amount of volcanic glass. The volcanic glass is slightly devitrified. Apatite, titaniferrous magnetite and ilmenite are contained as accessories. Large amounts of basalt fragments are included in this specimen.

The basaltic andesite of specimen No. 9110705 occurs as a dark-colored and banded-structured lava. It is composed of small amounts of phenocrysts of plagioclase and a hyalopilitic and trachytic textured groundmass. Plagioclase occurs as an euhedral crystal up to 3 mm in size. Small amounts of euhedral clinopyroxene grains up to 0.9 mm in size and of euhedral orthopyroxene grains up to 0.3 mm in size are commonly found as microphenocrysts. Clinopyroxene exceeds orthopyroxene in amount. A glomeroporphyritic aggregate of plagioclase, clinopyroxene and orthopyroxene grains is sometimes found. A minor amount of olivine grain up to 0.1 mm in size is also found as a microphenocryst. The groundmass is composed of microlites of plagioclase, clinopyroxene and orthopyroxene and a large amount of volcanic glass. Apatite, titaniferrous magnetite and ilmenite are contained as accessories. Large amounts of olivine basalt fragments are commonly included in this specimen.

5

The basaltic andesite of specimen No. 9110706 occurs as a dark-colored and flow-structured lava. It is composed of large amounts of phenocrysts of plagioclase and a trachytic textured groundmass. Plagioclase occurs as an euhedral crystal up to 2 mm in size. Minor amounts of anhedral olivine grains up to 0.1 mm in size, euhedral orthopyroxene grains up to 0.2 mm in size and euhedral clinopyroxene grains up to 0.1 mm in size are found as microphenocrysts. The groundmass is composed of microlites of plagioclase, clinopyroxene and orthopyroxene and a large amount of volcanic glass. The volcanic glass is slightly devitrified. Apatite, titaniferrous magnetite and ilmenite are contained as accessories.

Petrochemistry

The rock samples collected from the Antuco volcano were chemically analyzed with the Rigaku XRF Spectrometer 3070-E. Chemical compositions analyzed and CIPW norms calculated are listed in Table 1, and the variation diagram is shown in Fig. 2.

The SiO_2 content of rocks from the Lava-1 ranges from 55 wt.% to 60 wt.%, and they are compositionally basaltic andesitic to andesitic. The SiO_2 content of rocks from the Lava-3 ranges from 52 wt.% to 55 wt.%, and they are compositionally basaltic andesitic. The SiO_2 content of rocks from the Lava-5

Table 2. Chemical analyses and CIPW norms of lavas from the Antuco volcano

No.	1	2	3	4	5	6
Sp. No.	91B2401	91B2402	91B2403	9210604	9210610	9210603
SiO_2	50.84	52.19	51.81	52.08	52.55	51.99
TiO_2	1.00	1.06	1.01	1.07	1.07	1.01
Al_2O_3	16.75	18.58	18.25	17.92	18.76	17.20
Fe_2O_3	3.60	3.68	3.69	3.56	3.39	3.67
FeO	5.92	4.50	4.62	4.90	4.68	4.99
MnO	0.15	0.14	0.14	0.14	0.14	0.14
MgO	8.65	5.18	5.94	5.50	4.96	7.07
CaO	8.61	9.75	9.59	9.76	9.56	8.87
Na_2O	3.17	3.41	3.34	3.39	3.60	3.27
K_2O	0.68	0.74	0.71	0.74	0.74	0.83
H_2O^+	0.18	0.24	0.25	0.19	0.21	0.22
H_2O^-	0.09	0.07	0.07	0.07	0.05	0.09
P_2O_5	0.18	0.19	0.18	0.18	0.20	0.18
Total	99.82	99.73	99.60	99.50	99.91	99.53

Table 2. (continued)

Q	-	2.75	1.89	2.25	2.37	1.41
Or	4.02	4.37	4.20	4.37	4.37	4.91
Ab	26.82	28.86	28.26	28.69	30.46	27.67
An	29.47	33.21	32.71	31.50	32.85	29.80
Di	9.65	11.12	10.92	12.63	10.65	10.39
Wo	5.04	5.81	5.72	6.58	5.54	5.44
En	3.54	4.12	4.09	4.54	3.79	3.90
Fs	1.07	1.19	1.11	1.51	1.32	1.05
Hy	18.49	11.32	13.61	12.20	11.53	17.39
En	14.19	8.78	10.70	9.16	8.56	13.71
Fs	4.30	2.54	2.91	3.04	2.97	3.68
Ol	3.56	-	-	-	-	-
Fo	2.67	-	-	-	-	-
Fa	0.89	-	-	-	-	-
Il	1.90	2.01	1.92	2.03	2.03	1.92
Mt	5.22	5.34	5.35	5.16	4.92	5.32
Ap	0.42	0.44	0.42	0.42	0.46	0.42

| No.	7	8	9	10	11	12
Sp. No.	9210601	9210602A	9210602B	91B2404	9210705	9210706
SiO_2	52.96	54.76	54.15	55.56	59.61	55.52
TiO_2	1.13	1.48	1.46	1.57	1.36	1.58
Al_2O_3	19.15	16.43	16.74	16.11	15.75	16.21
Fe_2O_3	3.28	4.09	3.82	4.48	2.11	2.91
FeO	4.78	5.75	5.90	5.36	5.85	6.82
MnO	0.14	0.17	0.17	0.17	0.16	0.17
MgO	3.61	3.70	3.74	3.18	2.15	3.24
CaO	9.30	7.59	7.87	6.96	5.35	7.03
Na_2O	3.71	4.08	4.15	4.37	4.80	4.42
K_2O	0.76	1.00	0.97	1.21	1.73	1.20
H_2O^+	0.36	0.13	0.12	0.13	0.33	0.14
H_2O^-	0.13	0.09	0.09	0.07	0.07	0.08
P_2O_5	0.18	0.24	0.23	0.29	0.35	0.29
Total	99.49	99.51	99.41	99.46	99.62	99.61
Q	4.14	6.50	4.85	7.47	9.89	5.20
Or	4.49	5.91	5.73	7.15	10.22	7.09
Ab	31.39	34.53	35.12	36.98	40.62	37.40
An	33.36	23.56	24.19	20.77	16.32	20.85
Di	9.40	10.17	10.87	9.59	6.62	10.03
Wo	4.85	5.23	5.58	4.95	3.31	5.07
En	3.04	3.19	3.31	3.12	1.43	2.52
Fs	1.51	1.75	1.98	1.52	1.88	2.44
Hy	8.90	9.33	9.61	7.14	9.09	10.93
En	5.95	6.03	6.01	4.80	3.92	5.55
Fs	2.95	3.30	3.60	2.34	5.17	5.38
Ol	-	-	-	-	-	-
Fo	-	-	-	-	-	-
Fa	-	-	-	-	-	-
Il	2.15	2.81	2.77	2.98	2.58	3.00
Mt	4.76	5.93	5.54	6.50	3.06	4.22
Ap	0.42	0.56	0.53	0.67	0.81	0.67

Oxides wt.%
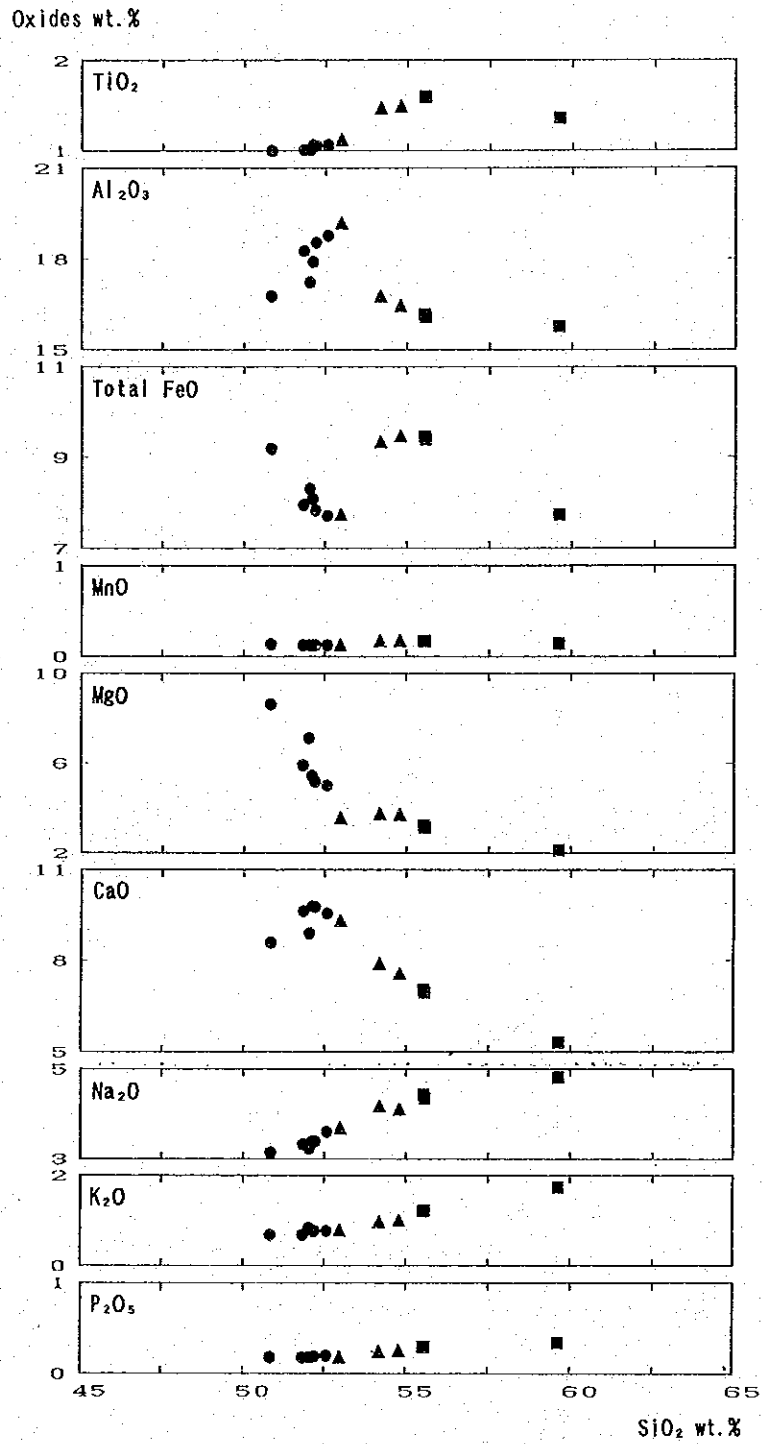
Fig. 2. Variation diagram of lavas from the Antuco volcano.
Squares: Lava-1, Triangles: Lava-3, Circles: Lava-5.

8

ranges from 50 wt.% to 53 wt.% and they are compositionally basaltic to basaltic andesitic. The SiO_2 content of analyzed rocks decreases in stratigraphically ascending order.

In norms, almost all analyzed rocks are of quartz normative, but the olivine basalt No. 91B2401 having the most basic composition is of hypersthene normative. Normative C is not calculated in all analyzed rocks, and they are metaluminous.

In Fig. 2, the amounts of MnO, Na_2O, K_2O and P_2O_5 vary regularly, but those of TiO_2, Al_2O_3, total FeO, MgO and CaO vary irregularly. Especially, compositional gaps in Al_2O_3, total FeO and MgO can be seen around 53 wt.% in SiO_2.

Figure 3 shows the FAM diagram of analyzed rocks. In Fig. 3, a solid line represents the boundary curve between calc-alkaline and tholeiitic series reported by Irvine and Baragar (1971). The analyzed rocks are plotted in the field of calc-alkaline suite. Figure 4 shows the relation between SiO_2 and Na_2O+K_2O of analyzed rocks. In Fig. 4, solid lines represent the boundary curves between alkali olivine basalt, high-alumina basalt and tholeiitic series reported by Kuno (1966). The analyzed rocks are plotted in the field of high-alumina basalt.
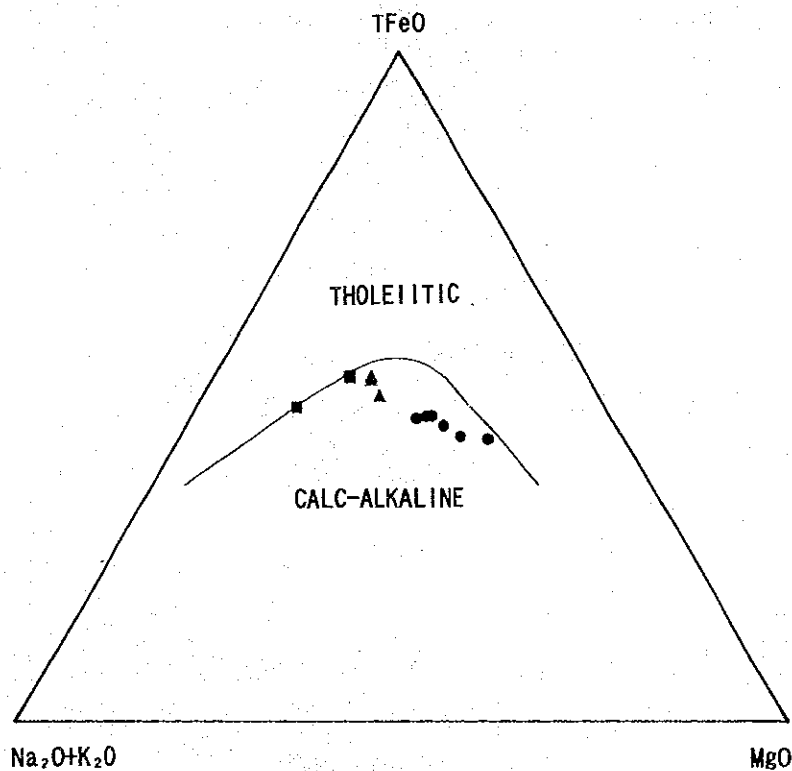

Fig. 3. FAM diagram of lavas from the Antuco volcano.
The symbols are the same as in Fig. 2.

Genetical Considerations

The olivine basalts and the basalt in the Lava-5 of later stage can be chemically divided into two types: one is rich in MgO and total FeO; and the other is rich in CaO and Al_2O_3. These rocks contain large amounts of olivine and plagioclase with small amounts of pyroxenes. These facts indicate that the rock rich in total FeO and MgO is a magnesian olivine accumulated rock and the rock rich in Al_2O_3 and CaO is a calcic plagioclase accumulated rock. It is indicated therefore that these rocks were resulted from fractionation of magnesian olivine and calcic plagioclase in a basaltic magma.

The basaltic andesites in the Lava-3 of middle stage is rich in total FeO and poor in MgO, CaO and Al_2O_3, as compared to the olivine basalts and the basalt in the Lava-5. The compositional variation of rocks in the Lava-3 is similar to that of rocks in the Lava-5. It is indicated therefore that the basaltic andesites were formed by fractionation of both magnesian olivine and calcic plagioclase in a basaltic magma.

Some basaltic andesites in the Lava-1 of earlier stage contain a large amount of xenolith. However, the chemical compositions is similar between basaltic andesites in the Lava-1 and the Lava-3. These facts suggest that the xenolith is an cognate. It is indicated therefore that the basaltic andesites in the Lava-5 were formed by fractionation of both magnesian olivine and calcic plagioclase in a basaltic magma, as well as the basaltic andesites in the Lava-3.
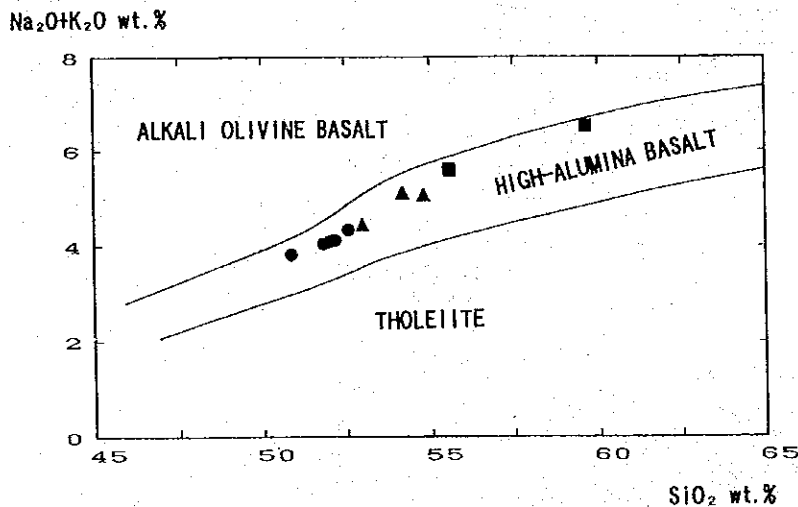

Fig. 4. Relation between SIO_2 and Na_2O+K_2O of lavas from the Antuco volcano. The symbols are the same as in Fig. 2.

The basaltic andesite of specimen No. 9210705 is rich in SiO_2 and contains a large amount of xenolith. It has a banded structure composed of a hyalopilitic groundmass and a trachytic one. It may be indicated that the basaltic andesite was formed through mixing between a basaltic magma and residual liquid after fractionation.

There is no evidence for contamination of crustal materials in all analyzed rocks from the Antuco volcano.

Acknowledgments

References

Deruelle, B. (1982): Petrology of the Plio-Quaternary volcanism of the South-Central and Meridional Andes. *J. Volcanol. Geotherm. Res.*, 14, 77-124.

Irvine, A.J. and Baragar, W.R. (1971): A guide to the chemical classification of the common igneous rocks. *Can. J. Earth Sci.*, 8, 523-548.

Kuno, H. (1966): Lateral variation of basalt magma type across continental margins and island arcs. *Bull. Volcanol.*, 29, 195-222.

Nishido,H., Yamamoto, M., and Frutos, J. (in press): Composition and K-Ar age of granitic intrusive body in Antuco, southern Chile.

Nishido,H., Yamamoto, M., and Frutos, J. (in preparation): Petrography, petrochemistry and K-Ar dating of Neogene volcanic rocks in Antuco, southern Chile.

Vergara, M. and Katsui, Y. (1969): Contribution a la geología y petrología del volcan Antuco, Cordillera de los Andes, Chile central. Univ. (Santiago) Chile Inst. Geol. Pub., 35, 25-47.

CHEMICAL COMPOSITIONS OF SILICATE MINERALS IN PLUTONIC AND DYKE ROCKS FROM THE WESTERN COPIAPO REGION OF NORTHERN CHILE

Hisao Tanaka*, Laura Hernández** and Osvaldo Rabbia**
*Faculty of Science, Yamagata University, Koshirakawamachi 1-4-12,
Yamagata 990, Japan. **Instituto GEA, Universidad de Concepción,
Casilla 4107, Concepción 3, Chile.

Introduction

A great part of the Coastal Cordillera of Northern Chile (CCNC), located at the western verge of the Andes, is underlain by granitoids and gabbroids of late Paleozoic to Mesozoic age (Ishihara *et al.*, 1984; Scheuber and Reutter, 1992). In an area of more than 500 km long of the CCNC between 24°S and 28°S, the plutonic rocks are penetrated by mafic to felsic dyke swarms, most of which run in two predominant directions of NW-SE and NE-SW (Pichowiak and Breitkreuz, 1984). The mafic to felsic dykes span in age from Triassic to Cretaceous (Naranjo, 1978; Herve and Marinovic, 1989). The mafic to felsic dykes are also spatially and temporally related with Mesozoic volcanic rocks (Scheuber and Reutter, 1992). Some of the dyke swarms are considered to represent subvolcanic equivalents or feeder channels intimately connected with volcanic rocks (Pichowiak and Breitkreuz, 1984; Scheuber and Reutter, 1992). The plutonic rocks, mafic to felsic dykes and volcanic rocks in the CCNC were probably linked to an extensional tectonic regime (Scheuber and Reutter, 1992). In this report mineral chemistry, obtained by using a JEOL-8600M electron-probe microanalyser (EPMA) installed at GEA, Universidad de Concepción, are presented for plutonic and dyke rocks from the western Copiapo region in the CCNC between 27°S and 28°S.

Outline of geology

The simplified geological map of the Copiapo region and sampling locality are shown in Fig. 1. The western Copiapo region between 27° and 28° is widely occupied by a batholithic complex of Jurassic to Cretaceous age. The western part of the batholithic complex intrudes into an upper Paleozoic accretionary prism
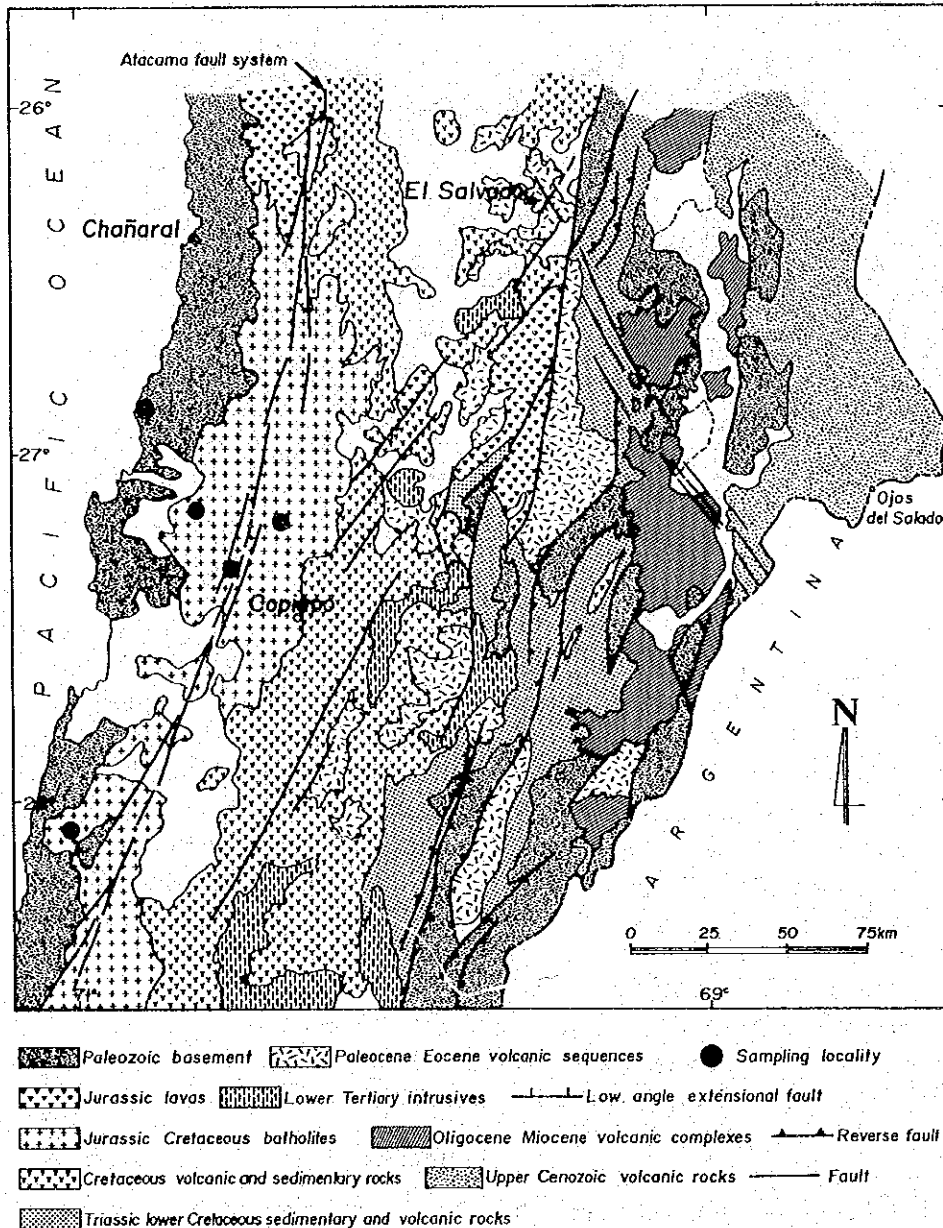

Fig. 1. Simplified geological map of the Copiapo region and sampling locality.

("Melange" de Chañaral) and Permian plutonic rocks (Mercado, 1980; Berg and Baumann, 1985). Thick volcano-sedimentary sequences, being mainly composed of Neocomian limestone and andesitic rocks (Segerstrom, 1968), are distributed on the east side of the complex. The batholithic complex consists mainly of tonalitic granitoids and is cut by dense dike swarms of mafic to felsic compositions. The Atacama fault system, which has been active since Jurassic (Brown, in press) and has long axis striking nearly N-S, crosses the batholithic complex.

Description of rocks

Six rock samples were selected for a study of mineral chemistry; that is 38 (Carrizal Alto), 61 (Copiapo), 67-A and 67-B (Sierra de la Gloria), 70 (Cerro Chamonate) and OF-1 (Caldera). Rock type and mineral assemblage of the samples are shown in Table 1. The analysed samples include host intrusive rocks (61, 67-B and 70) and mafic to intermediate dykes (38, 67-A and Of.-1). They are commonly altered to some degree, expressed in the plagioclase as incipient and sometimes advanced saussuritisation, and by the alteration of pyroxene and amphibole to secondary fibrous amphibole.

Table 1. Rock type and mineral assemblage of the analysed samples.
    Abbreviations are as follows; pl: plagioclase, qt: quartz, cpx: clinopyroxene, amp: amphibole, bi: biotite, opa: opaque minerals, ap: apatite, sph; sphene, phe: phenocryst, gr: groundmass. The mineral assemblage is aranged in a decreasing order of abundance.

Samp. Name	Rock Type	Mineral Assemblage
OF1	dolerite	(phe) pl+cpx
		(gr) pl+cpx+bi+opa
61	quartz diorite	pl+amp+qt+opa+sph
67A	porphyry	pl+amp+qt+opa+sph
67B	gabbro	amp+pl+cpx+opa
70	quartz diorite	pl+amp+qt+bi+cpx+opa+ap
38	porphyry	(phe) pl+amp
		(gr) pl+amp+bi+qt+opa+sph

Analytical conditions of silicate minerals

Mineral analyses were done with a JEOL-8600M EPMA using a wave-dispersive X-ray analytical system. A detailed instrumental explanation and manual of the EPMA is presented by Fukuoka (1991). An accelerating voltage of 15 kv and a filament current of $1 \ 10^{-8}$ A were used for the mineral analyses. An

analysing crystal TAP of channel 1 was used for the measurement of SiO_2, Al_2O_3, MgO and Na_2O, and LiF of channel 2 for FeO and MnO, and PET of channel 3 for TiO_2, Cr_2O_3 and CaO. Iron contents were expressed as total FeO.

Chemical compositions of silicate minerals

Representative chemical compositions of clinopyroxenes in OF1 dolerite are shown in Table 2 and plotted in the Ca-Mg-Fe+Mn diagram (Fig. 2). Their total

Table 2. Representative chemical compositions of clinopyroxenes.

Anal. No.	OF1-1	OF1-2	OF1-3	OF1-4	OF1-5
SiO2	52.25	52.29	52.36	51.35	50.76
TiO2	0.57	0.51	0.53	0.67	0.71
Al2O3	1.96	1.85	1.76	2.34	2.42
Cr2O3	0.14	0.08	0.09	0.00	0.04
FeO	9.69	9.98	9.59	11.43	12.07
MnO	0.27	0.37	0.30	0.39	0.22
MgO	17.02	17.03	17.33	15.65	15.67
CaO	18.43	17.54	17.70	17.49	17.85
Na2O	0.33	0.19	0.28	0.37	0.40
Total	100.66	99.84	99.94	99.69	100.14
O=6 Si	1.926	1.940	1.939	1.924	1.903
Ti	0.016	0.014	0.015	0.019	0.020
Al	0.085	0.081	0.077	0.103	0.107
Cr	0.004	0.002	0.003	0.000	0.001
Fe	0.299	0.310	0.297	0.358	0.378
Mn	0.009	0.012	0.010	0.012	0.007
Mg	0.935	0.942	0.956	0.874	0.876
Ca	0.728	0.697	0.702	0.702	0.717
Na	0.024	0.014	0.020	0.027	0.029
Total	4.026	4.012	4.019	4.019	4.038
Ca	0.369	0.355	0.357	0.361	0.362
Mg	0.474	0.480	0.487	0.449	0.443
Fe+Mn	0.156	0.164	0.156	0.190	0.195
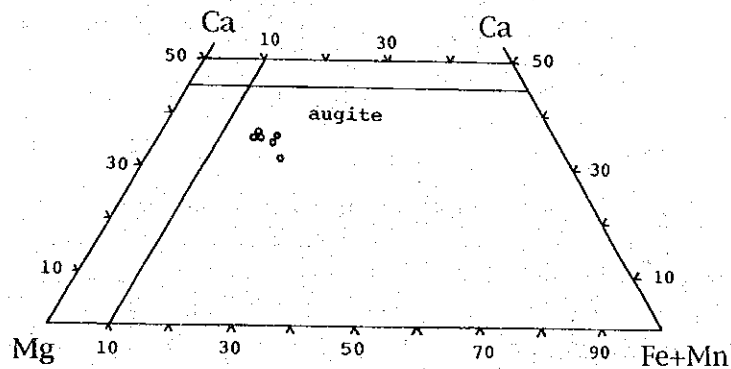
Fig. 2. Compositons of clinopyroxenes in the Ca - Fe+Mn diagram.

wt.% and total cations on the basis of O=6 are almost identical to 100 wt.% and 4 atom, respectively. The pyroxenes are augite in the classification scheme of Poldervaart and Hess (1951) and have relatively low TiO_2 (0.51-0.77 wt.%) and Al_2O_3 (1.76-2.55 wt.%), typical of clinopyroxenes from non-alkaline basalts (Leterrier *et al.*, 1982).

Representative chemical compositions of amphiboles are given in Table 3, and all amphibole analyses are plotted in Si - Mg/ (Mg+Fe) diagrams (Fig. 3). The amphiboles are classified on the basis of the nomenclature of Leake (1978). Amphiboles in 61 quartz diorite are mainly greenish brown and partly colorless to pale green in Z-axial color. The greenish brown amphiboles have chemical compositions of magnesio-hornblende, and the colorless to pale green amphiboles are actinolite to actinolitic hornblende. Amphiboles in 67B gabbro are composed of colorless to pale green parts and brown parts. The colorless to pale green amphiboles are predominant and occur as deuteric fibrous crystals replacing brown amphiboles. The colorless to pale green amphiboles have chemical

Fig. 3. Classification of the analysed amphiboles after Leake (1978).
a: actinolite, b: actinolite hornblende, c: magnesio-hornblende, d: tschermakitic hornblende.

17

Table 3. Representative chemical compositions of amphiboles.

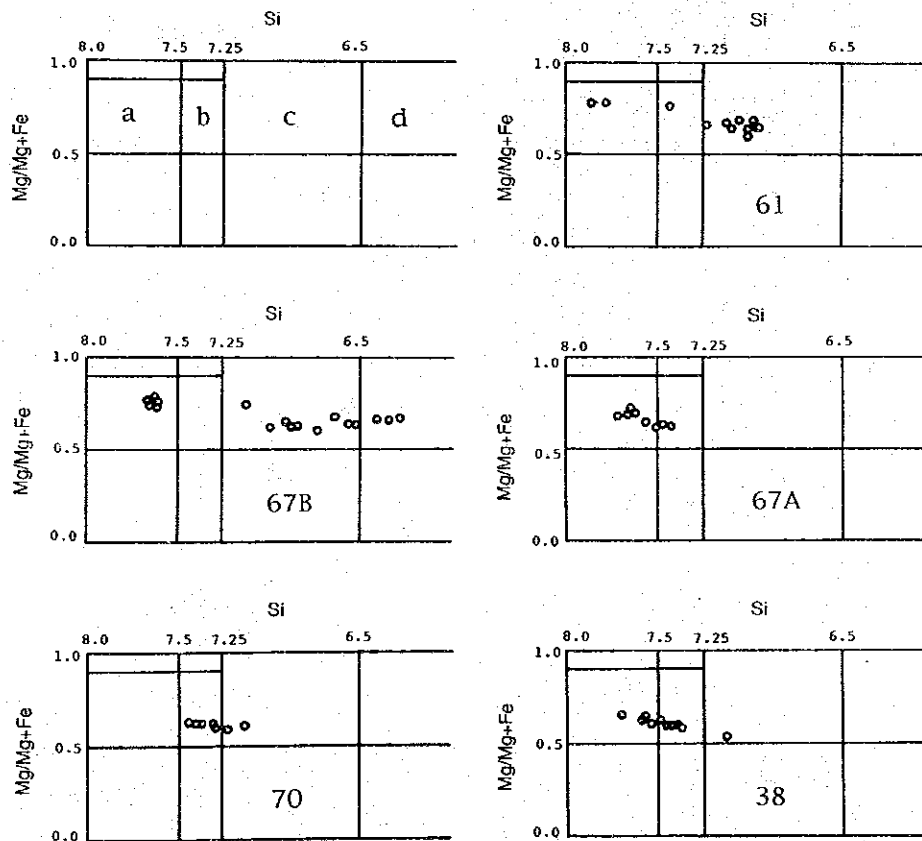| Anal. No.	61-1	61-2	61-3	67A-1	67A-2	67A-3	67B-1	67B-2	67B-3	70-1	70-2	70-3	38-1	38-2	38-3
SiO_2	47.39	48.86	47.99	52.08	51.77	53.76	43.72	44.67	54.38	49.10	50.64	50.18	52.52	53.42	50.16
TiO_2	1.17	1.10	1.72	0.19	0.25	0.12	3.52	0.73	0.12	1.00	0.43	0.74	0.18	0.17	0.39
Al_2O_3	6.66	6.23	7.15	3.70	4.38	2.10	10.53	10.46	3.31	6.04	5.07	5.43	3.81	2.71	5.54
Cr_2O_3	0.00	0.02	0.00	0.15	0.14	0.20	0.03	0.04	0.01	0.02	0.02	0.01	0.06	0.00	0.06
FeO	14.97	12.66	11.69	14.22	15.76	13.61	11.76	13.18	10.04	15.86	15.73	15.92	14.65	13.86	15.91
MnO	0.34	0.27	0.27	0.16	0.11	0.09	0.07	0.20	0.10	0.29	0.48	0.40	0.26	0.35	0.30
MgO	13.66	14.90	15.47	14.78	14.08	16.24	14.04	14.43	18.69	13.16	13.98	13.95	14.03	14.88	12.75
CaO	11.60	12.06	11.57	11.86	11.21	11.64	11.23	11.55	11.83	11.37	11.02	11.24	12.49	12.50	12.27
Na_2O	1.13	1.06	1.46	0.47	0.45	0.30	2.09	2.32	0.38	0.12	0.08	0.13	0.04	0.03	0.06
K_2O	0.49	0.49	0.72	0.03	0.00	0.00	0.90	0.49	0.06	0.53	0.33	0.42	0.11	0.10	0.27
Total	97.41	97.65	98.04	97.64	98.15	98.06	97.89	98.07	98.92	97.49	97.78	98.42	98.15	98.02	97.71
O=23 Si	7.017	7.126	6.962	7.562	7.511	7.725	6.411	6.560	7.616	7.230	7.399	7.306	7.598	7.706	7.363
Ti	0.130	0.120	0.187	0.021	0.027	0.013	0.388	0.081	0.012	0.111	0.048	0.081	0.020	0.019	0.043
Al	1.162	1.071	1.222	0.632	0.749	0.355	1.821	1.810	0.546	1.049	0.873	0.932	0.650	0.461	0.959
Cr	0.000	0.002	0.000	0.017	0.016	0.023	0.004	0.005	0.001	0.002	0.002	0.010	0.007	0.000	0.007
Fe	1.854	1.545	1.419	1.727	1.912	1.635	1.442	1.619	1.176	1.954	1.922	1.938	1.772	1.672	1.953
Mn	0.043	0.033	0.033	0.020	0.013	0.010	0.009	0.025	0.012	0.036	0.060	0.049	0.031	0.042	0.037
Mg	3.016	3.239	3.346	3.198	3.046	3.478	3.068	3.159	3.903	2.889	3.046	3.028	3.025	3.200	2.789
Ca	1.841	1.885	1.798	1.844	1.742	1.792	1.766	1.818	1.775	1.795	1.725	1.753	1.937	1.932	1.930
Na	0.324	0.300	0.411	0.133	0.126	0.083	0.593	0.661	0.102	0.033	0.023	0.037	0.010	0.009	0.016
K	0.093	0.091	0.133	0.006	0.000	0.000	0.168	0.091	0.001	0.100	0.062	0.078	0.021	0.018	0.050
Total	15.480	15.412	15.511	15.160	15.142	15.114	15.670	15.829	15.144	15.199	15.160	15.212	15.071	15.059	15.147
Mg/Mg+Fe	0.619	0.677	0.702	0.649	0.614	0.680	0.680	0.661	0.768	0.597	0.613	0.610	0.631	0.657	0.588

18

compositions of actinolite, and brown amphiboles of magnesio-hornblende to tschermakitic hornblende. Amphiboles in two porphyries (67A and 38) are pale green to green under the microscope, and are characterized by homogeneous compositions with low Al_2O_3, TiO_2, Na_2O and K_2O and high SiO_2. All the amphiboles except one in the porphyries are plotted in fairly restricted areas straddling actinolite and actinolitic hornblende. The low Al_2O_3 contents of the amphiboles may indicate that the two porphyries had intruded at shallow depths (Johnson and Rutherford, 1989; Schmidt, 1992). Amphiboles in 70 quartz diorite are green under the microscope, and show homegeneous compositions being relatively poor in Al_2O_3, Na_2O and K_2O.

Chemical compositions of biotites are given in Table 4, and are plotted in the Si - Mg/ (Mg+Fe) diagram (Fig. 4). Biotite in 67A porphyry occurs as minute anhedral grains replacing amphibole. Biotite in 38 porphyry is present as tiny flakes constituting a groundmass. The biotites from the two porphyries have low TiO_2 (1.72-2.13 wt.% and 2.27-2.60 wt.%), which may indicate low crystallization temperatures. Microscopic features indicate that the biotites in the two porphyry have formed at the latest stage of crystallization, by replacement of amphibole and/or by direct crystallization form an interstitial melt. Biotite in 70 quartz diorite shows slightly heterogeneous compositions. It is considerably rich in TiO_2 (3;62-5.46 wt.) and have high Mg/ (Mg+Fe) ratios (0.53-0.65) compared with the biotites from the porphyries.

Table 4. Representative chemical compositions of biotites.

Anal. No.	67A-1	67A-2	67A-3	70-1	70-2	70-3	38-1	38-2	38-3
SiO2	36.93	37.29	37.66	38.47	38.56	37.85	38.34	39.07	37.26
TiO2	2.13	2.05	2.09	3.79	4.67	4.84	2.56	2.60	2.47
Al2O3	15.70	15.48	14.79	13.52	13.64	13.83	14.59	14.07	14.69
Cr2O3	0.19	0.20	0.22	0.00	0.01	0.01	0.00	0.01	0.02
FeO	18.83	19.56	20.42	15.04	16.32	18.22	19.86	20.23	21.00
MnO	0.01	0.12	0.02	0.07	0.13	0.04	0.20	0.19	0.25
MgO	12.39	12.31	12.24	15.33	13.75	11.96	11.99	11.71	11.08
CaO	0.00	0.07	0.35	0.00	0.00	0.01	0.09	0.09	0.08
Na2O	0.09	0.06	0.07	0.01	0.01	0.01	0.01	0.01	0.01
K2O	9.53	9.15	9.79	9.40	8.96	9.04	9.00	8.97	9.16
Total	95.80	96.29	97.65	95.63	96.05	95.81	96.64	96.95	96.02
O=22 Si	5.587	5.617	5.640	5.717	5.722	5.692	5.745	5.836	5.675
Ti	0.242	0.232	0.235	0.424	0.521	0.548	0.288	0.292	0.283
Al	2.800	2.748	2.611	2.368	2.385	2.450	2.577	2.477	2.636
Cr	0.022	0.024	0.027	0.000	0.001	0.001	0.000	0.002	0.003
Fe	2.383	2.464	2.558	1.869	2.025	2.291	2.489	2.527	2.674
Mn	0.001	0.015	0.003	0.009	0.017	0.005	0.026	0.024	0.032
Mg	2.793	2.764	2.733	3.396	3.043	2.680	2.679	2.607	2.516
Ca	0.000	0.012	0.056	0.000	0.000	0.002	0.014	0.014	0.014
Na	0.025	0.019	0.019	0.002	0.002	0.002	0.002	0.002	0.002
K	1.840	1.759	1.870	1.783	1.697	1.734	1.721	1.710	1.780
Total	15.693	15.654	15.752	15.568	15.413	15.405	15.541	15.491	15.615
Mg/Mg+Fe	0.540	0.529	0.517	0.645	0.600	0.539	0.518	0.508	0.485

Compositions of plagioclases are plotted in Fig. 5, and their representative analyses are presented in Table 5. Plagioclases in OF1 dolerite are characterized by a restricted anorthite (An) range from 60 to 65, and high FeO content (0.75-0.99 wt.%). Plagioclase in 67B gabbro and 70 quartz diorite have homogeneous An content of 50 to 61 and 39-48, respectively. Plagioclases in 61 quartz diorite have An content from 37 to 58, and show a decrease of An mole % toward the crystal rim (normal zoning with respect to the An content). Plagioclases in 67A porphyry, which has intruded into 67B gabbro, show a wide range of An from 14 to 59, and some grains display a remarkable decrease of more than 30 An mole % toward the crystal rim. The plagioclases in the porphyry exhibit a general decrease of FeO from 0.50 to 0.05 wt.% with decreasing An mole %. Plagioclases in 38 porphyry also have a wide variation in An from 30 to 76, and FeO contents decrease from 0.99 to 0.12 wt.% with a decrease of An mole %.
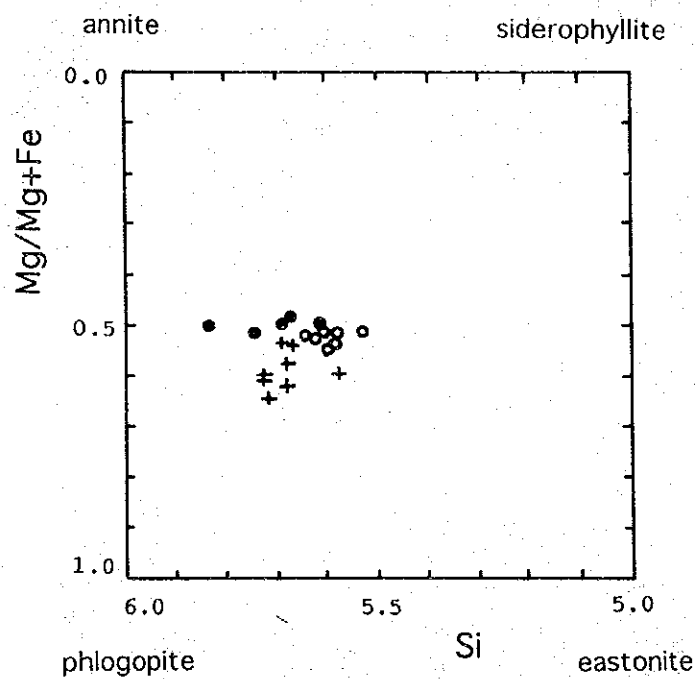

Fig. 4. Compositions of biotites in the phologopite - annite - eastonite - siderophyllite quadrilateral. Open circle: 67A porphyry, plus: 70 quartz diorite, closed circle: 38 porhyry.

Table 5. Representative chemical compositions of plagioclases.

Anal. No.	OF1-1	OF1-2	OF1-3	61-1	61-2	61-3	67A-1	67A-2	67A-3
SiO2	52.46	52.71	53.35	54.31	56.88	59.72	54.63	61.02	64.66
Al2O3	29.59	29.10	29.50	29.52	27.23	25.78	29.04	25.00	22.32
FeO	0.89	0.88	0.94	0.22	0.17	0.07	0.29	0.25	0.05
CaO	13.15	12.55	12.28	12.04	10.40	7.94	11.55	6.22	2.88
Na2O	3.87	4.23	4.20	4.91	6.07	7.61	5.18	7.98	9.74
K2O	0.27	0.33	0.30	0.09	0.03	0.19	0.06	0.07	0.06
Total	100.23	99.80	100.57	101.09	100.78	101.31	100.75	100.54	99.71
O=8 Si	2.385	2.405	2.411	2.431	2.541	2.638	2.452	2.699	2.852
Al	1.586	1.565	1.571	1.558	1.434	1.342	1.536	1.303	1.160
Fe	0.034	0.034	0.035	0.008	0.006	0.003	0.011	0.009	0.002
Ca	0.641	0.613	0.595	0.577	0.498	0.376	0.555	0.295	0.136
Na	0.341	0.374	0.368	0.427	0.526	0.652	0.450	0.684	0.833
K	0.015	0.019	0.018	0.005	0.002	0.011	0.003	0.004	0.004
Total	5.002	5.010	4.998	5.006	5.007	5.022	5.007	4.994	4.987
An/An+Ab	0.653	0.621	0.618	0.575	0.486	0.366	0.552	0.301	0.140

| Anal.No.	67B-1	67B-2	67B-3	70-1	70-2	70-3	38-1	38-2	38-3
SiO2	53.49	54.98	55.76	56.90	57.42	58.74	52.18	54.56	61.12
Al2O3	30.01	28.55	28.28	27.18	26.49	25.75	30.49	28.86	24.84
FeO	0.28	0.24	0.18	0.33	0.26	0.27	0.79	0.32	0.22
CaO	12.53	11.36	10.34	9.64	8.94	8.04	13.09	11.32	6.26
Na2O	4.47	5.25	5.73	5.88	6.53	7.03	3.74	5.38	8.25
K2O	0.00	0.00	0.02	0.27	0.26	0.05	0.00	0.02	0.06
Total	100.78	100.38	100.31	100.20	99.90	99.88	100.29	100.46	100.75
O=8 Si	2.404	2.472	2.502	2.553	2.581	2.630	2.364	2.455	2.700
Al	1.590	1.514	1.496	1.437	1.403	1.359	1.628	1.531	1.294
Fe	0.011	0.009	0.007	0.012	0.010	0.010	0.030	0.012	0.008
Ca	0.604	0.547	0.497	0.464	0.430	0.386	0.636	0.546	0.297
Na	0.390	0.458	0.498	0.512	0.569	0.610	0.328	0.469	0.706
K	0.000	0.000	0.001	0.015	0.015	0.003	0.000	0.001	0.004
Total	4.999	5.000	5.001	4.993	5.008	4.998	4.986	5.014	5.009
An/An+Ab	0.608	0.544	0.499	0.475	0.430	0.388	0.660	0.538	0.296
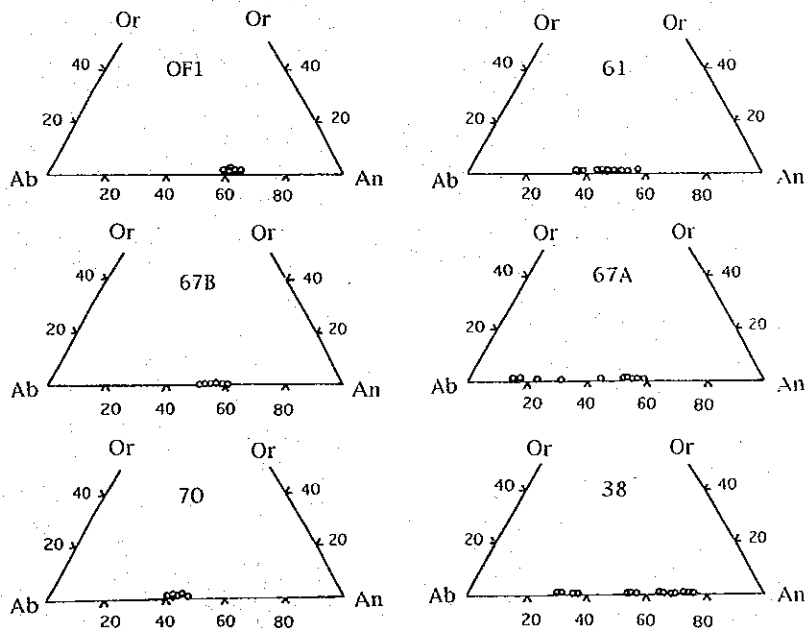
Fig. 5. Compositions of plagioclases in the anorthite (An) - albite (Ab) - orthoclase (Or) diagram.

References

Berg, K. and Baumann, A. (1985) Plutonic and metasedimentary rocks from the Coastal Range of Northern Chile: Rb-Sr and U-Pb isotopic systematics. Earth Planet. Sci. Lett., 75, 101-115.

Fukuoka, M (1991) Electron probe X-ray microanalysis. In: Textbook for Instrumental Analyses on Economic Geology and Related Sciences. H. Sugaki (ed.), pp. 61-87, JICA.

Herve, F. and Marinovic, N. (1989) Geocronología y evolución del batolito Vicuña Mackenna, Cordillera de la Costa, Sur de Antofagasta (24°-25°S). Rev. Geol. Chile, 16, 31-49.

Ishihara, S., Uleiksen, C.E., Sato, K., Terashima, S., Sato, T. and Endo, Y. (1984) Plutonic rocks of North-Central Chile. Bull. Geol. Surv. Japan. 35, 503-536.

Johnson, M.C. and Rutherford, M.J. (1989) Experimental calibration of an aluminium-in-hornblende geobarometer applicable to calcalkaline rocks. Geology, 17, 837-841.

Leake, B.E. (1978) Nomenclature of amphiboles. Can. Mineral., 16, 501-520.

Leterrier, J., Maury, R.C., Thonon, P., Girard, D. and Marchal M. (1982) Clinopyroxene compositions as a method of identification of the magmatic affinities of paleo-volcanic series. Earth Planet. Sci. Lett., 59, 139-154.

Mercado, M. (1980) Geología del área de Pan de Azúcar, Región de Atacama. Escala 1:100,000. Carta Nº 37 IIG.

Naranjo, J.A. (1978) Geología de la zona interior de la Cordillera de la Costa entre los 26°00, y 26°20, Región de Atacama. Escala 1:100,000. Carta No. 34, IIG.

Pichowiak, S. and Breitkreu, C. (1984) Volcanic dykes in the north Chilean Coast Range. Geol. Rdsch., 73, 853-868.

Poldervaart, A. and Hess, H.H. (1951) Pyroxene in the crystallization of basaltic magma. Jour. Geol., 59, 472-489.

Scheuber, E. and Reutter, K.J. (1992) Magmatic arc tectonics in the Central Andes between 21 and 25°S. Tectonophysics, 205, 127-140.

Schmidt, M.W. (1992) Amphibole composition in tonalite as a function of pressure: an experimental calibration of the Al-in-hornblende barometer. Contrib. Mineral. Petrol., 110, 304-310.

Segerstrom, K. (1968) Geología de las hojas Copiapo y Ojos del Salado. Inst. Invest. Geolog., Bol., No. 24, p.58. Santiago de Chile.

SCAPOLITE AND CHLORITE IN QUARTZ-DIORITE FROM CALDERA COASTAL AREA, COPIAPO PROVINCE, NORTHERN CHILE

Morihiro Aoki*, Shoji Kojima**, Shoji Higashi***
and Kiyoshige Ochiai****
*Miyagi University of Education, Aramaki Aoba, Sendai 980, Japan.
**Yagiyama Hon-cho 1-24-11, Taihaku, Sendai 982, Japan.
***Department of Geology, Faculty of Science, Kochi University,
Akebono 2-5-1, Kochi 780, Japan.
****Science Education Institute, Karita 4-13-23, Sumiyoshi,
Osaka 558, Japan.

Introduction

In the Copiapo province, one of the most important mining districts, a great deal of granitic rock is extensively distributed. Particularly in the Caldera coastal area situated at the western region of the province, dioritic to tonalitic rock occurs with varying amount (Ishihara et al., 1984). Recently, Sugaki and his co-workers collected such a granitic rock for the purpose of making a study on its K-Ar age (Sample No. 92102926), and have reported K-Ar ages of 162-155 Ma in middle Jurassic (Sugaki and Shimada, 1994). According to Farrar et al. (1970), however, the tonalitic rock in this area is regarded to have formed at 187-181 Ma in earlier Jurassic. This discrepancy suggests that the younger K-Ar age is attributed to hydrothermal metasomatism in the later ages, and has led us to check constituent minerals of the Caldera granitic rock. Indeed, we have found that the Caldera rock contains considerable amounts of scapolite - and chlorite - group minerals as metasomatic products. In the present study, we try to make a preliminary description on the scapolite and chlorite through microscopic observations and X-ray powder diffraction analysis.

23

Mineral descriptions

The granitic rock collected from the Caldera coastal area, north of the Caldera City (approximately 27°01'S, 70° 47'W) was used for the present study. Macroscopically the rock is fine to coarse-grained, showing distinct heterogeneities in grain size and distribution of lenticular to weakly layering light-colored portions. A detailed observation leads us to recognize that the light-colored portion is subdivided into pinkish white layer (low crystalline part) and colorless

Fig. 1. Photomicrographs showing paragenetic relations among scapolite, chlorite, plagioclase and hornblende in the Caldera quartz-diorite. A, sericitized plagioclase surrounded by chlorite: B, chloritized plagioclase: C, plagioclase replaced by chlorite: D, plagioclase relict in chlorite: E, fractured hornblende (plane-polarized): F, identical field to E, primary hornblende intersticed with scapolite aggregate (crossed polars).

layer (highly crystalline part). As described later, the former contains plagioclase relict and the latter includes considerable amount of well-crystallized scapolite and chlorite. In contrast, green-colored hornblende is uniformly distributed in no relation to the layered alteration fabrics. Two thin-sections, which were from the low crystalline and highly crystalline parts, were prepared for microscopic observations.

The present rock consists mainly of scapolite, chlorite, plagioclase and hornblende as major minerals, and quartz, sphene, zoisite, sericite, rutile, carbonate
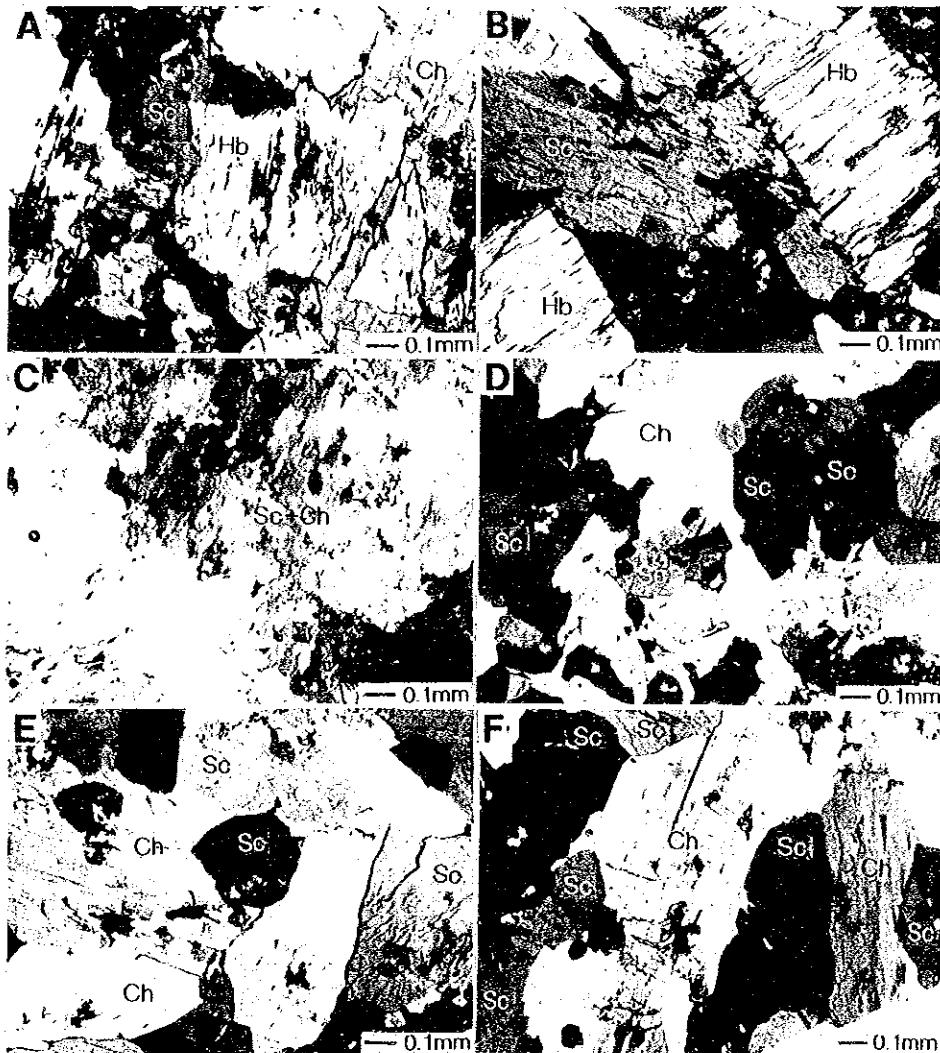

Fig. 2. Photomicrographs showing paragenetic relations among scapolite, chlorite and hornblende in the Caldera quartz-diorite. A, fracturing of primary hornblende filled by chlorite and scapolite grains: B, primary hornblende intersticed with scapolite: C, fine-grained aggregate of scapolite and chlorite: D, sacchaloidal aggregate of scapolite and chlorite: E-F well-crystallized scapolite and chlorite.

25

(calcite) and apatite as minor minerals. Microscopic features of the major minerals and their paragenetic relations are shown in Figs. 1 and 2, and are summarized as follows.

Scapolite, the most abundant mineral in the colorless layer occurs as fine-grained aggregate to well-crystallized grains, varying in grain size. Usually scapolite is colorless in plane-polarized light, and its refractive index and birefringence are low. Optically, scapolite is uniaxial (-), showing the length fast character. Although scapolite resembles some other minerals such as nepheline, it is usually distinguished by its uniaxial (-) character, straight extinction and the (100) and (110) cleavages at right-angles to one another. As shown in Fig. 1-E F, the scapolite partially cuts across primary hornblende crystals.

Chlorite is colorless to pale greenish in plane-polarized light, occurring as well-crystallized prismatic grains. The present chlorite has low refractive indices, and its birefringence is moderate. Optically, chlorite is biaxial (+), exhibiting the length fast character. The chlorite shows straight extinction, having small $2V$ values ranging in $20°$ ($\pm$). These results suggest that the chlorite presents corresponds to a clinochlore. The chlorite replaces partially plagioclase grains (Fig. 1-D).

Plagioclase suffered mostly sericitization, remaining as a relict phase (Fig. 1-A B C D). Under the microscope, distribution of plagioclase is restricted in the low crystalline layer. In such a part, primary plagioclase with typical albite twinnig is observed (Fig. 1-D). As shown in Fig. 1-A-D, considerable part of plagioclase is strongly substituted by chlorite. Plagioclase and chlorite have no certain crystallographic relations, varying in their mode of occurrence.

Hornblende (common hornblende) appears in both the low crystalline and highly crystalline parts of the rock, and partially intersticed by scapolite (Fig. 1-E F) and cut by chlorite (Fig. 2-A B). In the case of the latter, fracture profiles of the hornblende separated by chlorite are well accordant each other. This means that the hornblende was not replaced but only fragmented by chlorite.

Quartz develops intersticially as the latest stage mineral. From the presence of hornblende and plagioclase in addition to such a crystallization of excess silica (quartz), the original rock is estimated as quartz-diorite.

X-ray diffraction analysis

X-ray powder diffraction analysis was made for the colorless layer of the rock, so as to check the presence of scapolite and chlorite. The colorless part was separated by hand picking under a stereoscopic microscope. The X-ray analysis was carried out using Cu-Kα radiation under the operating conditions of 40 kV and 20 mA.

From the diffraction profile obtained, it has been proved that the colorless

Table 1. X-ray diffraction data for scapolite in the Caldera quartz-diorite

hkl	Caldera d(Å)	I	Schetland* d(Å)	I
110	8.50	45	8.54	10
101	6.45	10	6.43	8
200	6.05	25	6.04	16
211	4.41	5	4.40	4
220	4.27	25	4.27	8
310	3.81	80	3.82	45
301	3.56	40	3.56	20
112	3.47	100	3.47	100
321	3.06	90	3.06	65
400	3.02	60	3.02	30
222	2.84	25	2.84	8
411	2.734	20	2.731	14
312	2.694	55	2.691	32
510	2.368	2	2.367	2
431	2.301	20	2.300	10
422	2.200	2	2.199	2
303	2.145	10	2.144	6b
530	2.071	2	2.070	4
600	2.021	8	2.015	4b
413	1.915	25	1.914	14
620	1.908	25	1.908	12
004	1.901	20	1.897	8
541	1.829	2	1.830	2
532	1.818	8	1.817	4
433	1.749	4	1.746	4
550	1.707	10	1.707	6
640	1.674	4	1.674	2
721	1.620	4	1.619	2
404	1.607	2	1.606	<2
730	1.585	2	1.584	<2
613	1.562	4	1.561	6

*Marialite from Schetland Islands, United Kingdam (JCPDS 31-1279).

part of the rock is composed mainly of scapolite and chlorite. X-ray powder diffraction data for scapolite are listed in Table 1, together with those for calcian marialite given in JCPDS (1986). They are in excellent agreement each other, so that the present scapolite is regarded as calcian marialite $(Na, Ca)_4(Si, Al)_{12}O_{24}(Cl, CO_3)$.

Concluding remarks

By means of microscopic observations and X-ray powder diffraction analysis, scapolite (calcian marialite) and chlorite as metasomatic minerals were found in

the quartz-diorite from the Caldera coastal area, Copiapo province. Detailed observations under the microscope has led the following paragenetic sequences.

(1) First, calcian marialite substituted a part of plagioclase, developing as an idiomorphic phase.
(2) Second, chlorite replaced selectively plagioclase. While, hornblende was only physically fragmented by chlorite, and remains as a primary phase.
(3) Finally, small amount of quartz crystallized as the latest stage mineral, filling up interspace of the previously crystallized minerals.

The present chlorite is well-crystallized, corresponding probably to clinoclore from the viewpoint of the optical properties. The occurrence of scapolite group mineral means that the original rock, quartz-diorite has suffered hydrothermal metasomatic reaction under high CO_2 pressure condition or in the presence of abundant brine (NaCl). It is well known that certain hypersaline brines were responsible for formation of the hydrothermal ore deposits in the Copiapo province (e.g., Campos 1991). Accordingly, although no mineralization is known related to the coastal plutonic rocks in the Caldera area (Ishihara *et al.*, 1984), the scapolitic (alkaline) metasomatism in granitic rocks may be a significant sign of hydrothermal activity in middle Jurassic.

Acknowledgment

References

Campos, E. (1991): Estudios mineralógicos y microtermométricos en vetillas de cuarzo, Mina Marte. Sci. Rept. Econ. Geol. Res. Proyect, Universidad de Concepción, No. 1, 57-73.

Farrar, E., Clark, A.H., Haynes, S.J. And Quirt, G.S. (1970): K-Ar evidence for the post-paleozoic migration of granitic intrusion foci in the Andes of Northern Chile. Earth Planet. Sci. Lett., 10, 60-66.

Ishihara, S., Ulriksen, C.E., Sato, K., Terashima, S., Sato, T. and Endo, Y. (1984): Plutonic rocks of North-Central Chile. Bull. Geol. Surv. Japan, 35, 503-536.

JCPDS (1986): Mineral Powder Diffraction File Data Book, No. 31-1279, International Centre for Diffraction Data, Swarthmore.

Sugaki. A. and Shimada, N. (1994): K-Ar dating on rocks and minerals related to ore deposits in Chile (2). Sci. Rept. Econ. Geol. Res.Project, Univ. Concepción, No. 4, 71-80.

SYNTHESIS OF SIMPLE SULFIDE MINERALS

Asahiko Sugaki*, Eduardo Campos** and Ricardo Alvarez***
***Kadan 4-30-503, Aoba, Sendai 980, Japan. **Instituto GEA,**
Universidad de Concepción, Casilla 4107, Concepción 3, Chile.
*****Depto. Ciencias de la Tierra, Universidad de Concepción,**
Casilla 3-C, Concepción, Chile.

1. Introduction

The phase diagrams of sulfide minerals are necessary when the genesis of the ore-forming minerals in the ore deposits is discussed. To determine experimentally the phase relations in the diagrams of sulfide system, artificially prepared sulfide minerals are used, owing to the difficulty in obtaining the necessary amounts of natural sulfide minerals of sufficient purity. Accordingly, the synthesis of pure sulfide minerals is the first step in the studies on the phase diagram.

Sulfide crystals synthesized by using high-purity metals and sulfur are generally employed as a standard material for chemical analyses, for example, electron probe microanalysis (EPMA), X-ray diffraction and X-ray fluorescence.

Some metal sulfides are also used as materials of semiconductor, piezoelectricity and cathode luminescence. The phase relation data of these materials in the diagram are fundamentally necessary to develop them in the material sciences, and those investigations have to start from synthesis of sulfides.

Such phase diagram also plays an important role to interpret the behavior of the sulfide minerals in the smelting furnace in metallurgy.

As mentioned above, the sulfide synthesis works need by all means, to play an important role in the development of investigation in all the fields of ore mineralogy, economic geology, geochemistry, analytical chemistry, material sciences and metallurgy.

The synthesis methods of sulfide minerals, in general, are roughly divided into two kinds the evacuated glass-tube (dry) and hydrothermal crystallization (wet) methods.

29

In this paper, the experimental procedure on the synthesis of simple sulfides, such as covellite (CuS), chalcocite (Cu$_2$S), troilite (FeS), galena (PbS), sphalerite (ZnS), alabandite (MnS), greenockite (CdS), bismuthinite (Bi$_2$S$_3$) and stibnite (Sb$_2$S$_3$), by the evacuated glass-tube method and mineralogical data of synthesized products are described in the concrete as below.

2. Synthetic method

As simple and more popular method of sulfide synthesis, the reaction between pure metal and sulfur under vacuum is commonly used. In this case, the evacuated and sealed glass-tube is employed as a container of the reaction. The procedures and equipments of this method were already described by Kullerud (1971), Scott (1974), Sugaki & Shima (1965a, b), Vaughan & Craig (1978) and Sugaki (1992). So, the present authors will explain about concretely and necessarily things only to synthesize such simple sulfides as mentioned above. The synthesis of simple sulfides is, in particular, significance that they are often used as a starting material for synthesis of three or more component sulfide and sulfosalt minerals which occur in nature.

2.1. Reaction vessel

The transparent fused quartz glass-tube was, in general, used as a container of sulfide synthesis. ThePyrex glass-tube was also employed at lower temperatures than 550°C. The quartz glass-tube was stable up to about 1,100°C, and did not react with sulfur and most kinds of metals below that temperature.

· The size of the glass-tube was chosen in part by amount of the charge to be reacted. Usually, the tubes of inside diameter, 4 to 8 mm, with wall thickness of 0.5 to 1.5 mm were used in most synthetic works. The tubes, 6 to 8 mm in inside diameter and 0.7 to 1.5 mm in wall-thickness, were necessary for starting materials of several hundred milligrams to one gram. Commonly, about 300 to 500 mg, sometimes 1.0 g of starting materials were sealed in the glass-tube, 4 to 8 mm inside diameter, 0.5 to 1.0 mm thick and 30 to 50 mm long.

The procedure sealing the evacuated glass-tube is illustrated by Fig. 1. After a glass-tube (Fig. 1-A) of about 20 cm long was sufficiently cleaned in the distilled water bath by using ultrasonic wave and was dried, it was separated in two tubes, about 10 cm long, closed the end as shown in Fig. 1-B by melting the glass-tube in small propane gas-oxygen flames of the welding torch.

Then, pure metals and sulfur as a starting material of the sulfide synthesis were exactly weighed by the chemical balance in the proportions to metal and sulfur ratio in the composition of sulfide mineral synthesized. The starting
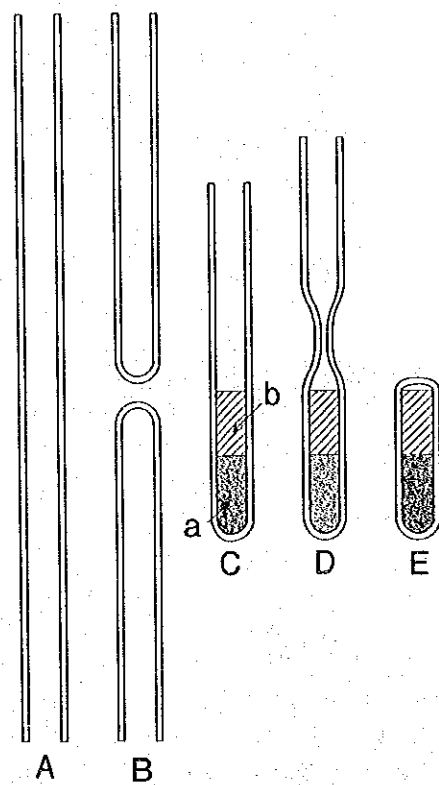
Fig. 1. Glasswork procedure on a reaction
vessel using the evacuated glass-
tube method. a. charge, b. quartz
glass-rod.

materials were put carefully so as not to lose into the bottom of the tube closed
at the end. Sulfur was usually put first place at the bottom of the tube to keep it
away from the welding flames as far as possible, and then the metal was added.

After all sulfur and metal were completely transferred into the glass-tube so
as not to lose them, a tightly fitting short piece, 1 to 2 cm long, of transparent
quartz glass-rod was put on the metal in the upper part of the glass-tube to
decrease much of the vapor space in the sealed tube (Fig. 1-C). The glass-tube was
necked down as to become a fine pipe with less than 1 mm in inside diameter just
above the filler quartz glass-rod by the flames as shown in Fig. 1-D. In this case,
to protect sulfur and metal from vaporization and oxidation, respectively, by
heating during the glasswork, a lower portion of the glass-tube contained the
charge, extending about 2 to 3 cm to the bottom side from the end of the quartz
glass-rod was wrapped in a wet cloth.

The necked glass-tube was connected to a rubber tube of vacuum pump line, and
then was evacuated to approximately 10^{-3} Torr. After reaching at about 10^{-3} Torr, the
fine pipe portion of the necked glass-tube was sealed off in the flames, and the top

31

end of the sealed tube was melted around the filler quartz glass-rod (Fig. 1-E). In that case, the pumping for vacuum should has been carried out carefully to avoid suction of the fine-grained or powdered charges into the vacuum line. This suction loss was able to be usually prevented by rapidly flipping the rotary pump switch on-and-off a few times, initially.

2.2. Starting materials

As the starting materials, pure sulfur and metals were employed for synthesis of a simple sulfide. Sulfur with four nine (99.99%) in purity was commonly used as grains after breaking and sieving. Most metals were available four to six nine pure as block, lump, grain, scrap, plate, sheet, rod, wire, sponge or powder. If possible, it was better not to use powders of metal and sulfur because they are likely to adhere to watch-glass or paper used in weighing and wall of the glass-tube of a reaction vessel when transferring them, and as a result, they were lost. The powder was also likely to be sucked into the vacuum pump line, and it was lost. When metals were at a large scale as block, lump, sheet, plate, rod and wire, they were crushed, cut and shaved so as not to be contaminated, and then sized through a sieve. Grain size of metals employed synthesis was in general a few millimeters, 0.5 to 3 mm, meanwhile sulfur, 0.2 to 3 mm. Some powdered metals, for example, copper acted quickly upon sulfur with intense exothermic reaction at room temperature, and then sulfur burnt before the evacuation.

Also, some metals, particulary iron and copper, were often coated with their oxide film. This oxide film had to be taken away before weighing them as a starting material. In this case, such metals coated with the oxide film were usually reduced at temperatures below their melting points in a stream of hydrogen gas cleaned off from water and oxygen contained in the gas through a desiccant (silica-gel) and copper net heated at about 400° to 450°C, respectively (Sugaki, 1992). For example, the oxide films of iron and copper were able to be completely taken away in the purified hydrogen gas stream at 900°C and 800°C, respectively, for 1 to 2 hours.

2.3. Heating procedure

The charge of metal and sulfur which were sealed into the evacuated glass-tube was put into an electric furnace, and kept at desired temperature until their reaction that produced sulfide compound finishs perfectly, namely, up to complete consumption (or disappearance) of sulfur. In this case, the vapor pressure of sulfur rises rapidly above 445°C of its boiling point. So, the charges had to be preheated at lower temperature below 450°C to combine the metal and sulfur as much as possible before heating at the desired temperature.

32

After heating the charges at the desired temperature until all sulfur was spent in order to form sulfide completely with metal, the sealed glass-tube was taken out from the furnace and cooled in air. The glass-tube was broken and then the sulfide charge of the product was taken out from the tube. In the case of removing the charge from the tube, it was important not to lose the product and not to remain it in the tube. Namely, all the product had to be taken out from the tube. The product was thoroughly ground so as not to lose it, to get a homogeneous powdered mixture in an agate mortar under acetone to prevent oxidation in air.

Then, the powdered product was sealed again with the quartz glass-rod in the glass-tube under vacuum by the same procedure as mentioned above, and it was reheated in the furnace kept at desired temperature during suitable time for equilibrium. After reheating the charge was cooled in air, and was taken out again from the tube. The product was examined on its homogeneity using a microscope and X-ray powder diffraction. The product usually became homogeneous by reheating. If original metal still remained or the product was heterogeneous, the preparations of grinding under acetone in the agate mortar, sealing the evacuated glass-tube and reheating in the furnace were repeated until the product became homogeneous.

2.4. Synthetic apparatus of sulfide minerals

Furnace: Six vertical and cylindrical type furnaces, 5 cm in inside diameter, 30 cm in outside diameter and 50 cm long, were used in the synthetic works (Fig. 2). The furnaces which are wound with Kanthal resistance wire, 1.6 mm in diameter, were able to be use commonly at temperatures up to 800°C, but only temporarily up to 1,000°C for a short time. The temperature distribution of hot spot (maximum temperature) within ±1°C in the furnace was over a vertical distance of 8 cm at 600°C. The charge in the sealed glass-tube was suspended with iron or nickel wires into the hot spot zone of the furnace, so as to touch to thermocouple.

Temperature measurement system: Temperatures at a hot spot zone in the furnace were measured by a sheath-type chromel-alumel (K-type) thermocouple (Fig. 2-b). Exact temperature of the charge was also measured by touching the thermocouple to the sealed sample glass-tube suspended in the hot spot zone of the furnace.

The extension lead-wire of the thermocouple was joined to a digital thermometer (Fig. 3). We were able to know easily an exact temperature of the furnace by a display in the thermometer. By this single thermometer hooked up with the multichannel switching unit, the temperatures of the six furnaces were measured (Fig. 3). Also the furnace temperatures were more exactly measured by using DC precision potentiometer assembled with standard cell, electronic galvanometer and DC precision current supply (Fig. 3-b).
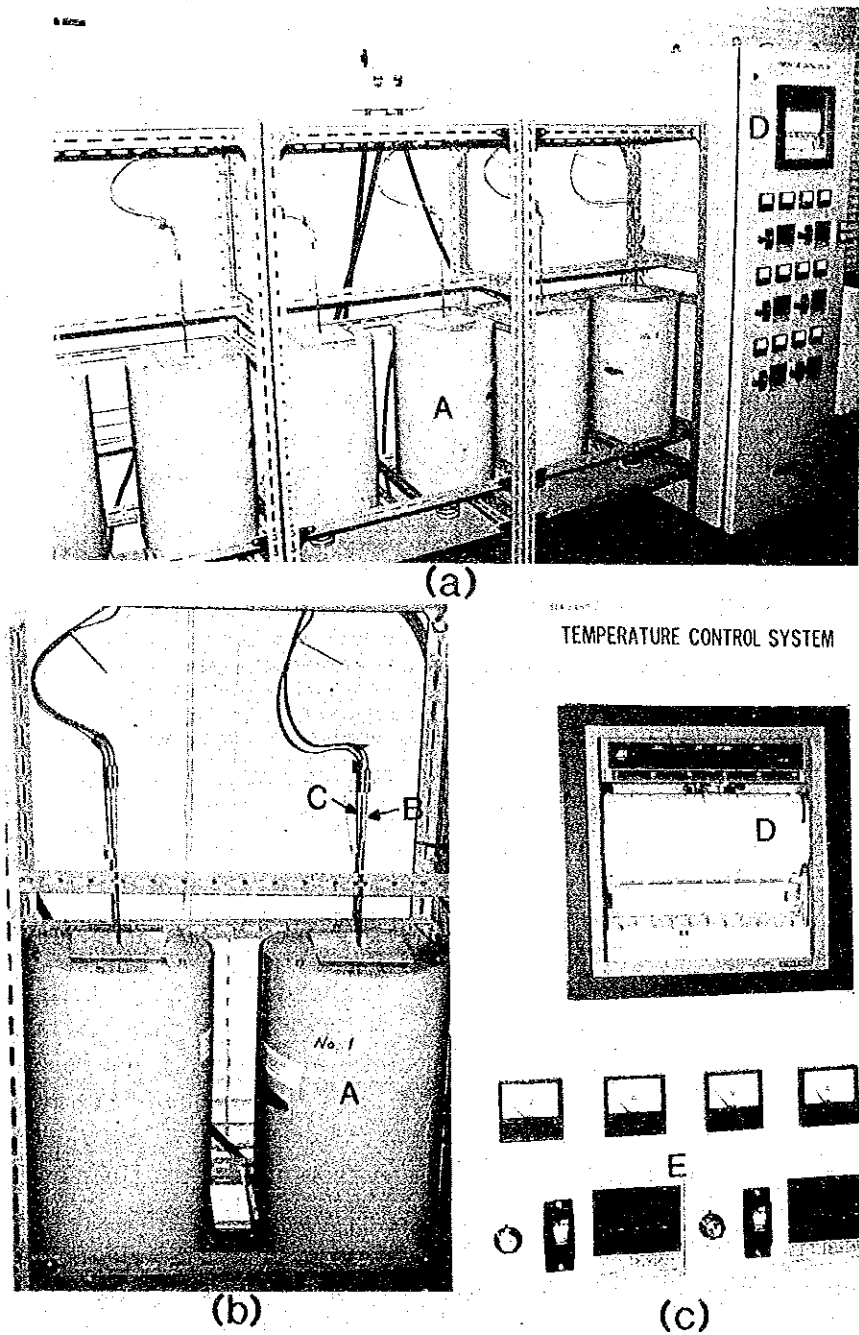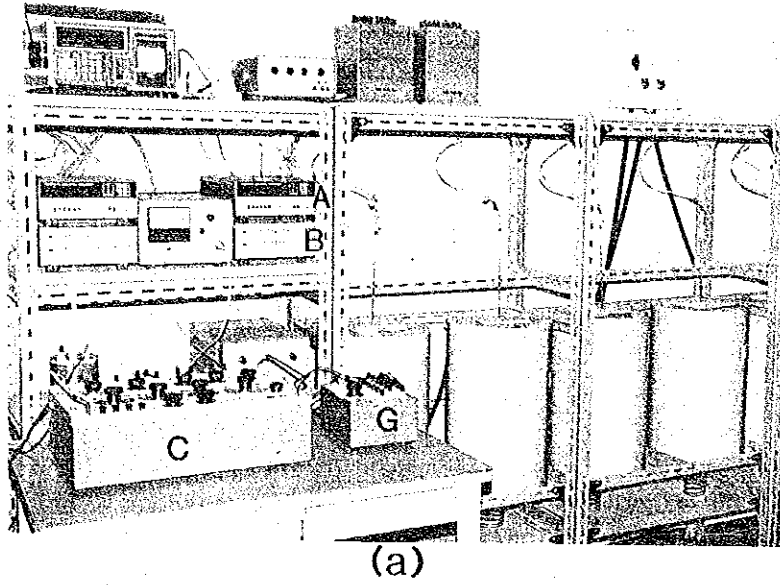
Fig. 2. Electric furnace using the sulfide synthesis. A: Electric furnace of vertical and cylindrical type (a,b), B: Sheath-type chromel-alumel thermocouple for temperature measurement (b), C: Thermocouples for temperature-control and recording (b) D: Temperature recorder (a, c), E: Temperature controller (a, c).

34
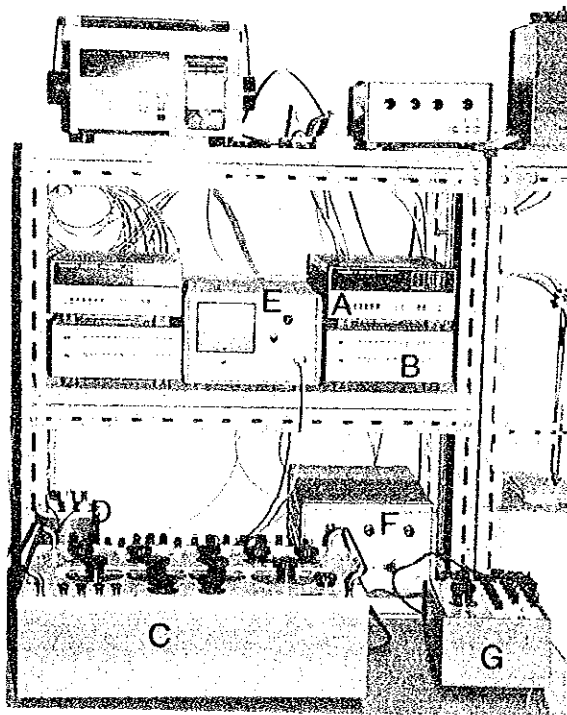
Fig. 3. Temperature measurement system (a, b).
A: digital thermometer (millivoltmeter), B: Multichannel switching
unit, C: DC precision potentiometer, D: Standard cell, E: Electronic
galvanometer, F: DC precision current supply, G: Selector switch.

Temperature controller and recorder: The temperature of the furnace was continuously adjusted by the PID digital indicating controller to keep it at desirable temperature for a long time. As a temperature detector, one of the chromel-alumel double thermocouples was used. The extension lead wires of the thermocouple were connected to the PID digital controller. It was important to select fitting values of P, I and D so as to maintain at exactly fixed temperature within ±1°C or less. For example, the furnaces used in this synthetic experiment were able to perform a suitable control within ±1°C at temperature range from 200° to 700°C by setting the following values, P: 5%, I: 600 sec., and D: 0 sec.

The controller of power for the electric furnaces was a silicon controlled rectifier whose function is to automatically keep the furnace temperature at a constant value for a long time, connected with the PID digital indicating controller.

To keep an eye on the furnace temperatures for a long time, a hybrid recorder was used. This recorder is six-point sequential display type to be able to dot by different colors on temperatures of the six-furnaces. The extension lead wire of one of the double chromel-alumel thermocouples in each furnace was connected directly to the recorder. A dot interval of the recorder was approximately 5 seconds per dot. Speed of recording chart was 25mm per hour although it can be set from 1 to 1500 mm per hour.

3. Identification of synthetic products

Macroscopic properties: Physical properties of the products such as crystal color, luster, morphology, magnetic behavior and hardness were used as means of identification of synthetic sulfide mineral.

Microscopic properties: The small amounts of the products were mounted with acrylic acid resin at room temperature in a plastic cylinder vessel. After hardened, they were ground and polished as for a normal polished section of ores. The polished section was observed under ore microscope with illuminator about homogeneity, size, form, and optical properties such as color, bireflence, anisotropy, internal reflection, reflectance etc., of the product.

Scanning electron microscopy : The products synthesized occasionally have euhedral crystal macroscopically. In such a case, the crystal was examined on its morphology under scanning electron microscope (SEM).

X-ray powder diffraction: The product was routinely identified by its X-ray powder diffraction data. The synthesized minerals have very distinct and characteristic X-ray patterns which allow fast and sure identification. These patterns were always obtained by using Guinier camera with quartz monochromator in this study to obtain the most exact data so as to be able to employ as a standard, although they usually were got by the diffractometer or Debye-Scherrer camera.

The film of the camera was exposed for 10 to 15 hours using Cu-Kα radiation (fine focus type of Cu X-ray tube) of 35 kV and 15 mA. High purity silicon was always used as an internal standard. The Guinier film reading and calculation programs which were developed by Kitakaze (1992) were employed to obtain fast the exact data of the d-spacings and cell constants of the synthesized product.

Thermal analysis: Differential thermal analysis (DTA) was performed on synthesized sulfides to detect their thermal behavior such as phase transformation, decomposition and melting which are of characteristic for each product. The analysis was carried out by the means using sealed vacuum quartz glass-tube (Sugaki, 1991). Calcined aluminum oxide (α-alumina) was used as an inert material. The heating rate was 5°C/min. exactly. Both, the temperature of the product rising with the heating rate and the potential difference of the thermoelectric motiveforce of the differential thermocouples were continuously and automatically recorded. The amounts of the sulfide product used in the DTA were about 300mg.

4. Synthesized sulfide minerals

4.1. Covellite (CuS)

Synthesis of covellite was carried out by reaction between pure copper metal (5N), which was taken off coating oxide film by reduction of hydrogen gas, and sulfur (4N) in the evacuated glass-tube, after they were accurately weighed in the proportion to one to one in atomic ratio. They were treated at 450°C for 2 to 4 days after preheating at 400°C for a day to be consumed sulfur below its boiling temperature, 445°C, as much as possible, and then cooled in air. If the product was found heterogeneous under the ore microscope, it was again sealed in the evacuated glass-tube after thoroughly grinding under acetone, and then reheated at 450°C for 2 days. By this reheating, a homogeneous phase was usually obtained.

Covellite synthesized is in granular aggregate, indigo-blue in color with submetallic luster megascopically. Under the microscope, it has distinct pleochroism changing its interference color from deep reddish brown to purple under the crossed nicols. Its hardness is low. These optical properties agree with those of natural covellite described by Ramdohr (1969), Uytenbogaardt & Burke (1971), Picot & Johan (1982) and Spray & Gedlinske (1987).

Synthesized covellite sometimes shows macroscopically a crystal form in its aggregate. Photomicrograph of the covellite crystal by scanning electron microscope (SEM) is shown in Fig. 4-A. The crystals in the figure have besal and pyramidal faces.

The data of X-ray powder diffraction of synthetic covellite obtained by Guinier camera are given in Table 1. Its cell parameters obtained from these data
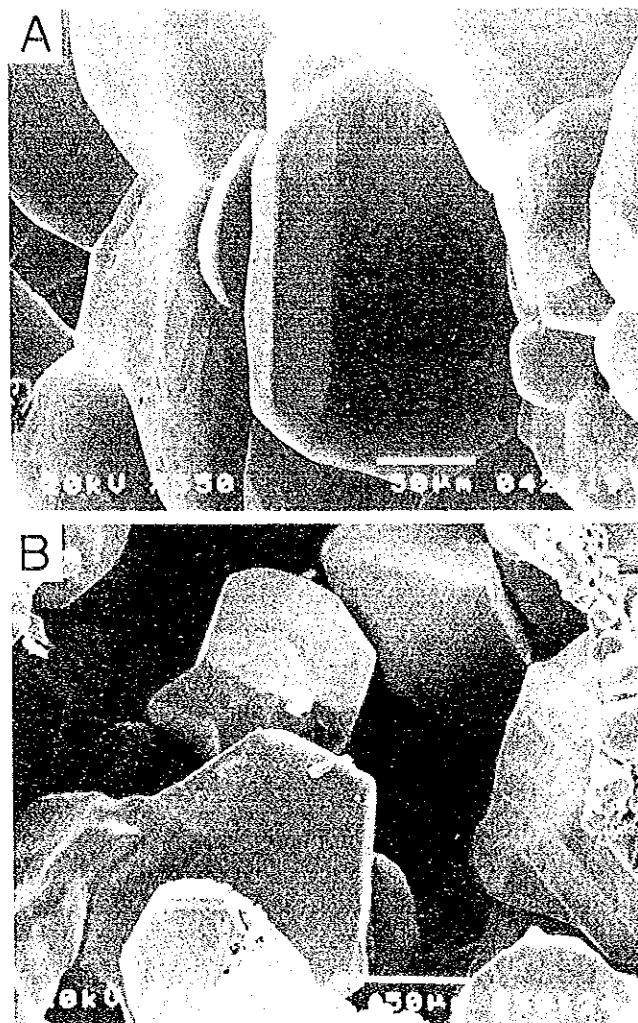
Fig. 4. Photomicrographs of scanning electron microscope
(SEM) for sulfide minerals synthesized by the
evacuated glass-tube method. A: Covellite, B:
Chalcocite.

are hexagonal, a=3.7923 (1)Å and c=16.3504(8)Å. Its data are in good accordance
with those of Berry & Thompson (1962) and Mineral Powder diffraction File
(Data Book) compiled by the JCPDS (1986).

The DTA curve of covellite is shown in Fig. 5. The curve represents a strong
endothermic reaction begining at 503°C, indicating formation of high-digenite
by breakdown (507°C) of covellite.

38

Table 1. The data of X-ray powder diffraction by Guinier camera for covellite synthesized by evacuated glass-tube method

I	h	k	l	d(obs)	d(calc)	Δd
5.3	0	0	2	8.1760	8.1752	0.0008
11.7	1	0	0	3.2847	3.2842	0.0005
30.9	1	0	1	3.2201	3.2199	0.0002
81.0	1	0	2	3.0484	3.0475	0.0009
99.9	1	0	3	2.8132	2.8130	0.0003
49.0	0	0	6	2.7245	2.7251	-0.0005
8.7	1	0	5	2.3172	2.3173	-0.0001
3.2	1	0	6	2.0967	2.0971	-0.0004
5.0	0	0	8	2.0432	2.0438	-0.0006
18.4	1	0	7	1.9030	1.9035	-0.0004
100.0	1	1	0	1.8962	1.8961	0.0000
27.4	1	0	8	1.7352	1.7352	-0.0000
8.8	2	0	2	1.6100	1.6100	0.0001
15.1	2	0	3	1.5722	1.5723	-0.0001
37.3	1	1	6	1.5566	1.5564	0.0001
2.1	1	0	10	1.4639	1.4637	0.0002
4.3	1	1	8	1.3901	1.3900	0.0000
6.2	1	0	11	1.3542	1.3542	0.0000
4.4	2	0	7	1.3433	1.3434	-0.0001
8.9	2	0	8	1.2802	1.2801	0.0001
5.9	2	1	2	1.2272	1.2273	-0.0001
10.6	2	1	3	1.2103	1.2103	0.0000

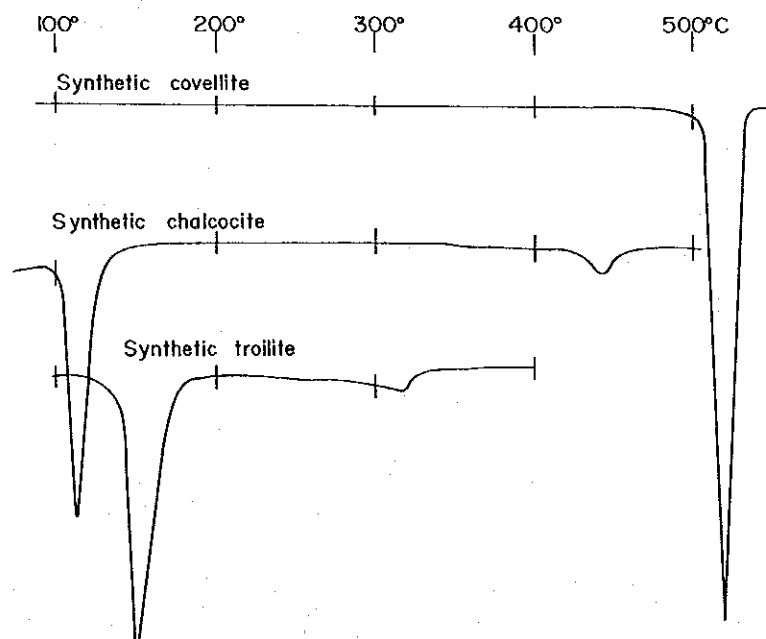CELL PARAMETERS

a = 3.7923 (1) Å   c = 16.3504 (8) Å

Fig. 5. The curves of differential thermal analysis (DTA) for synthetic covellite, chalcocite and troilite.

4.2. Chalcocite (Cu_2S)

Copper metal, 5N purity, in a chip-shaped form scraped off by a lathe from a copper rod, and sulfur, 4N purity, in grain were used as starting materials for synthesis of chalcocite. The copper metal covered with a oxide film its surface was reduced by hydrogen gas at 800°C for 1 to 2 hours before weighing. They were exactly weighed in the proportion to two copper and one sulfur in atomic ratio, and were sealed in Pyrex glass-tube under vacuum in 10^{-3} Torr. The sealed tube with charge was put into a hot point of the electric furnace and was kept at 500°C for 2 days after preheating at 400°C for a day, and then was cooled in air. By this heating, copper and sulfur easily reacted each other to form a cuprous sulfide. Then, the polished product was observed under microscope. If copper remained or the product was heterogeneous, the product was ground in an agate mortar to get a homogeneous mixture with acetone, and was again sealed in the glass-tube under vacuum. Then, it was reheated in the furnace at 500°C for 2 days. By this reheating, homogeneous chalcocite was formed.

Chalcocite produced is aggregate of fine grains showing steel gray in color with metallic luster. Under the microscope, it is grayish white in color and shows anisotropism changing its color from grayish blue to grayish brown under the crossed nicols. These optical properties are in good accordance with those of natural chalcocite described by Ramdohr (1969), Uytenbogaardt & Burke (1971), Picot & Johan (1982), and Spray & Gedlinske (1987).

A SEM photomicrograph of synthetic chalcocite is shown in Fig. 4-B. The chalcocite crystals consist of (111) and (110) faces of the cubic form with a growth twin.

X-ray powder diffraction for chalcocite synthesized was carried out by using Guinier camera, and its data are given in Table 2.

DTA curve of synthetic chalcocite is shown in Fig. 5. The curve has a distinct endothermic peak beginning at 102°C and a gentle and small endothermic peak beginning at 430°C. The former one indicates a latent heat of inversion (103°C) from the monoclinic (low) form to the hexagonal form. The latter also represents an inversion (435°C) from the hexagonal to the cubic form.

4.3. Troilite (FeS)

Stoichiometric iron sulfide, FeS, was synthesized by reaction between iron (4N) and sulfur (4N) in the evacuated quartz glass-tube. The powdered iron metal with oxide film was reduced in the stream of hydrogen gas at 900° to 950°C for 1 to 2 hours before weighing. By this heating, iron powder was sintered as a hard mass as a rod-like shape. The hard mass of the sintered iron powder was crushed and sized to a few mm across as a powder aggregate by sieving. Then, such

Table 2. The X-ray powder diffraction data obtained by Guinier
camera for synthetic chalcocite

I/I0	d(obs.)	I/I0	d(obs.)
3.5	6.4217	15.0	2.1210
4.0	4.2407	7.6	2.0285
4.1	3.8574	13.7	2.0107
2.0	3.7746	4.6	2.0021
30.0	3.7365	36.2	1.9817
21.9	3.5989	100.0	1.9746
6.2	3.3337	12.5	1.9610
16.3	3.3157	19.3	1.9521
33.7	3.2769	16.0	1.9103
30.4	3.1874	5.7	1.8948
37.6	3.1587	97.5	1.8805
20.2	3.0570	6.8	1.8089
37.9	2.9529	12.5	1.7983
15.2	2.9325	13.1	1.7882
10.4	2.8868	4.1	1.7797
7.3	2.8697	5.5	1.7274
4.9	2.8281	15.3	1.7086
35.6	2.7279	13.4	1.7038
22.2	2.6691	3.2	1.6958
5.2	2.6446	22.8	1.6871
19.0	2.6204	9.1	1.6725
4.9	2.6106	9.2	1.6612
8.0	2.5645	3.9	1.6555
35.1	2.5313	3.6	1.6256
35.7	2.4781	12.5	1.5280
12.1	2.4695	8.1	1.3965
98.4	2.4034	7.9	1.3492
4.8	2.3775	12.3	1.2830
5.2	2.3716	5.5	1.2702
38.7	2.3313	4.7	1.2240
7.9	2.3050	3.7	1.1810
19.4	2.2424	5.5	1.1680
7.3	2.2195	5.8	1.1338
44.1	2.2108		

sintered aggregate of iron powder was used as a starting material. They were exactly weighed in the proportion to composition of stoichiometric FeS, and then sealed in the quartz glass-tube under vacuum in 10^{-3} Torr. The tube with the charge was kept 800°C for 3 days after preheating from 450° to 700°C for 3 days and then was cooled in air. By this heating, the starting materials were completely reacted to produce iron sulfide. If the product was heterogeneous or iron metal remained under the microscope, it was necessary to reheat them after thoroughly grinding under acetone and sealing in the evacuated glass-tube. The reheating at 800°C for 2 days was generally enough to produce a homogeneous ferrous sulfide.

The iron sulfide formed is fine grained aggregate of bronze yellow in color with metallic luster. Under the microscope with vertical illuminator, it has pleochroism changing its color from pale brown to yellowish cream. It also shows strong anisotropism changing its interference color from bluish gray to reddish brown under the crossed nicols. Its hardness is medium. These optical properties are in good agreement with those of natural troilite by Ramdohr (1969), Uytenbogaardt & Burke (1971), Picot & Johan (1982), and Spray & Gedlinske (1987).

The data of X-ray powder diffraction by Guinier camera are given in Table 3. Using all the d-spacing values, cell parameters of synthetic troilite were obtained as follows: Hexagonal, a=3.4451 (3)Å, c=5.8802 (8)Å. These data of synthetic troilite correspond to those of a NC type sub-cell of natural troilite described by Berry & Thompson (1962), and JCPDS (1986).

Table 3. The X-ray powder data of synthesized troilite, obtained by Guinier camera

I	h	k	l	d(obs)	d(calc)	Δd
44.4	1	0	0	2.9831	2.9835	-0.0005
8.2	0	0	2	2.9401	2.9401	-0.0001
46.4	1	0	1	2.6603	2.6606	-0.0003
100.0	1	0	2	2.0939	2.0942	-0.0003
31.7	1	1	0	1.7221	1.7225	-0.0004
8.7	0	0	4	1.4697	1.4701	-0.0003
6.1	2	0	1	1.4461	1.4460	0.0001
7.9	2	0	2	1.3301	1.3303	-0.0003
4.8	1	0	4	1.3185	1.3187	-0.0001
8.9	1	1	4	1.1185	1.1182	0.0003

CELL PARAMETERS
a= 3.4451 (3) Å   c= 5.8802 (8) Å

The DTA curve synthetic troilite is shown in Fig. 5. The curve has an intensely endothermic reaction beginning at 140°C and a small endothermic peak at 320°C. The former reaction represents the inversion from hexagonal ordered superlattice to disordered form (1C), and the latter corresponds to Néel point above which arrangement of magnetic spins in sub-lattice becomes disordered.

4.4. Galena (PbS)

Because lead metal is malleable, its block was not able to crush and grind to a small grain. A thin plate of lead which was deformed from original block was cut a small chip with scissors, and its chip was used as a starting materials.

Synthesis of galena was carried out by reaction between lead metal (6N) and sulfur (4N) in the evacuated Pyrex glass-tube.

Lead and sulfur were exactly weighed in the proportion to one to one in atomic ratio, and were sealed in the evacuated Pyrex glass tube at 10^{-3} Torr. The tube with charge was heated at 450° or 500°C for 3 days after preheating at 300°C for a half day below melting point of lead and at 400°C for a day below a boiling point of sulfur. By this heating, lead was completely reacted with sulfur to produce galena. However, if lead still remained or the product was heterogeneous, the charge was reheated after grinding thoroughly under acetone and sealing again in the evacuated glass-tube.

The product synthesized is a fine grained aggregate of lead gray color with metallic luster. Under the microscope, it is white in color with high reflectance and isotropic.

X-ray powder data for synthesized galena, obtained by Guinier camera are given in Table 4. Its cell parameter calculated using all the d-spacing in the table is cubic, a=5.9369(1)Å. This value is in good accordance with that of natural galena by Berry & Thompson (1962) and JCPDS (1986).

Table 4. Guinier camera data of X-ray powder diffraction for synthetic galena

I	h	k	l	d(obs)	d(calc)	Δd
90.9	1	1	1	3.4293	3.4277	0.0016
100.0	2	0	0	2.9692	2.9685	0.0007
86.2	2	2	0	2.0993	2.0990	0.0003
68.2	3	1	1	1.7901	1.7901	0.0001
42.0	2	2	2	1.7138	1.7138	-0.0000
27.7	4	0	0	1.4841	1.4842	-0.0002
31.6	3	3	1	1.3620	1.3620	-0.0000
51.4	4	2	0	1.3274	1.3275	-0.0001
36.7	4	2	2	1.2119	1.2119	0.0000
23.7	3	3	3	1.1426	1.1426	0.0000
~	5	1	1	~	1.1426	0.0000

CELL PARAMETERS
a= 5.9369 (1) Å

4.5. Sphalerite (ZnS)

The reaction between zinc metal and sulfur to produce zinc sulfide is very slow. Therefore, it is necessary to obtain zinc metal of flaky or film-like forms to be reacted more easy. So, a rod-shaped zinc metal formed by melting high-purity (6N) zinc grains in the evacuated quartz glass-tube was shaved by a lathe. Its thin scrap was used as a starting material. Also, drilling scrap of a zinc ingot (4N) was employed. The zinc scrap and sulfur granule were exactly weighed in the

proportion to one to one in atomic ratio, and were sealed in the evacuated quartz glass-tube. The sealed tube with the charge was kept at 700°C for 3 days after rising gradually temperatures from 350° to 650°C for 6 days. By this heating, the charge was completely reacted to form zinc sulfide, sphalerite.

The product synthesized shows macroscopically a white colored flaky form consisting of granular aggregate of sphalerite. Under the microscope on the polished section, it is gray in color and isotropic, but shows an internal reflection. It is transparent in the thin section.

The synthesized product sometimes represents crystal habits as shown in a SEM photomicrograph of Fig. 6-A. The sphalerite crystals consisting of (101) and (001) faces are found in the photomicrograph.
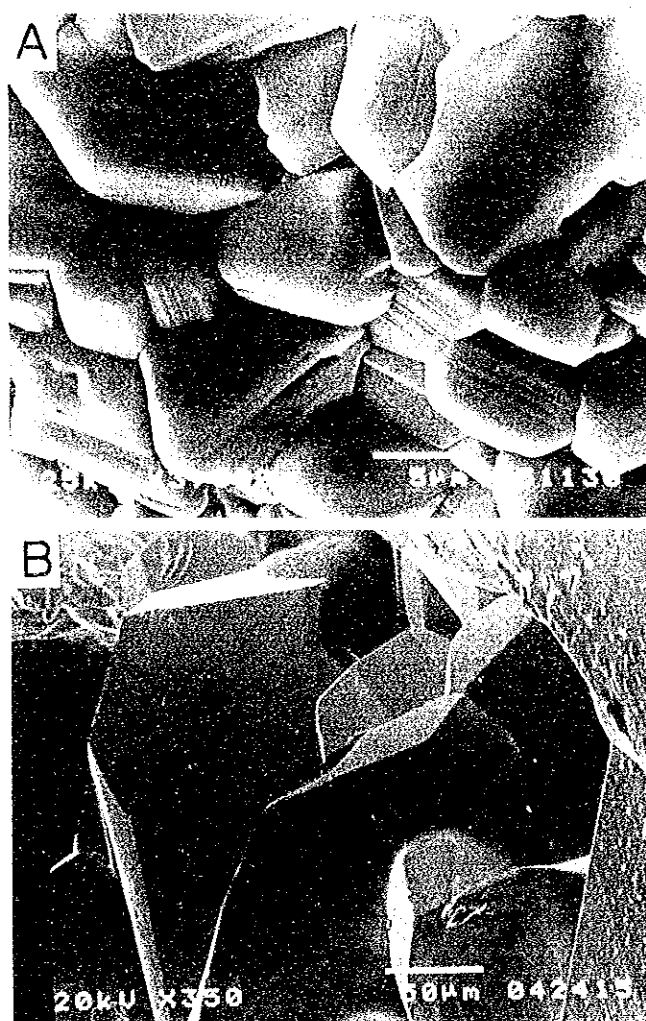
Fig. 6. SEM photomicrographs of synthetic sphalerite (A) and greenockite (B).

44

X-ray powder data of synthetic sphalerite are given in Table 5. Cell parameter obtained from the X-ray powder data is cubic, a=5.4103(2)Å. This value is in good accordance with that of natural sphalerite by Berry & Thompson (1962) and JCPDS (1986).

Table 5.The data of X-ray powder diffraction using Guinier camera for sphalerite synthesized

I	h	k	l	d(obs)	d(calc)	Δ d
100.0	1	1	1	3.1236	3.1236	-0.0000
20.1	2	0	0	2.7050	2.7051	-0.0002
83.8	2	2	0	1.9126	1.9128	-0.0002
65.3	3	1	1	1.6313	1.6313	0.0000
7.3	2	2	2	1.5619	1.5618	0.0001
21.1	4	0	0	1.3524	1.3526	-0.0002
36.9	3	3	1	1.2412	1.2412	0.0000
6.0	4	2	0	1.2097	1.2098	-0.0001
43.4	4	2	2	1.1045	1.1044	0.0001

CELL PARAMETERS
a= 5.4103 (2) Å

4.6. Alabandite (MnS)

Because the reaction between manganese and sulfur is very slow, powdered manganese (4N) was used as a starting material. After manganese and sulfur were weighed in the proportion to one to one in atomic ratio, they were sealed in the evacuated quartz glass-tube. The glass-tube with the charge was kept at 750°C for 10 days after slowly rising the heating temperatures from 350° to 700°C during 9 days, and was cooled in air. The reaction between manganese and sulfur to synthesize alabandite was almost finished, but very small amounts of sulfur remained. The synthesis works of alabandite by this method were difficult because the quartz glass-tube was often cracked and exploded due to difference of expansion coefficient between manganese sulfide and quartz glass besides very slow reaction of them.

The product synthesized is a fine grained aggregate of steel gray in color with submetallic luster macroscopically. Its powder ground shows green color. Under the microscope on the polished section, it is gray, sometimes with greenish internal reflection. It is isotropic.

The data of the X-ray powder diffraction for synthetic alabandite are given in Table 6. Its cell parameter obtained from the powder data is cubic, a=5.2244(2)Å.

45

Table 6.The X-ray powder data of synthetic alabandite, obtained by
Guinier camera.

I	h	k	l	d(obs)	d(calc)	Δd
15.1	1	1	1	3.0165	3.0163	0.0002
100.0	2	0	0	2.6115	2.6122	-0.0007
55.3	2	2	0	1.8468	1.8471	-0.0003
5.0	3	1	1	1.5755	1.5752	0.0003
21.7	2	2	2	1.5084	1.5082	0.0002
9.8	4	0	0	1.3061	1.3061	0.0000
22.6	4	2	0	1.1681	1.1682	-0.0001

CELL PARAMETERS
a= 5.2244 (2) Å

4.7. Greenockite (CdS)

The reaction between cadmium metal and sulfur to produce greenockite is not so easy similar to that of zinc and manganese with sulfur as mentioned above. Thus, flaky cadmium metal (3N) was chosen. It was cut a small chip with scissors to use as a starting material. Cadmium and sulfur were sealed in the evacuated quartz glass-tube after they were exactly weighed by chemical balance in the proportion to one to one in atomic ratio. Then, the quartz glass-tube with starting materials was kept at 800°C for 4 days and then at 900°C for 3 days after very slowly rising the heating temperatures from 500° to 750°C for 25 days. By this heating during a long time more than a month, the reaction to form greenockite was completely done.

The product is granular aggregate of orange yellow color with resinous luster. Many crystals occur. Under the reflecting microscope, it is gray in color with yellow internal reflection. A SEM photomicrograph of greenockite crystals produced is shown in Fig. 6-B. The crystals consist of (001), (100) and (503) faces.

The X-ray powder data for synthetic greenockite are given in Table 7. Its cell constants obtained from these data are hexagonal, a=4.1371(1)Å and c=6.7161(2)Å.

4.8. Argentite (Ag₂S)

Synthesis of argentite was carried out by the reaction between silver metal and sulfur in the evacuated glass-tube. A granule of silver (5N) was use as starting material. Silver and sulfur were sealed in the evacuated Pyrex glass-tube at 10^{-3} Torr after they were exactly weighed in the proportion to two silver and one sulfur in atomic ratio. Then, the sealed tube with the charge was kept at 500°C for 3 days after preheating at 400°C for a day. The reaction between them to form argentite was fast, and was completely finished by this heating.

Table 7. The data of the X-ray powder diffraction using Guinier camera
for synthetic greenockite

I	h	k	l	d(obs)	d(calc)	Δd
69.5	1	0	0	3.5830	3.5828	0.0002
75.0	0	0	2	3.3576	3.3581	-0.0005
100.0	1	0	1	3.1610	3.1611	-0.0001
40.6	1	0	2	2.4496	2.4501	-0.0005
53.3	1	1	0	2.0682	2.0685	-0.0003
69.5	1	0	3	1.8986	1.8986	0.0001
10.7	2	0	0	1.7914	1.7914	0.0000
43.0	1	1	2	1.7613	1.7612	0.0001
23.4	2	0	1	1.7308	1.7309	-0.0001
8.5	0	0	4	1.6792	1.6790	0.0001
8.1	2	0	2	1.5806	1.5806	-0.0000
6.2	1	0	4	1.5203	1.5204	-0.0001
20.4	2	0	3	1.3985	1.3987	-0.0002
11.3	2	1	0	1.3543	1.3542	0.0001
15.0	2	1	1	1.3274	1.3275	-0.0000
8.2	1	1	4	1.3036	1.3036	-0.0000
21.6	1	0	5	1.2578	1.2577	0.0000
7.7	2	1	2	1.2558	1.2559	-0.0001
9.0	3	0	0	1.1943	1.1943	0.0000
15.1	2	1	3	1.1588	1.1587	0.0001
8.3	3	0	2	1.1252	1.1252	-0.0000

CELL PARAMETERS
a= 4.1371 (1) Å   c= 6.7161 (2) Å

The product is a massive form of dark lead-gray in color with metallic luster macroscopically. Under the ore microscope, it is light gray with a greenish shade, and shows very weak pleochroism. It is difficult to polish because of its softness. Its anisotropism is distinctly visible though weak, because argentite inverted to arcanthite below 173°C during cooling.

Synthetic argentite sometimes shows its crystal form with (100), (110) and (111). As shown in a SEM photomicrograph of Fig. 7-A, long prismatic or needle-like crystals of argentite elongate to direction of perpendicular to (111), namely parallel to (110). Dendrite is also observed.

X-ray powder diffraction data were not able to obtain because argentite is malleable and cannot powder.

4.9. Stibnite (Sb$_2$S$_3$)

Stibnite was synthesized by reaction between antimony metal and sulfur in the evacuated glass-tube. As a starting material, small fragment and piece crushed a block of antimony metal (6N) were used. Antimony and sulfur were exactly
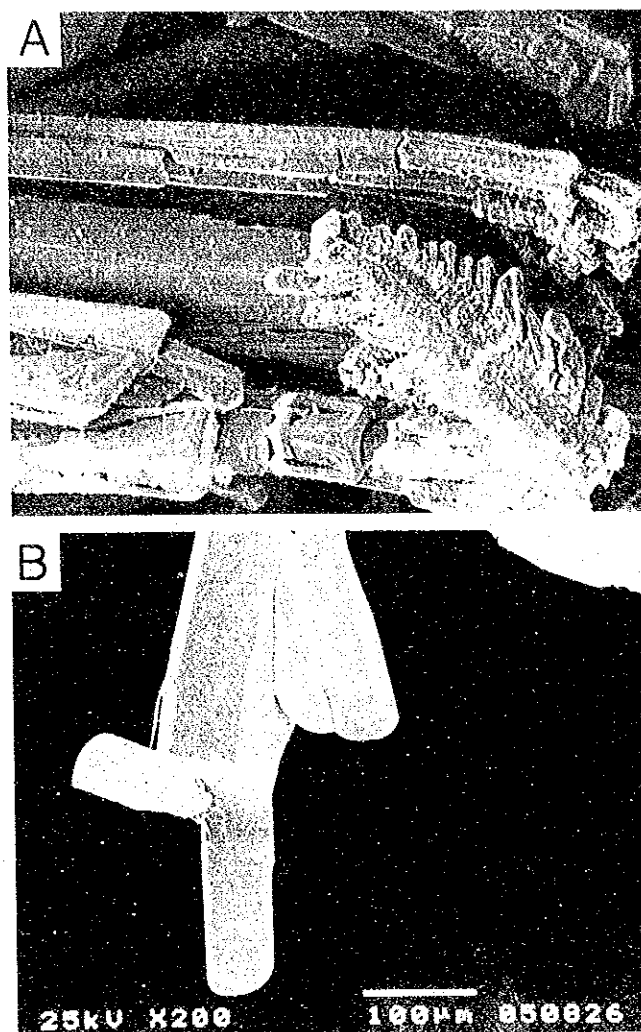
Fig. 7.   Photomicrographs by SEM for synthetic argentite (A)
and stibnite (B).

weighed in the proportion to two antimony and three sulfur in atomic ratio, and were sealed in the Pyrex glass-tube under vacuum of 10^{-3} Torr. The sealed glass-tube with the charge was heated at 400° to 450°C for 12 hours to a day, at 500°C for 1 to 3 days, at 550°C for a day, and finally at 600°C for 5 hours to a day (and at 550°C for a day) in this order, and then was cooled in air. The charge melted completely at 600°C and sulfur disappeared entirely, though small amounts of sulfur still remained at 500°C. By this heating process, the reaction of metal and sulfur was completely finished.

The product is composed of radially fibrous aggregates and melted mass of

silver-white in color. Under the microscope, it is aggregate of long prismatic and needle-like crystals, and shows distinct pleochroism from grayish white to grayish brown. It also has strong anisotropism changing its colors from dark brown to bluish gray under the crossed nicols, and shows twinning. These optical properties agree with those of natural stibnite described by Ramdohr (1969), Uytenbogaadt & Burke (1971), Picot & Johan (1982), and Spray & Gedlinske (1987).

A SEM photomicrograph of synthetic crystal is shown in Fig. 7-B. As seen in the photograph, the prismatic crystal elongates to parallel to the c-axis direction, and consists of the (110) and (010) faces.

The data of the X-ray powder diffraction by Guinier camera for synthetic stibnite are given in Table 8. Cell parameters of synthetic stibnite calculated using the data are orthorhombic, a=11.2337(7) Å, b=11.3123(7) Å and c=3.8387(3) Å. These data of synthetic stibnite are in good accordance with those of natural stibnite by Berry & Thompson (1962) and JCPDS (1986).

The DTA curve of synthetic stibnite is shown in Fig. 8. The curve indicates only a distinct endothermic reaction beginning at 553°C which represents the latent heat of its congruent melting.

4.10. Bismuthinite (Bi_2S_3)

Bismuthinite was able to be synthesized in a relatively easy way by the reaction between bismuth metal and sulfur in the evacuated glass-tube. A small fragment and piece of bismuth metal and sulfur were sealed in the evacuated Pyrex glass-tube after weighed exactly in the proportion to two bismuth and three sulfur in atomic ratio. The charge in the glass-tube was kept at 550°C for 3 days after preheated at 250°C for 12 hours and then at 450°C for a day. It was better to heat first at temperatures below melting point (273°C) of bismuth, because the reaction of bismuth liquid and sulfur is sometimes not easy. By the heating as above, the charge was completely changed to bismuthinite.

The product is massive and granular aggregate of lead-gray in color. Under the ore microscope, it is aggregate of granular and blade-like crystal. It shows distinct pleochroism changing its colors from creamy white to purplish gray, and has also strong anisotropism changing from pale brownish gray to dark violet with inclined extinction under the crossed nicols. These optical properties are in good agreement with those of natural bismuthinite described by Ramdohr (1969), Uytenbogaadt & Burke (1971), Picot & Johan (1982) and Spray & Gedlinske (1987).

The X-ray powder data of synthetic bismuthinite by Guinier camera are given in Table 9. Its cell parameters obtained from these data are orthorhombic, a=11.1491(6) Å, b=11.3024(7) Å and c=3.9812(2) Å. These data agree well with those of natural bismuthinite described by Berry & Thompson (1962) and JCPDS (1986).

Table 8. The X-ray powder data of synthetic stibnite by Guinier camera

I	h	k	l	d(obs)	d(calc)	Δ d
6.8	1	1	0	7.9783	7.9715	0.0068
18.4	0	2	0	5.6615	5.6562	0.0054
8.7	2	0	0	5.6164	5.6174	-0.0010
33.3	1	2	0	5.0529	5.0520	0.0009
20.9	2	2	0	3.9860	3.9857	0.0002
22.6	1	0	1	3.6317	3.6325	-0.0008
39.7	1	3	0	3.5761	3.5748	0.0013
66.1	3	1	0	3.5541	3.5552	-0.0011
31.2	1	1	1	3.4592	3.4586	0.0006
10.1	0	2	1	3.1785	3.1763	0.0022
9.4	3	2	0	3.1228	3.1225	0.0002
100.0	2	1	1	3.0541	3.0518	0.0023
81.6	2	2	1	2.7653	2.7649	0.0005
6.0	4	1	0	2.7261	2.7259	0.0001
58.1	3	0	1	2.6811	2.6806	0.0005
27.7	3	1	1	2.6093	2.6084	0.0010
33.1	2	4	0	2.5275	2.5260	0.0014
16.7	4	2	0	2.5162	2.5156	0.0005
17.9	2	3	1	2.4264	2.4262	0.0002
18.2	0	4	1	2.2782	2.2769	0.0013
3.2	3	4	0	2.2579	2.2569	0.0010
7.3	4	3	0	2.2538	2.2525	0.0013
20.5	1	4	1	2.2320	2.2315	0.0005
14.2	4	1	1	2.2232	2.2226	0.0006
5.9	5	1	0	2.2034	2.2039	-0.0005
2.8	3	3	1	2.1845	2.1848	-0.0003
21.0	4	2	1	2.1046	2.1041	0.0006
13.7	2	5	0	2.0995	2.0987	0.0009
13.0	5	2	0	2.0883	2.0882	0.0001
6.9	4	4	0	1.9933	1.9929	0.0004
35.5	4	3	1	1.9434	1.9427	0.0007
40.4	5	0	1	1.9397	1.9392	0.0005
14.9	5	3	0	1.9306	1.9303	0.0004
3.8	0	6	0	1.8857	1.8854	0.0003
8.4	6	0	0	1.8726	1.8725	0.0001
9.5	6	1	0	1.8474	1.8473	0.0000
5.1	0	2	2	1.8176	1.8175	0.0000
7.9	1	2	2	1.7944	1.7942	0.0002
5.2	6	2	0	1.7776	1.7776	0.0000
4.5	5	4	0	1.7595	1.7593	0.0002
20.5	3	5	1	1.7288	1.7290	-0.0001
10.9	5	3	1	1.7244	1.7245	-0.0001
25.4	0	6	1	1.6920	1.6923	-0.0003
24.5	3	1	2	1.6889	1.6889	-0.0001
6.0	3	6	0	1.6839	1.6840	-0.0001
2.6	6	1	1	1.6642	1.6646	-0.0004
14.1	7	2	0	1.5437	1.5440	-0.0003
14.8	2	4	2	1.5282	1.5282	-0.0000
5.8	4	2	2	1.5257	1.5259	-0.0002
4.3	3	7	0	1.4837	1.4838	-0.0001
2.6	1	7	1	1.4763	1.4765	-0.0002
4.9	4	3	2	1.4608	1.4609	-0.0002
4.7	5	6	0	1.4440	1.4443	-0.0003

CELL PARAMETERS

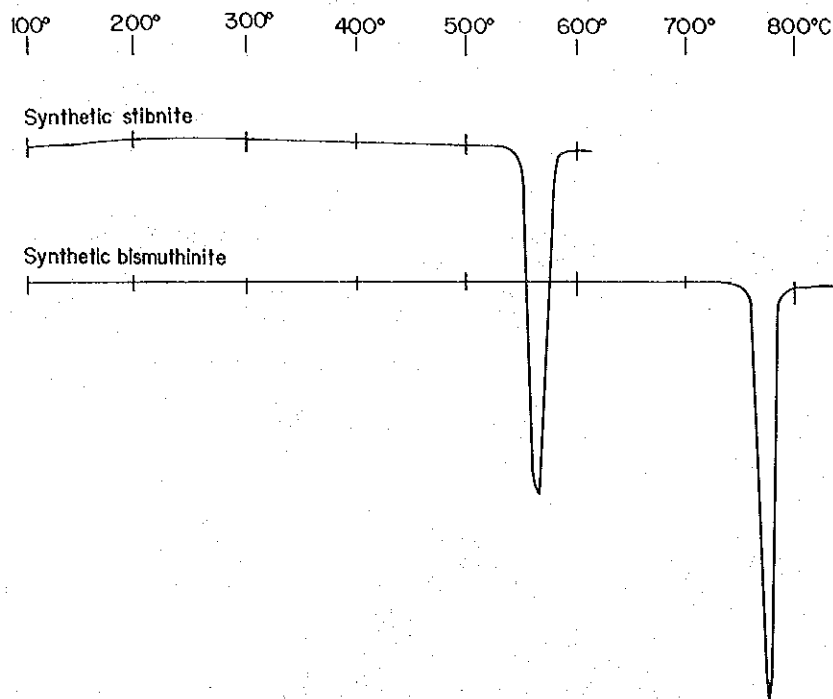   a= 11.2337 (7) Å   b= 11.3123 (7) Å   c= 3.8387 (3) Å

50

Fig. 8. The DTA curves of synthesized stibnite and bismuthinite.

The DTA curve of synthetic bismuthinite is shown in Fig. 8. It represents an intensely endothermic reaction beginning at 761°C, corresponding to the congruent melting (760°C) of bismuthinite.

5. Summary

Simple sulfide minerals such as covellite, chalcocite, troilite, galena, sphalerite, alabandite, greenockite, argentite, stibnite and bismuthinite were synthesized by the reaction between metals and sulfur in the evacuated glass-tube. Among them, covellite, chalcocite, galena, argentite, stibnite and bismuthinite were artificially produced at comparatively lower temperatures than 600°C, while troilite, sphalerite, alabandite and greenockite were formed at higher temperatures than 600°C, for example, sphalerite at 700°C, alabandite at 750°C, troilite at 800°C and greenockite at 800° to 900°C. In the latter case, the quartz glass-tube had to be used as a reaction vessel, meanwhile in the former the Pyrex glass-tube was very useful without trouble.

In the case that the reaction between starting materials is very slow, it was important that a shape of metal as to be apt to react with sulfur has to be devised, for example, powder, granule, piece, scrap, foliation and film.

Table 9. The data of the X-ray powder diffraction for synthetic bismuthinite by Guinier camera

I	h	k	l	d(obs)	d(calc)	Δd	I	h	k	l	d(obs)	d(calc)	Δd
16.5	0	2	0	5.6534	5.6512	0.0022	13.6	2	5	1	1.8533	1.8539	-0.0005
9.8	0	2	0	5.5776	5.5745	0.0030	10.3	6	1	1	1.8340	1.8336	0.0004
20.3	1	2	0	5.0413	5.0407	0.0006	17.6	2	2	2	1.7794	1.7793	0.0000
9.9	2	1	0	4.9998	4.9995	0.0003	7.8	6	2	0	1.7652	1.7652	0.0000
43.2	2	2	0	3.9701	3.9686	0.0015	5.1	5	4	0	1.7505	1.7504	0.0001
35.9	1	0	0	3.7514	3.7494	0.0020	44.0	4	4	2	1.7384	1.7385	-0.0001
78.8	1	3	0	3.5673	3.5692	-0.0019	36.4	3	1	2	1.7340	1.7340	0.0000
73.0	3	1	0	3.5331	3.5304	0.0027	6.3	5	3	1	1.7284	1.7286	-0.0001
26.4	0	2	1	3.2560	3.2547	0.0013	10.2	0	6	1	1.7028	1.7028	0.0000
100.0	2	1	0	3.1181	3.1144	0.0037	3.3	5	1	1	1.6833	1.6832	0.0000
80.0	2	2	1	2.8123	2.8107	0.0016	5.4	2	6	2	1.6790	1.6784	0.0007
49.3	3	0	1	2.7180	2.7167	0.0013	7.0	3	2	2	1.6759	1.6758	0.0000
9.7	4	1	0	2.7069	2.7062	0.0007	6.7	6	1	1	1.6654	1.6654	0.0001
37.2	3	1	0	2.6431	2.6415	0.0017	4.6	2	4	2	1.6035	1.6035	-0.0001
35.4	2	4	0	2.5217	2.5203	0.0014	21.3	4	2	2	1.5620	1.5621	-0.0001
17.6	4	2	0	2.5009	2.4998	0.0011	9.3	6	4	0	1.5572	1.5572	0.0000
18.4	2	3	1	2.4576	2.4565	0.0011	5.5	4	3	2	1.5523	1.5526	-0.0003
21.7	0	4	1	2.3053	2.3043	0.0008	4.8	6	3	0	1.5479	1.5480	-0.0001
34.3	1	4	1	2.2574	2.2566	0.0008	4.5	3	2	1	1.5372	1.5373	-0.0001
5.0	3	4	0	2.2495	2.2493	0.0002	13.0	7	4	0	1.5328	1.5330	-0.0002
24.1	4	3	0	2.2393	2.2407	-0.0014	3.3	3	4	2	1.4906	1.4907	-0.0001
2.6	3	3	1	2.2041	2.2035	0.0006	2.3	4	3	1	1.4881	1.4882	-0.0001
5.7	5	1	0	2.1887	2.1877	0.0010	7.9	1	7	1	1.4827	1.4830	-0.0003
7.9	2	4	1	2.1303	2.1295	0.0008	9.2	5	5	2	1.4807	1.4807	0.0000
21.3	4	2	1	2.1176	2.1170	0.0005	3.4	6	1	2	1.4722	1.4723	-0.0001
8.6	2	5	0	2.0953	2.0948	0.0007	5.8	2	7	1	1.4455	1.4451	0.0003
14.8	5	2	0	2.0749	2.0742	0.0005	6.5	5	5	2	1.4432	1.4430	0.0002
53.2	0	0	2	1.9911	1.9906	0.0005	10.5	7	2	0	1.4360	1.4362	-0.0003
60.8	4	3	1	1.9532	1.9527	0.0005	21.0	4	4	2	1.4305	1.4306	-0.0001
43.8	5	0	1	1.9458	1.9455	0.0003	5.8	4	5	2	1.4052	1.4053	-0.0003
10.1	1	1	1	1.9362	1.9359	0.0003	4.4	3	3	2	1.3969	1.3971	-0.0002
9.6	3	5	0	1.9313	1.9313	0.0000	8.3	5	6	0	1.3860	1.3861	-0.0001
11.7	0	6	0	1.8839	1.8837	0.0002	17.3	3	3	2	1.3815	1.3815	0.0000
6.1	0	2	2	1.8772	1.8775	-0.0003	9.5	0	6	2	1.3682	1.3682	-0.0002
14.7	6	2	0	1.8582	1.8582	0.0000							

CELL PARAMETERS

a= 11.1491 (6) Å   b= 11.3024 (7) Å   c= 3.9812 (2) Å

In the case using such metals with a low melting point as bismuth, lead and zinc it was necessary to preheat at lower temperatures than the melting point of the metals for some time, a half to a day, because metal liquid was accumulated in the bottom of the glass-tube and the reaction with sulfur was not carried out completely.

In general, the reaction between metal and sulfur was done at temperature below a melting point of sulfide minerals which are synthesized, because a part of sulfur vaporized and the product often was heterogeneous when melted. However, in the case of synthesis of stibnite, the product was melted at 600°C because sulfur still remained at 500°C and as results, sulfur entirely disappeared and homogeneous stibnite was able to obtain.

Synthesis of manganese sulfide, alabandite, was one of difficulty because the quartz glass-tube was often cracked due to difference of expansion coefficients of manganese sulfide and quartz glass, and direct reaction between manganese metal and quartz glass at high temperature, in addition to very slow reaction between them.

All the products synthesized were cooled in air after a finish of synthetic experiments. The synthesized sulfides become a stable form at room temperature after cooling notwithstanding that such minerals as chalcocite and argentite were high forms when synthesized. However, in the case of troilite, the change to a stable low form (2C type) by air cooling was incomplete. So, it was necessary to anneal at temperatures below its inversion point (137°C) to obtain the low form. Thus, the X-ray powder data of synthesized troilite given in Table 3 correspond to those of a metastable phase.

The optical properties of synthetic products were in good accordance with those of natural minerals. Especially, it is significant to have been able to synthesize greenockite with a crystal form which is very rare in nature.

The data of X-ray powder diffraction by Guinier camera for synthetic sulfide minerals agreed well with those of natural minerals except those of synthetic troilite of which the data indicate its metastable phase (NC type).

Thermal properties of some synthetic minerals as covellite, chalcocite, troilite, stibnite and bismuthinite were entirely the same as those of natural minerals.

The sulfide minerals synthesized by reaction between metal and sulfur in the evacuated glass-tube are a high purity with a stoichiometric composition. Therefore, they thoroughly can be used as the standard materials of the electron probe microanalyser, X-ray diffraction, fluorescence X-ray analysis, and reflectance of ore microscopy, etc. Also, these simple sulfides synthesized can fully be used as starting material of the investigations on the ternary, quaternary and polycomponent sulfide systems. Indeed, chalcopyrite ($CuFeS_2$), bornite (Cu_5FeS_4) and nukundamite ($Cu_{3.39}Fe_{0.61}S_4$) in the Cu-Fe-S system, enargite (Cu_3AsS_4) in the Cu-As-S system and famatinite (Cu_3SbS_4) in the Cu-Sb-S system were

synthesized by using of CuS, Cu_2S and FeS, CuS and AsS, and CuS, Cu_2S and Sb_2S_3, respectively, as the starting materials.

Acknowledgments

References

Berry, L.G. & Thompson, R.M. (1962), *X-ray Powder Data for Ore Minerals*. Geol. Soc. Amer., Memoir 85, Nos. 45, 63, 83, 93, 110, 111.

JCPDS (1986), *Mineral Diffraction File*. Data Book. Int. Nat. Center for Diffraction Data. Swarthmore, Pa., U.S.A., 126, 1099, 1114.

Kitakaze, A. (1992), Guinier film reading and calculation system. In *Textbook for Instrumental Analyses on Economic Geology and Related Sciences*, ed. A. Sugaki, No. 2, JICA, 47-72.

Kullerud, G. (1971), Experimental techniques in dry sulfide research. In *Research Techniques for High Pressure and High Temperature*, ed. G.C. Ulmer, Springer, New York, 288-315.

Picot, P. & Johan, Z. (1982), *Atlas of Ore Minerals*, B.R.G.M., Orleans-Elsevier, Amsterdam, 92, 116, 132, 172, 315, 353.

Ramdohr, P. (1969), *The Ore Minerals and Their Intergrowths*. Pergamon Press, Oxford, 438, 582, 634,665, 698.

Scott, S.D. (1974), Experimental methods in sulfide synthesis. In *Sulfide Mineralogy*, ed. P.H. Ribbe, Miner. Soc. Amer. Short Course Notes, 1, S1-S38.

Spry, P.G. & Gedlinske, B.L. (1987), *Tables for the Determination of Common Opaque Minerals*. Economic Geology, Pub. Co., New Haven, 1, 6, 18, 38, 42, 50.

Sugaki, A. (1991), Differential thermal analysis. In *Textbook for Instrumental Analyses in Economic Geology and Related Sciences*, ed. A. Sugaki, No. 1, JICA, 30-60.

Sugaki, A. (1992), Synthetic method of sulfide minerals -Evacuated glass-tube method. In *Textbook for Instrumental Analyses on Economic Geology and Related Sciences*, ed. A. Sugaki, JICA, No. 2, 73-105.

Sugaki, A. & Shima, H. (1965a), Synthetic sulfide minerals (I). *Mem. Fac. Eng. Yamaguchi Univ.*, 15, 15-31.

Sugaki, A. & Shima, H. (1965b), Synthetic sulfide minerals (II). *Mem. Fac. Eng. Yamaguchi Univ.*, 15, 33-47.

Uytenbogaadt, W. & Burke, E.A.J. (1971), *Tables for Microscopic Identification of Ore Minerals*. Elsevier, Amsterdam, 42, 54, 58, 64, 66, 138.

Vaughan, D.J. & Craig, J.R. (1978), *Mineral Chemistry of Metal Sulfides*. Cambridge Univ. Press, Cambridge, 284-272.

PETROGRAPHY, PETROCHEMISTRY AND K-Ar DATING OF NEOGENE VOLCANIC ROCKS IN ANTUCO, SOUTHERN CHILE

Hirotsugu Nishido*, Masahiko Yamamoto** and José Frutos***
*Hiruzen Research Institute, Okayama University of Science, Kawakami, Okayama 717-06, Japan. **Institute of Earth Sciences, Faculty of Science, Kagoshima University, Kagoshima 890, Japan. ***Programa de Geología Económica Aplicada, Universidad de Concepción, Concepción 3, Chile.

Abstract

Volcanic and volcani-sedimentary rocks of Neogene age in Antuco, southern Chile were petrologically studied. They are accompanied with granitic intrusive bodies of Miocene age. The volcanic rocks are composed of an olivine basalt to an andesite. The volcanic rocks of pre-intrusion of granitic rocks contain tholeiites in composition, and those of post-intrusion of granitic rocks are mainly composed of calc-alkaline rocks. The calc-alkaline rocks show a regular compositional variation, and the basaltic rocks in them are compositionally similar to the Recent Antuco lavas. The K-Ar ages indicate that the tholeiitic rocks of pre-granite were formed during the Middle Miocene time and the calc-alkaline rocks of post-granite were formed during Pliocene time.

Introduction

Large amounts of volcanic and volcani-sedimentary rocks of Neogene age are zonally distributed in the coastal area of western side of Andes in Chile. Studies on these rocks are important to know historical evolution of volcanic activities in Andes ranging in age from Neogene to Recent, however, there are little petrological data on them. The present paper presents the results of petrographical, petrochemical and K-Ar dating studies of volcanic rock samples collected from outcrops in the Antuco area, southern Chile.

Geological Setting

Volcanic and volcani-sedimentary rocks are widely distributed in the Antuco area, southern Chile. A geologic map compiled from Instituto de Investigaciones Geológicas (1980a, b) is shown in Fig. 1. Strata composed of volcanic and volcani-sedimentary rocks in this area can be stratigraphically divided into two formations: one formation is unconformably underlain by the Cretaceous to Paleogene terruginous rocks and intruded by the Miocene granitic intrusives (Nishido *et al.*, in press); and the other formation covers pre-granite strata and the granitic intrusives and is unconformably overlain by the Quaternary volcanics. There are also many dikes which intrude the formation of pre-granite in this area.
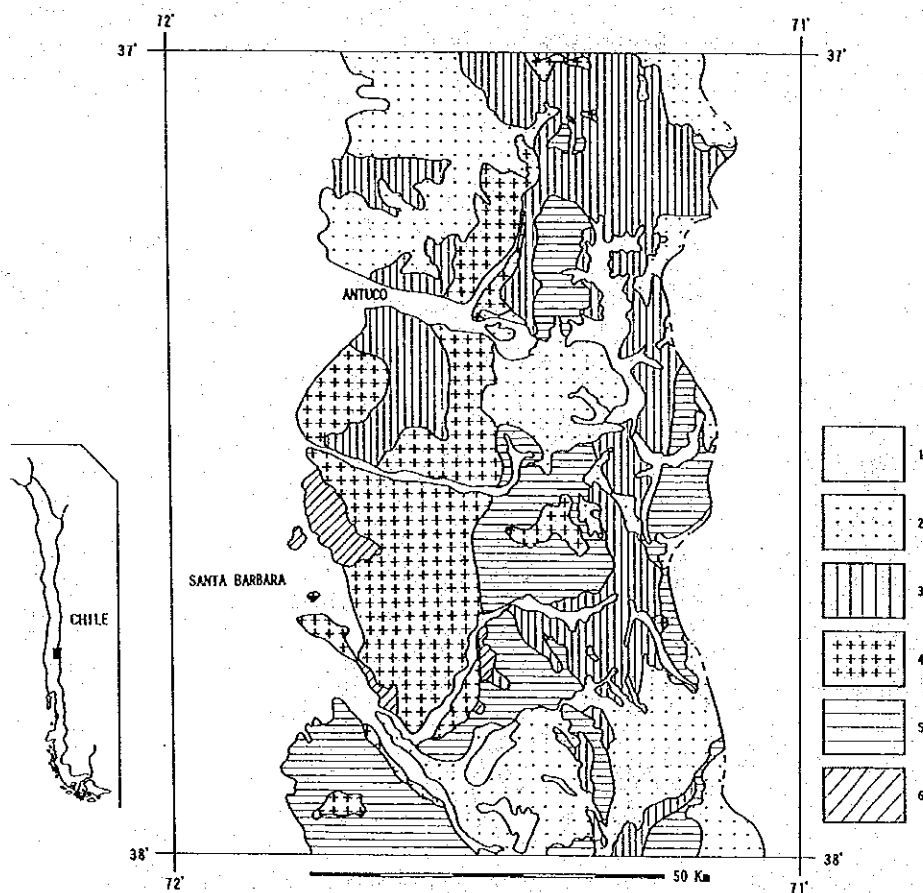
Fig. 1. Index and geologic maps of the Antuco area.
The geologic map is compiled from Instituto de Investigaciones Geológicas (1980a, b).
Stratigraphic sequences: 1. Alluvial deposits, 2. Quaternary volcanics, 3. Pliocene volcanics, 4. Miocene granitic intrusives, 5. Miocene volcanics, 6. Cretaceous to Paleogene strata.

Two rock samples of lavas were collected from the formation of pre-granite, and four rock samples of lavas and welded tuff were also collected from the formation of post-granite. Additionally, one rock sample was collected from a dike which intrudes the formation of pre-granite. The rock samples collected from outcrops in the Antuco area are listed in Table 1.

Table 1. Rock samples collected from the Neogene volcanic rocks in the Antuco area

No.	Sp. No.	Latitude (S)	Longitude (W)	Altitude (m)	Rock	Remarks
			(a) Pliocene Rocks			
1	9210703	37° 22' 45"	71° 22' 38"	1410	Welded Tuff	
2	9210608	37° 22' 32"	71° 22' 24"	1410	Altered Andesite	Dike
3	9210701	37° 22' 32"	71° 22' 26"	1410	Ol Basalt	Lava
4	9210607	37° 22' 29"	71° 22' 22"	1410	Ol Basalt	Lava
5	9210609	37° 22' 34"	71° 22' 28"	1410	Andesite	Lava
			(b) Miocene Rocks			
6	9210708	37° 20' 18"	71° 36' 14"	700	Ol Basalt	Lava
7	9210709	37° 20' 18"	71° 36' 14"	700	Ol Basalt	Lava

Petrography

The rock samples collected from the Antuco area were petrographically studied under a petrographic microscope. The rock samples collected from the formation of pre-granite are composed of an olivine basalt, and those collected from the formation of post-granite are composed of an olivine basalt, an andesite and a welded tuff.

The olivine basalt of pre-granite is a pale greenish dark-colored rock, and is composed of large amounts of phenocrysts of olivine and a trachytic textured groundmass. Olivine occurs as euhedral to subhedral grains up to 2.5 mm in size, but is mostly altered to an assemblage of serpentine, chlorite and iddingsite. Large amounts of euhedral plagioclase laths up to 0.3 mm in size and euhedral to subhedral clinopyroxene grains up to 0.9 mm in size are commonly found as microphenocrysts. Clinopyroxene is commonly crystallized around the olivine phenocrysts. A glomeroporphyritic aggregate of clinopyroxene grains is sometimes found. A Small amount of euhedral to subhedral orthopyroxene grain up to 0.3 mm in size is also found as a microphenocryst. The groundmass is composed of microlites of plagioclase, clinopyroxene and orthopyroxene and a large amount of volcanic glass. The volcanic glass is slightly altered. Apatite, titaniferrous magnetite and ilmenite are contained as accessories.

The olivine basalt of post-granite is a pale greenish dark-colored rock, and is composed of large amounts of phenocrysts of olivine, small amounts of phenocrysts of plagioclase and clinopyroxene and a trachytic textured groundmass. Olivine occurs as euhedral to subhedral grains up to 3 mm in size, but is mostly altered to an assemblage of serpentine, chlorite and green mica. Both plagioclase and clinopyroxene occur as euhedral crystals up to 1.5 mm in size. A small amount of euhedral orthopyroxene garin up to 0.6 mm in size is commonly found as a microphenocryst. The groundmass is composed of microlites of plagioclase, clinopyroxene and orthopyroxene and a large amount of volcanic glass. The volcanic glass is commonly altered. Apatite, titaniferrous magnetite and ilmenite are contained as accessories.

The andesite of post-granite is a dark brown-colored rock, and is composed of large amounts of phenocrysts of plagioclase and clinopyroxene, small amounts of phenocrysts of orthopyroxene and an intersertal textured groundmass. Plagioclase occurs as euhedral crystals up to 6 mm in size. Both clinopyroxene and orthopyroxene occur as euhedral crystals up to 1.5 mm in size. The groundmass is composed of microlites of plagioclase, clinopyroxene and orthopyroxene and a small amount of volcanic glass. The volcanic glass is commonly devitrified. Apatite, titaniferrous magnetite and ilmenite are contained as accessories.

The welded tuff of post-granite is a brown-colored rock and mainly composed of phenocrysts of plagioclase, quartz and hornblende.

The andesite collected from the dike wich intrudes the formation of pre-granite is a porous greenish gray-colored rock, and is composed of small amounts of phenocrysts of plagioclase and pseudomorphs of olivine and a hyalopilite textured groundmass. Plagioclase occurs as euhedral crystals up to 3 mm in size. The olivine pseudomorph occurs as euhedral to subhedral form up to 1.5 mm in size, and is composed of an assemblage of alteration minerals such as serpentine, chlorite, green mica, sphene and iddingsite. Trace amounts of both clinopyroxene and orthopyroxene grains up to 0.3 mm in size occur as microphenocrysts. The groundmass is composed of microlites of plagioclase and a large amount of volcanic glass. The volcanic glass is strongly altered, and spotted albitic plagioclase is commonly found in the groundmass as a secondary mineral. Druzy calcite, quartz and some zeolite minerals are also found.

Petrochemistry

The rock samples collected from the Antuco area were chemically analyzed with the Rigaku XRF Spectrometer 3070-E. Chemical compositions analyzed and CIPW norms calculated are listed in Table 1, and the variation diagram is shown in Fig. 2. CO_2 contents were measured with a CHN analyzer of Okayama University of Science, but were not used for norm calculations.

The SiO_2 content of rocks from the formation of pre-granite is about 50 wt. % and their compositions are basaltic. They are rich in MgO and poor in Al_2O_3 and Na_2O. Normative Q is calcultated.

The SiO_2 content of rocks from the formation of post-granite ranges from 47 wt. % to 69 wt. %, and their compositions are basaltic to dacitic. As seen in Fig. 2, they show a regular compositional variation. Normative Q is calculated in all analyzed rocks. Normative C is calculated only in the dacitic welded tuff No. 9210703, but normative Di is calculated in other rocks.

The SiO_2 content of the andesite dike is 62.5 wt. % and its composition is andesitic. It is rich in Al_2O_3 and Na_2O, because secondary spotted albitic plagioclase is contained in its groundmass. Normative Q is also calculated.

Figure 3 shows the FAM diagram of analyzed rocks. In Fig. 3, a solid line represents the boundary curve between calc-alkaline and tholeiitic rock series

Table 2. Chemical analyses and CIPW norms of Neogene volcanic rocks

No.	1	2	3	4	5	6	7
Sp. No.	9210703	9210608	9210701	9210607	9210609	9210708	9210709
SiO_2	68.56	62.54	46.96	49.39	54.90	49.87	50.98
TiO_2	0.49	0.48	0.92	0.91	1.47	0.49	0.50
Al_2O_3	15.71	17.25	15.43	19.84	16.17	12.76	13.17
Fe_2O_3	1.90	1.90	4.96	4.87	4.16	3.53	3.68
FeO	1.36	2.65	3.18	3.69	3.89	4.29	4.19
MnO	0.06	0.09	0.13	0.16	0.13	0.14	0.13
MgO	0.40	0.83	7.86	4.24	3.80	13.35	12.08
CaO	3.18	3.80	9.26	10.75	7.21	10.23	9.94
Na_2O	4.32	5.22	2.33	2.54	3.78	1.30	1.49
K_2O	2.63	2.65	0.63	0.33	1.82	0.21	0.55
H_2O^+	1.05	1.52	3.91	1.99	1.39	3.73	3.16
H_2O^-	0.44	0.49	4.33	1.29	1.42	0.52	0.67
P_2O_5	0.10	0.16	0.12	0.11	0.35	0.09	0.09
CO_2	nd.	0.69	0.37	0.30	0.04	nd.	0.06
Total	100.20	100.27	100.39	100.41	100.53	100.51	100.69
Q	26.13	12.32	2.88	5.94	7.65	2.63	3.86
Or	15.54	15.66	3.72	1.95	10.76	1.24	3.25
Ab	36.56	44.17	19.72	21.49	31.99	11.00	12.61
An	15.12	15.81	29.78	41.76	21.78	28.36	27.62
C	0.21	-	-	-	-	-	-
DI	-	1.66	12.00	8.57	9.25	17.20	16.64
Wo	-	0.83	6.42	4.53	4.89	9.10	8.81
En	-	0.36	5.45	3.52	3.76	7.15	6.90
Fs	-	0.47	0.13	0.52	0.60	0.95	0.93
Hy	1.23	3.90	14.47	8.07	6.62	29.56	26.32
En	1.00	1.70	14.13	7.04	5.70	26.10	23.18
Fs	0.23	2.20	0.34	1.03	0.92	3.46	3.14
II	0.93	0.91	1.75	1.73	2.79	0.93	0.95
Mt	2.75	2.75	7.19	7.06	6.03	5.12	5.34
Ap	0.23	0.37	0.28	0.25	0.81	0.21	0.21

CO_2 was not used for norm calculaytions.
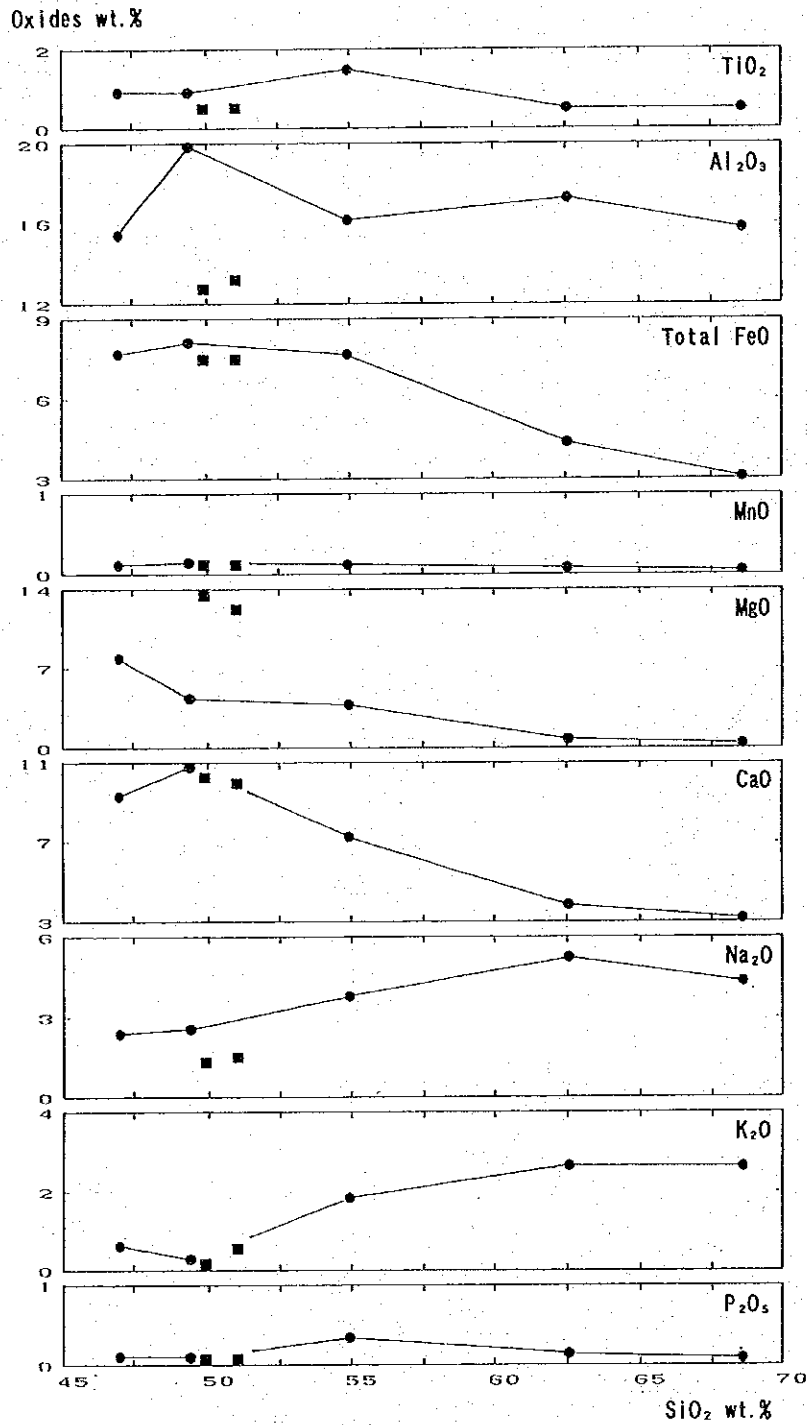
Oxides wt.%

Fig. 2. Variation diagram of Neogene volcanic rocks.
Squares: Rocks of pre-granite, Circles: Rocks of post-granite and andesite dike.

reported by Irvine and Baragar (1971). The rocks of pre-granite are plotted in the field of tholeiitic suite, on the other hand, those of post-granite are plotted in the field of calc-alkaline suite. Figure 4 shows plot of Na_2O+K_2O against SiO_2 for analyzed rocks. In Fig. 4, solid lines represent the boundary curves between alkali olivine basalt, high-alumina basalt and tholeiitic series reported by Kuno (1966). The rocks of pre-granite are plotted in the field of tholeiite. The rocks of post-granite are plotted in the field of high-alumina basalt. However, only the andesite No. 9210608 of dike is plotted in the field of alkali olivine basalt, in order to contain secondary spotted albitic plagioclase.
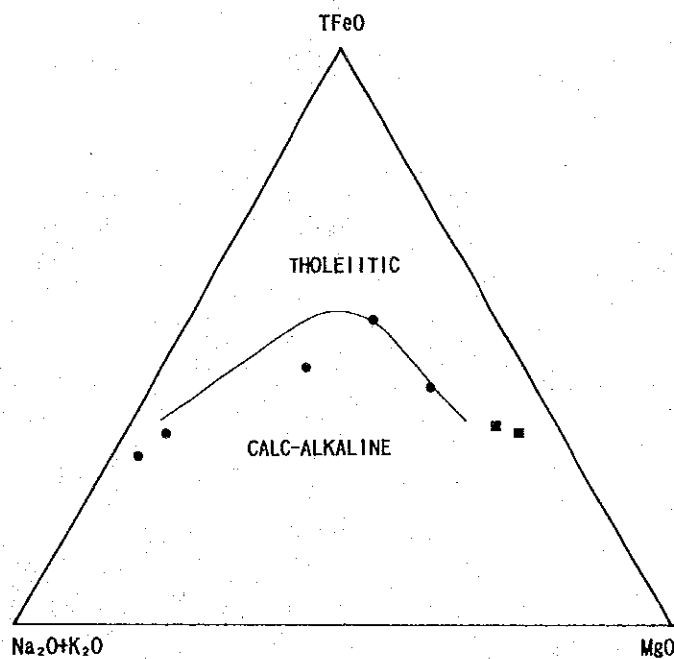
Fig. 3. FAM diagram of Neogene volcanic rocks. The symbols are the same as in Fig. 2.

K-Ar Dating

K-Ar ages of three whole rock samples collected were determined with a mass spectrometer of Okayama University of Science. The results are presented in Table 3.

The K-Ar age of olivine basalt No. 9210709 of pre-granite is 12.2±3.9 Ma during the Middle Miocene time, that of dacitic welded tuff No. 9210703 of post-granite is 4.04±0.4 Ma during the Pliocene time, and that of dike andesite No. 9210608 is 6.6±0.5 Ma during the Mio-Pliocene time. These K-Ar ages are concordant with the K-Ar age of granitic intrusive body in this area (Nishido et al., in press).
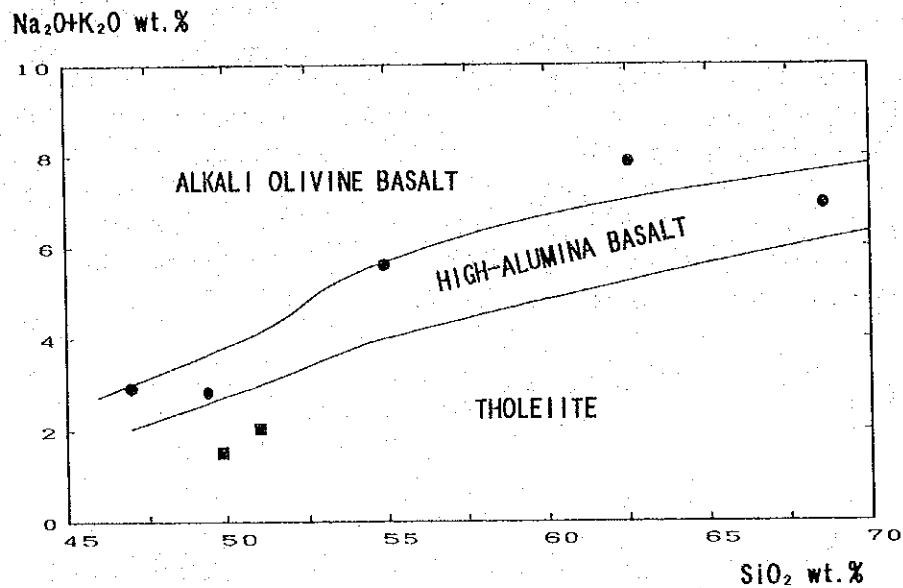
Na$_2$O+K$_2$O wt.%

Fig. 4. Plot of Na$_2$O+K$_2$O against SiO$_2$ for Neogene volcanic rocks.
The symbols are the same as in Fig. 2.

Table 3. K-Ar dating for the Neogene volcanic rocks

Sample No.	Sample	K-Ar Age (Ma)	K (wt.%)	Rad^{40}Ar (10^{-8} ccSTP/g)	Air Ar (%)
9210703	Whole Rock	4.0±0.4	2.18	34.0±3.7	87
9210608	Whole Rock	6.6±0.5	2.20	56.7±4.0	81
9210709	Whole Rock	12.2±3.9	0.457	21.8±6.9	95

Genetical Consideration

The olivine basalt of pre-granite contains strongly altered olivines and a slightly altered groundmass, but other constituent minerals are fresh. This mode of occurrence indicates that the K-Ar age obtained is not different from the age of formation of olivine basalt. Therefore, it is concluded that the olivine basalt composed of a tholeiite was formed during the Middle Miocene age.

The rocks of post-granite are composed of an olivine basalt, a pyroxene andesite and a dacitic welded tuff, and show a regular compositional variation of calc-alkaline rock series. The K-Ar age indicates that the welded tuff was erupted during the Pliocene time.

The andesitic dike intrudes the formation of pre-granite. The andesite is strongly altered. So, the K-Ar age obtained is thought to be too young. Because the andesite is composed of a calc-alkaline rock, it is considered that this andesite

dike intruded during probably the Late Miocene time, the post of intrusion of Middle Miocene granitic bodies.

As seen in Fig. 2, a fractionation scheme of olivine is found in the Pliocene olivine basalt as well as in the Recent Antuco lavas (Yamamoto *et al.*, in press). This fact suggests that the calc-alkaline volcanic activity is intermittently continuing from Pliocene to Recent.

Acknowledgments

References

Instituto de Investigaciones Geológicas (1982a): Mapa Geológico de Chile, 1:1.000.000, N° 3. Servicio Nacional de Geología y Minería, Santiago.

Instituto de Investigaciones Geológicas (1982b): Mapa Geológico de Chile, 1:1.000.000, N°4. Servicio Nacional de Geología y Minería, Santiago.

Irvine, A. J. and Baragar, W. R. (1971): A guide to the chemical classification of the common igneous rock. *Can. J. Earth. Sci.*, 8, 523-548.

Kuno, H. (1966): Lateral variation of basalt magna type across continental margins and island arcs. *Bull. Volcanol.*, 29, 195-222.

Nishido, H., Yamamoto, M., and Frutos, J. (in press): Composition and K-Ar age of granitic intrusive body in Antuco, southern Chile.

Yamamoto, M., Nishido, H., and Helle, S. (in press): Petrography and petrochemistry of volcanic rocks of Antuco volcano, Chile.

COMPOSITION AND K-Ar AGE OF GRANITIC INTRUSIVE BODY IN ANTUCO, SOUTHERN CHILE

Hirotsugu Nishido*, Masahiko Yamamoto** and José Frutos***
*Hiruzen Research Institute, Okayama University of Science, Kawakami, Okayama 717-06, Japan. **Institute of Earth Sciences, Faculty of Science, Kagoshima University, Kagoshima 890, Japan. ***Programa de Geología Económica Aplicada, Universidad de Concepción, Concepción 3, Chile.

Abstract

The granitic intrusive body exposed in the Antuco area, southern Chile, was petrologically studied. The granitic body is composed of an I-type augite-bearing biotite-hornblende granodiorite. The whole rock K-Ar age indicates that the granitic body was emplaced in the epizone during Late Miocene age.

Introduction

A number of granitic intrusive masses are zonally distributed in the coastal area of western side of Andes in Chile (Aguirre, 1983). The granitic intrusive body is widely exposed in the Antuco area. However, there are little petrological data of granitic body. The present paper presents the results of petrographical, petrochemical and K-Ar dating studies of one rock sample collected from an outcrop near El Abanico.

Geological Setting

The granitic intrusive body is exposed in the Antuco area, southern Chile. A geologic map compiled from Instituto de Investigaciones Geológicas (1980a, b)

is shown in Fig. 1. The granitic body is batholithic in shape. In this area, it intrudes the altered volcanic and volcani-sedimentary rocks of probably Miocene age and is covered by the altered volcanic and volcani- sedimentary rocks of Pliocene age and the lava flows and the pyroclastic rocks of Quaternary age (Nishido *et al.*, in preparation; Yamamoto *et al.*, in press).

One rock sample was collected from an outcrop near El Abanico, 15 kilometers east of Antuco. The locality is shown in Fig. 2.
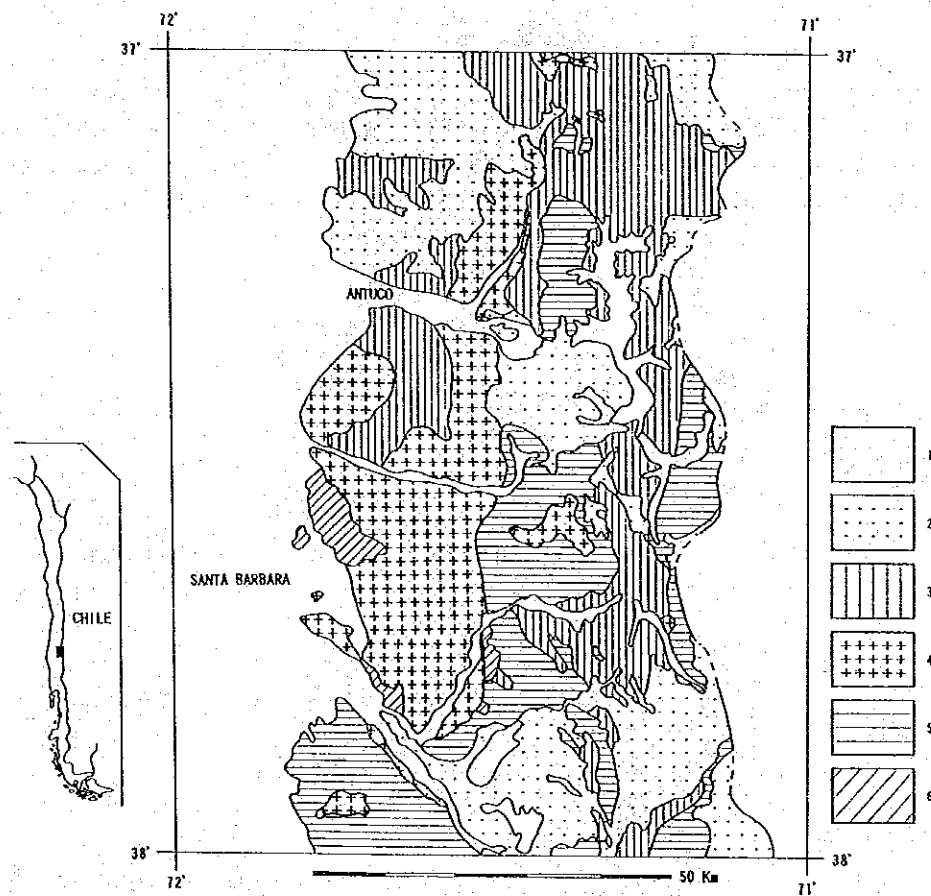

Fig. 1. Index and geologic maps of the granodiorite body in Antuco.
The geologic map is compiled from Instituto de Investigaciones Geológicas (1980a, b). Stratigraphic sequences: 1. Alluvial deposits, 2. Quaternary volcanics, 3. Pliocene volcanics, 4. Miocene granitic intrusives, 5. Miocene volcanics, 6. Cretaceous to Paleogene strata.

Petrography

The rock sample collected was petrographically studied under a petrographic microscope. The rock is a light grey-colored and medium-grained granodiorite. Large amounts of xenoliths of basic igneous rocks are included within the rock.

The rock is principally composed of plagioclase, quartz, K-feldspar, hornblende and biotite, with a small amount of augite. Plagioclase occurs as euhedral zoned and twinned crystals, and anti-perthitic texture is commonly found. K-feldspar occurs as subhedral to anhedral grains, and perthitic texture is commonly found. Both plagioclase and K-feldspar are sometimes sericitized. Quartz occurs in anhedral grains. Hornblende occurs as euhedral slightly zoned and twinned crystals, and is partly changed to actinolitic in composition. Biotite occurs as euhedral to subhedral flakes, and is largely chloritized. Augite occurs in subhedral to anhedral small-sized grains. Crystal clots composed of mainly augite, hornblende, biotite and opaque oxides are sometimes included in the rock. Accessory minerals are of apatite, zircon, magnetite, ilmenite and sphene, and secondary minerals are of sericite and chlorite.
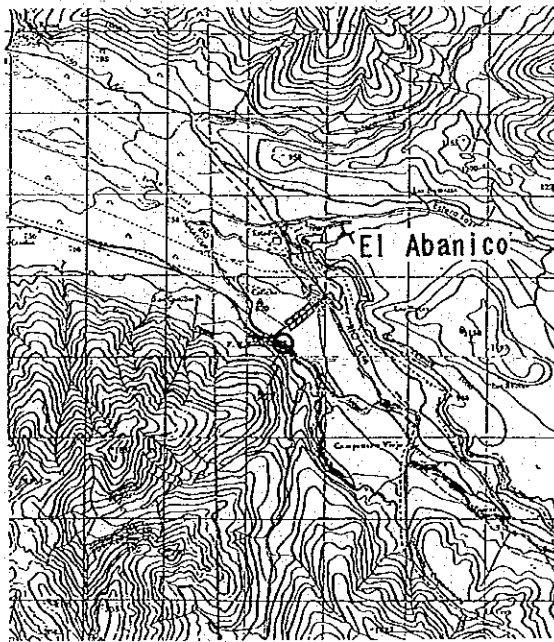

Fig. 2. Topographic map showing the locality
(open circle) of granodiorite sttudied.

Table 1. Chemical analysis and CIPW norm of the granodiorite No. 9210707 from Antuco

SiO_2	64.96	Q	21.93
TiO_2	0.55	Or	15.37
Al_2O_3	15.47	Ab	28.09
Fe_2O_3	1.72	An	19.63
FeO	2.91	DI	3.22
MnO	0.09	Wo	1.65
MgO	2.00	En	0.96
CaO	4.86	Fs	0.61
Na_2O	3.32	Hy	6.59
K_2O	2.60	En	4.02
H_2O^+	0.94	Fs	2.57
H_2O^-	0.14	Il	1.04
P_2O_5	0.08	Mt	2.49
		Ap	0.19
Total	99.64		

Petrochemistry

The rock sample collected was chemically analyzed with the Rigaku XRF Spectrometer 3070-E. The chemical composition analyzed and the CIPW norm calculated are listed in Table 1.

The SiO_2 content is 65 wt. %, and the rock is chemically granodioritic. The amount of Na_2O exceeds that of K_2O, and the amount of CaO is relatively high. Normative C is not calculated, but a large amount of normative Di is calculated; and the rock is metaluminous. The chemical composition indicates that the granodiorite is of I-type defined by Chappell and White (1974).

Table 2. K-Ar dating for the granodiorite No. 9210707 from Antuco

Sample	K-Ar Age (Ma)	K (wt.%)	Rad^{40}Ar (10^{-8}ccSTP/g)	AirAr (%)
Whole Rock	11.4±0.8	2.16	96.1±6.8	80

K-Ar Dating

The K-Ar age of whole rock sample collected was determined with a mass spectrometer of Okayama University of Science. The result is presented in Table 2.

The K-Ar age is 11.4±0.8 Ma, and indicates that the granitic intrusive body was emplaced during the Late Miocene age.

Genetical Consideration

The altered volcanic and volcani-sedimentary rocks of Neogene age are widely distributed in the Antuco area (Nishido et al., in preparation). The granitic body intrudes the volcanic and volcani-sedimentary rocks of Miocene age. This fact indicates that the granitic body was formed by volcano-plutonism of Miocene age, and that the granitic body was emplaced in the epizone, as well as most Tertiary stocks and batholiths of Peruvian Andes (Bussell et al., 1976; Atherron, 1981; Cobbing and Pitcher, 1983).

Acknowledgments

The authors are greatly indebted to Dr. A. Sugaki, Emeritus Professor of Tohoku University, who kindly gave an opportunity to study in Chile.

References

Aguirre, L. (1983): Granitoids in Chile. *Geol. Soc. Amer. Mem.*, 159, 293-316.

Atherton, M.P. (1981): Horizontal and vertical zoning in the Peruvian Coastal batholith., *J. Geol. Soc. London*, 138, 343-349.

Bussell, M.A., Pitcher. W.S., and Wilson, P.A. (1976): Ring complexes of Peruvian Coastal batholith; A long-standing subvolcanic regime. *Can. J. Earth Sci.*, 13, 1020-1030.

Chappell, B.W. and White, A.J.R. (1974): Two contrasting granite types. *Pac. Geol.*, 8, 173-174.

Cobbing, E.J. and Pitcher, W.S. (1983): Andean plutonism in Peru and its relationship to volcanism and metallogenesis at a segmented plate edge. *Geol. Soc. Amer. Mem.*, 159, 277-292.

Instituto de Investigaciones Geológicas (1982a): Mapa Geológico de Chile, 1:1.000.000, N° 3. Servicio Nacional de Geología y Minería, Santiago.

Instituto de Investigaciones Geológicas (1982b): Mapa Geológico de Chile, 1:1.000.000, N° 4. Servicio Nacional de Geología y Minería, Santiago.

Nishido, H., Yamamoto, M., and Frutos, J. (in preparation): Petrography, petrochemistry and K-Ar dating of Neogene volcanic rocks in Antuco, southern Chile.

Yamamoto, M., Nishido, H., and Helle, S. (in press): Petrography and petrochemistry of volcanic rocks of Antuco volcano, Chile.

K-Ar DATING ON ROCKS AND MINERALS RELATED TO ORE DEPOSITS IN CHILE (2)

Asahiko Sugaki* and Nobutaka Shimada**
*Kadan 4-30-503, Aoba, Sendai 980, Japan. **Faculty of Science, Kyushu University, Hakozaki 6-10-1, Fukuoka 812, Japan.

1. Introduction

This is a preliminary report of K-Ar age determinations on rocks and minerals related to Chilean ore deposits, followed by Sugaki and Shimada (1992). K-Ar age determinations were made at the Teledyne Isotopes, New Jersey, U.S.A., using separated K-bearing specimens (24 samples) and crushed whole-rock ones (11 samples). The former specimens were intended to define directly the mineralization epochs from hydrothermally deposited minerals or wall rock alteration products, and the latter the ages of igneous activities genetically related to metallic mineralizations.

2. Descriptions of dated samples

The modes of occurrence and types of ore deposits are briefly described as follows:

No. 1: Alunite separated from a yellowish brown colored, intensely altered rock (2022502), which is composed of alunite and quartz, associated with goethite and barite, collected at an open-pit, 4,780 m above sea level, of the Choquelimpie Au-Ag mine (see Gröpper *et al.,* 1991).

No. 2: Sericite fractions separated by elutriation from a bornite-bearing quartz-sericite veinlet (1030711), trending N80°E and dipping 80°N, less than 5 cm wide, which clearly cuts a stratiformed copper body, at the level 285 m of the Buena Esperanza mine (see Sugaki *et al.,* 1983; Losert, 1973).

No. 3: Sericite fractions separated from a hydrothermally altered dacite porphyry sample (1030901), which contains abundant sericite and quartz, together with atacamite and malachite, taken at 804 m above sea level on the Elvira open-pit of the Mantos Blancos mine (see Ruiz and Peebles, 1988).

No. 4: Almost pure jarosite (2022833), which occurred as a veinlet transecting a magnetite lava flow, at a middle bench of an open-pit of El Laco (see Frutos and Oyarzún, 1975).

No. 5: Alunite containing kaolinite and also accompanying supergene alteration products such as jarosite and goethite. This sample (2102707) was collected from the gold-bearing silicified zone, at an open-pit of the Farrellón ore body, the La Coipa gold mine (see Oviedo *et al.*, 1991).

No. 6: A crushed whole-rock sample of biotite-bearing hornblende diorite (2102926), taken at the outcrop, 5 km north of the Caldera Town, Copiapó. Biotite is partly chloritized, and also some parts of plagioclase and K-feldspar are sericitized under a microscope.

No. 7: Hornblende concentrates, divided by an isodynamic separator from the same rock as No. 6.

No. 8: Alunite, handpicked from kaolin-quartz-gypsum-bearing silicified andesite (3022522), collected at the Marte gold mine (see Vila *et al.*, 1991).

No. 9: Dark bluish-grey colored, fine grained andesite, intruded into the Punta de Cobre Formation (?), collected at Paipote, Copiapó.

No. 10: Fresh diorite (3022721), mainly composed of plagioclase and hornblende, taken from the outcrop at the northern foot of Mt. El Granate.

No. 11: Small amount of alunite with quartz, handpicked from gold-bearing silicified sample (3022632) taken at the Pantanillo gold mine (see Sillitoe *et al.*, 1991).

No. 12: Alunite-quartz from the same locality as No. 11.

No. 13: K-feldspar, handpicked from flesh colored veins, less than 2 cm wide, developed widely in the granodiorite pluton (3060112A), located at the southern foot of Mt. El Granate (see Segerstrom and Ruiz, 1962).

No. 14: K-feldspar, selectively collected from a portion of pinkish brown colored reaction rim, 0.3 to 1.5 cm wide, formed along the margin of altered andesite breccia with copper ores in the Punta de Cobre mine. The rim is mainly composed of fine-grained aggregates of K-feldspar, sometimes associating with veinlets of tourmaline, pyrite, chalcopyrite, chlorite and calcite.

No. 15: K-feldspar separated from the sample (3030101) of the Mantos de Cobre mine, showing nearly the same occurrence as No. 14.

No. 16: A lenticular or banded form of altered-andesite (3022824a), surrounded by and sometimes cut or replaced by garnet skarns.

No. 17: An andesite dyke (2102915), 50 cm wide, transecting the garnet-skarn zone of the same locality as No. 16.

No. 18: Altered andesite (2072901), the host rock of a stratified low grade copper ore body called Zona Mantiforme, mainly of chalcopyrite and pyrite, in the Socavón Rampa mine.

No. 19: Altered andesite (1031203), the host rock of brecciated copper ores, taken at the 7th level, 245 m above sea level, in the western part of the Agustina mine.

No. 20: K-feldspar, separated from hornblende-biotite granite (0062711), cropped out near the Fortuna skarn deposits.

No. 21: Biotite flakes, released from clinopyroxene-hornblende-biotite diorite (4061211), genetically related to the Panulcillo skarn deposits.

No.22: Light grey colored dacite (3011405), occurred as a stock along the Pan-American Highway, and collected at the north of Loncoche.

No.23: Crushed whole-rock sample (GA-R1) of intensely sericitized dacite at Río Futa.

No. 24: Hornblende-rich concentrate removed from clinopyroxene-bearing gabbro pegmatite (4040102) in granitic batholith at the east side of Lago Chapo.

No. 25: Biotite flakes, put apart from cordierite-bearing muscovite-biotite granite (4040104), taken at the east side of Lago Chapo.

No. 26: K-feldspar, disconnected from the same rock as No. 25.

No. 27: Biotite fractions, separated from hornblende-biotite diorite (4040202), cropped out widely as a batholith at Canutilla.

No. 28: K-feldspar grains, divided from the same rock as No. 27.

No. 29: Elutriated $2M_1$- sericite fractions from hydrothermally altered quartz-porphyry sill (3050602), cropped out in the main adit of the Doña Rosa ore body, El Toqui mine (see Wellmer *et al.*, 1983; Wellmer and Reeve, 1990).

No. 30: Pale flesh colored, nearly euhedral crystals of adularia, handpicked from an arsenopyrite-sphalerite-bearing adularia-quartz veinlet (3050615), less than 4 cm wide, occurred at the coordinate of N-5007368 and E-266835 in the Doña Rosa ore body, El Toqui mine.

No. 31: Metabasite (4031612), consisting of actinolite, epidote, chlorite, muscovite, albite, calcite and quartz, of the Complejo Sarmiento Formation (see Allen, 1982).

No. 32: Pulverized whole-rock sample of andalusite-bearing muscovite-biotite schist (4031710), a thermally metamorphosed rock of the Complejo Staines Formation (see Allen, 1982).

No. 33: K-feldspar or perthite, put apart from muscovite-bearing biotite granite (4031701) of the Patagonian batholith (see Allen, 1982).

No. 34: K-feldspar or perthite, derived from biotite granite (4031705) of the same batholith as No. 33.

No. 35: Biotite fractions, concentrated by an isodynamic separator from hornblende-biotite granodiorite (4031402), which intrudes the Complejo Sarmiento Formation (see Allen, 1982).

3. Results and considerations

The results of K-Ar age determinations are shown in Table 1. The data are divided into five districts for the sake of convenience and will be briefly considered. Radiometric ages reported in this paper are assigned to geological periods on the basis of Harland *et al.*, (1989).

3-1. Northern district between latitudes 18° and 24°S:

The mineralization age of the Choquelimpie epithermal gold deposit is given as 4.7±0.7 Ma from alunite (No. 1 in Table 1). But the age has relatively large analytical uncertainty, due to the low radiogenic ^{40}Ar percentages. And it does not agree with previous data, namely sericite ages of 6.0±0.3 Ma and 5.6±0.3 Ma, and also alunite age of 6.9±0.3 Ma, presented by Sugaki and Shimada (1992). In order to distinguish a hypogene vs. supergene origin (Field and Gustafson, 1976), it is further necessary to determine sulfur isotopes on the alunite samples with coexisting sulfides.

According to the mineralization age of Buena Esperanza, an age of 151±8 Ma is presented for a veinlet (No. 2), which definitely postdates the stratiformed copper mineralization. The age fairly agrees with 159±8 Ma (Sugaki and Shimada, 1992) within an analytical uncertainty. From these data, it is concluded that the mineralization took place before the age of 159±8 Ma.

The mineralization age of Mantos Blancos has been considered to be late Jurassic from a K-Ar age of 149±13 Ma on the dyke rock which evidently cuts the host volcanic rocks of the deposit (Ruiz and Peebles, 1988, p. 93). However, the present age, 96.2±4.8 Ma (No. 3), indicates that the hydrothermal alteration took place in late Cretaceous.

On the El Laco magnetite lava flow deposits, Oyarzún and Frutos (1984) indicated that they were formed in 1.9 Ma of late Pliocene, citing an unpublished age data. The present age of 1.99±0.10 Ma on alunite obviously postdates the El Laco magnetite flow, and is fully concordant with that age.

3-2. Copiapó mining district between latitudes 26.5° and 28.5° S:

On the diorite pluton at Caldera, two ages, 162±16 Ma and 155±8 Ma (Nos. 6 and 7), are fairly correlative to 182.1±2.8 Ma of tonalite at Caldera presented

Table 1. K-Ar ages on rocks and minerals related to ore deposits in Chile

No.	Locality (Mine)	Province	Latitude (South)	Longitude (West)	Sample No.	Material analyzed	K (wt%)	40Ar rad (10⁻⁵scc/g)	40Ar rad (%)	Age (Ma)
1	Choquelimpie	Parinacota	18° 17.0'	69° 14.2'	2022502	alunite	3.84±0.03	0.071±0.001	20.6	4.7 ± 0.7
2	Buena Esperanza	Tocopilla	22° 09.9'	70° 12.6'	1030711	sericite	7.09±0.02	4.33 ±0.01	98.1	151 ± 8
3	Mantos Blancos	Antofagasta	23° 25.3'	70° 04.3'	1030901	sericite	0.85±0.01	0.325±0.003	78.7	96.2 ± 4.8
4	El Laco	El Loa	23° 50.6'	67° 29.5'	2022833	jarosite	7.04±0.01	0.055±0.003	41.8	1.99± 0.10
5	La Coipa	Copiapó	26° 48.8'	69° 15.5'	2102707	alunite	4.76±0.01	0.312±0.002	67.8	16.8 ± 0.8
6	Caldera	Copiapó	27° 00.8'	70° 48.0'	2102926	whole rock	0.35±0.01	0.230±0.001	23.9	162 ±16
7	Caldera	Copiapó	27° 00.8'	70° 48.0'	2102926-H	hornbende	0.10±0.01	0.083±0.001	40.1	155 ± 8
8	Marte	Copiapó	27° 10.4'	69° 00.5'	3022522	alunite	1.87±0.02	0.084±0.001	28.4	11.5 ± 1.2
9	Paipote	Copiapó	27° 24.8'	70° 15.8'	3022701	whole rock	2.68±0.02	0.669±0.013	22.4	63.2 ± 8.1
10	Cerro Granate	Copiapó	27° 25.4'	70° 17.3'	3022721	whole rock	0.91±0.01	0.233±0.009	9.0	65.0 ±22.6
11	Pantanillo	Copiapó	27° 26.0'	69° 03.6'	3022632	alunite	0.56±0.01	0.038±0.002	22.8	17.7 ± 2.3
12	Pantanillo	Copiapó	27° 26.0'	69° 03.6'	3022633	alunite	3.00±0.02	0.231±0.001	68.5	19.7 ± 1.0
13	Cerro Granate,S	Copiapó	27° 27.6'	70° 16.7'	3060112A	K-feldspar	5.95±0.04	2.14 ±0.04	70.1	90.3 ± 4.5
14	Mantos de Cobre	Copiapó	27° 28.0'	70° 05.3'	PKf-JF-1	K-feldspar	3.24±0.01	0.922±0.005	63.5	71.1 ± 3.6
15	Mantos de Cobre	Copiapó	27° 28.0'	70° 05.3'	3030101	K-feldspar	9.04±0.03	2.67 ±0.02	85.7	74.4 ± 3.7
16	Tierra Amarilla	Copiapó	27° 28.2'	70° 16.5'	3022824a	whole rock	1.08±0.01	0.276±0.009	20.6	64.5 ± 8.1
17	Tierra Amarilla	Copiapó	27° 28.2'	70° 16.5'	2102915	whole rock	0.87±0.01	0.293±0.003	13.8	84.5 ±17.9
18	Socavón Rampa	Copiapó	27° 30.1'	70° 15.3'	2072901	whole rock	3.77±0.02	1.09 ±0.02	37.3	73.0 ± 4.1

Table 1. (Continued)

No.	Locality (Mine)	Province	Latitude (South)	Longitude (West)	Sample No.	Material analyzed	K (wt%)	^{40}Ar rad (10^{-5}scc/g)	^{40}Ar rad (%)	Age (Ma)
19	Agustina	Copiapo	27° 30.2'	70° 15.5'	1031203	whole rock	9.23±0.02	2.61 ±0.10	79.7	71.4 ± 3.6
20	Fortuna	Elqui	29° 47.8'	71° 03.0'	0062711	K-feldspar	4.12±0.01	1.67 ±0.02	66.7	101 ± 5
21	Panulcillo	Limarí	30° 26.0'	71° 12.0'	4061211	biotite	5.20±0.01	2.76 ±0.05	95.1	132 ± 7
22	Loncoche	Cautín	39° 19.5'	72° 40.2'	3011405	whole rock	1.92±0.01	0.196±0.005	9.0	26.1 ±10.6
23	Rio Puta	Valdivia	39° 51.9'	73° 14.8'	GA-R1	whole rock	2.71±0.01	0.448±0.004	66.8	42.1 ± 2.1
24	Lago Chapo	Llanquihue	41° 30.3'	72° 24.9'	4040102	hornblende	0.17±0.01	0.012±0.001	16.1	18.1 ± 3.0
25	Lago Chapo	Llanquihue	41° 30.3'	72° 24.1'	4040104	biotite	8.69±0.02	0.484±0.003	78.2	18.5 ± 0.9
26	Lago Chapo	Llanquihue	41° 30.3'	72° 24.1'	4040104	k-feldspar	2.73±0.01	0.208±0.002	77.0	19.4 ± 1.0
27	Canutillar	Llanquihue	41° 31.1'	72° 20.4'	4040202	biotite	6.57±0.01	0.586±0.004	64.5	22.8 ± 1.1
28	Canutillar	Llanquihue	41° 31.1'	72° 20.4'	4040202	k-feldspar	0.31±0.01	0.017±0.001	25.6	13.6 ± 1.3
29	El Toqui	Coihaique	45° 01.0'	71° 54.0'	3050602	sericite	5.82±0.03	2.39 ±0.01	97.3	103 ± 5
30	El Toqui	Coihaique	45° 01.0'	71° 54.0'	3050615	k-feldspar	12.8±0.1	3.63 ±0.07	85.1	72.6 ± 3.6
31	Península Staines	Ultima Esperanza	51° 30.2'	73° 35.6'	4031612	whole rock	0.44±0.01	0.200±0.003	71.9	113 ± 6
32	Península Staines	Ultima Espearnza	51° 32.3'	73° 48.7'	4031710	whole rock	3.09±0.01	0.684±0.001	93.3	56.2 ± 2.8
33	Península Staines	Ultima Esperanza	51° 32.5'	73° 49.8'	4031701	k-feldspar	3.55±0.03	1.37 ±0.03	93.0	98.4 ± 4.8
34	Península Staines	Ultima Esperanza	51° 33.2'	73° 49.3'	4031705	k-feldspar	5.27±0.02	0.891±0.003	86.6	43.0 ± 2.2
35	Puerto Fontaine	Ultima Esperanza	52° 03.7'	73° 26.8'	4031402	biotite	6.36±0.01	0.406±0.003	62.1	16.3 ± 0.8

The constants used are λ_β =4.962 x 10^{-10}/year, λ_ε =0.581 x 10^{-10}/year, and ^{40}K/K=1.167 x 10^{-2} atom% (Steiger and Jäger, 1977).

by Farrar *et al.* (1970). With other similar K-Ar ages from 177 to 191 Ma by Farrar *et al.* (1970), the coastal batholith in this district certainly belongs to Jurassic in age. Near the batholith, there occur several vein-type gold-copper deposits such as El Roble (Frutos, 1981, p. 138), but their minealization ages have not been defined.

From the eastern part of Caldera to the Copiapó Town, about 50 km wide, there widely crop out early Cretaceous granitoids with various lithologies (Segerstrom *et al.*, 1963; Segerstrom and Ruiz, 1962). This paper presents two age data, 65.0±22.6 Ma and 90.3±4.5 Ma (Nos. 10 and 13) for diorite and the potassic alteration of the granodiorite, respectively near Mt. El Granate. The former, however, can be regarded as an unreliable data due to the low potassium content and the very high atmospheric ^{40}Ar percentage. While, the latter age may indicate a hydrothermal alteration period followed by early Cretaceous granitoid intrusions, whose ages were previously reported to be 95.5±1.5 Ma and 106.9±1.7 Ma at Pampa Travesia, about 20 to 30 km SW of the Mt. El Granate (Farrar *et al.*, 1970).

It is clear that the potassic alteration at the Mantos de Cobre ore deposit, in which K-feldspar crystallized out as a reaction rim between andesite breccias and the hydrothermal solution, was taken place in 72.8±2.6 Ma, an averaged value of duplicated data of Nos. 14 and 15.

An altered andesite age from Socavón Rampa (73.0±4.1 Ma, No. 18) is in well agreement with that from Agustina (71.4±3.6 Ma, No. 19). But, these manto-type copper deposits are undoubtedly hosted in the upper andesite horizon of the Punta del Cobre Formation, whose sedimentation certainly occurred in Neocomian (Segerstrom, 1967). Thus, the ages presented here become a serious matter of great concern on the genesis of these ore deposits.

A whole rock age of andesite at Paipote indicates 63.2±8.1 Ma (No. 9). It may be noted that this age is correlative to the approximate K-Ar ages of 65-75 Ma for extrusive rocks in this district (McNutt *et al.*, 1975, Nos. 26 and 27).

By the way, the ages of Nos. 16 and 17 are full of inconsistencies with their modes of occurrence, although the latter age has large analytical uncertainty. Resolution must wait the more precise age determinations.

An alunite age from Marte (No. 8) yields 11.5±1.2 Ma, which is in reasonable agreement with an alunite age of 12.0±0.6 Ma reported by Mulja (1986) and also with that of 13.3±0.4 Ma by Sillitoe *et al.* (1991). While, two alunite ages, 17.7±2.3 Ma and 19.7±1.0 Ma from Pantanillo (Nos. 11 and 12) are distinct from an alunite age of 22.0±0.6 Ma reported by Sillitoe *et al.* (1991). These datings again need a further isotopic study as mentioned above.

3-3. *La Serena district between latitudes 29° and 30° 30' S:*

K-Ar mineral ages of hornblende-biotite granite and diorite related to skarn ore deposits of Fortuna and Panulcillo have been determined to be 101±5 Ma

(No. 20) and 132±7 Ma (No. 21), respectively. These ages have defined that the intrusion of granitoids in this district and the related skarnization were taken place in early Cretaceous.

3-4. Southern district between latitudes 39° and 45°30' S:

The area from Loncoche to Valdivia is principally composed of crystalline schist of the Cabo Tiura Unit, the Paleozoic Western Series (Oyarzún and Clemmey, 1986). However, small outcrops of dacite intrusion have been detected in the area. Dacite from Loncoche indicates 26.1±10.6 Ma (No. 22), and altered dacite from Río Futa 42.1±2.1 Ma (No. 23). These are the first age data indicating the presence of the Eocene-Oligocene igneous activity in this area.

Three mineal ages, 18.1±3.0 Ma (No. 24), 18.5±0.9 Ma (No. 25) and 19.4±1.0 Ma (No. 26), are in reasonable agreements in each other, so that the intrusion age of two-mica granite cropped out around Lago Chapo can be regarded to have an averaged value of 18.7±1.1 Ma in early Miocene. On the other hand, hornblende-biotite diorite shows two distinct mineral ages, namely 22.8±1.1 Ma for biotite (No. 27) and 13.6±1.3 Ma for K-feldspar (No. 28). Further duplicate study will be necessary to define the intrusion age of the diorite.

The minealization age of the El Toqui lead-zinc deposits has been estimated to be of early Cretaceous from the viewpoint of volcanogenetic exhalative origin and geologic correlations (Wellmer et al., 1983; Wellmer and Reeve, 1990). The quartz porphyry sill intrudes the Ore Series and the Upper Series, and has undergone potassic alteration (Wellmer and Reeve, 1990). The sericite age of 103±5 Ma (No. 29) entirely corresponds to the epoch of potassic alteration of the quartz porphyry sill, occurred in the Doña Rosa ore body. While, a K-feldspar age of 72.6±3.6 Ma (No. 30) displays the discordant minerlization epoch occurred in the massive sulfide lens, 6 m thick, of the Doña Rosa ore body. These two ages will contribute largely to an advanced understanding of more complicated and various kinds of minearlizations, such as three different stratiformed ore series and other discordant ore deposits, between ages 103±5 Ma and 72.6±3.6 Ma in the Toqui mining area.

3-5. Patagonia district between latitudes 51° and 52° S:

Allen (1982) reported that the Patagonian batholith in this district consists of diorite and granite, and probably shows the various intrusion episodes from late Jurassic to Tertiary. The present study represents the definite ages that the igneous intrusions were at least taken place in 96.4±4.8 Ma (No. 33), 43.0±2.2 Ma (No. 34) and 16.3±0.8 Ma (No. 35) from late Cretaceous to Miocene. A

whole rock age of 56.2±2.8 Ma (No. 32) is considered to indicate the epoch of contact metamorphism of biotite-quartz schist by a Patagonian granitic intrusion. Another whole rock age of 113±6 Ma (No. 31) may display the epoch of the regional metamorphism of basic tuff judging from the mineral associations.

Acknowledgements

References

Allen, R.E. (1982): Geología de la Cordillera Sarmiento, Andes Patagónicos, entre los 51° 00' y 52° 15' lat. S, Magallanes, Chile. *Servicio Nac. Geología y Minería, Chile, Boletín,* 38, 5-46.

Farrar, E., Clark, A.H., Haynes, S.J. and Quirt, G.S. (1970): K-Ar evidence for the post-Paleozoic migration of granitic intrusion foci in the Andes of Northern Chile. *Earth Planet. Sci. Letters,* 10, 60-66.

Field, C.W. and Gustafson, L.B. (1976): Sulfur isotopes in the porphyry copper deposit at El Salvador, Chile. *Econ. Geol.,* 71, 1533-1548.

Frutos, J. (1981): *Atlas of 1200 Chilean mines and prospects.* Vol. 1, 1-112, A. Sutulov, Inter. Pub.

Frutos, J. and Oyarzún, J. (1975): Tectonic and geochemical evidence concerning the genesis of El Laco magnetite lava flow deposits, Chile. *Econ. Geol.,* 70, 988-990.

Gröpper, H., Calvo, M., Crespo, H., Bisso, C.R., Cuadra, W.A., Dunkerley, P.M. and Aguirre, E. (1991): The epithermal gold-silver deposit of Choquelimpie, Northern Chile. *Econ. Geol.,* 86, 1206-1221.

Harland, W.B., Armstrong, R.L., Cox, A.V., Craig, L.E., Smith, A.G. and Smith, D.G. (1989): *A Geologic Time Scale.* 1-263, Cambridge Univ. Press.

Losert, J. (1973): Genesis of copper mineralizations and associated alterations in the Jurassic volcanic rocks of the Buena Esperanza mining area. (Antofagasta Province, Northern Chile). *Dep. Geol., Univ. of Chile,* 40, 1-64.

McNutt, R.H., Crocket, J.H., Clark, A.H., Caelles, J.C., Farra, E. and Haynes, S.J. (1975): Initial 87Sr/86Sr ratios of plutonic and volcanic rocks of the central Andes between latitudes 26° and 29° south. *Earth Plant. Sci. Letters,* 27, 305-313.

Mulja, R. (1986): Hydrothermal alteration, gold distribution and geochronology of epithermal gold mineralization in the Copiapó volcanic complex, Chile. *Unpub. B. Sc. Thesis, Halifax, Nova Scotia, Dalhousie Univ.,* 1-145.

Oviedo, L., Fuster, N., Tschischow, N., Ribba L., Zuccone, A., Grez, E. and Aguilar, A. (1991): General geology of La Coipa precious metal deposit, Atacama, Chile. *Econ. Geol.*, 86, 1287-1300.

Oyarzún, J. and Frutos, J. (1984): Tectonic and petrological frame of the Cretaceous iron deposits of North Chile. *Mining Geology, Japan*, 34, 21-31.

Oyarzún, R. and Clemmey, H. (1986): Las mineralizaciones bandeadas de hierro y de sulfuros masivos estratoligados de la Cordillera de Nahuelbuta, Chile. Parte A: Marco geológico, geoquímico y petrológico de la Cordillera de Nahuelbuta. In *Geología y Recursos Minerales de Chile*, Frutos, J. *et al.*, eds., 2, 739-753.

Ruiz, C. and Peebles, L. (1988): *Geología, distribución y génesis de los yacimientos metálicos chilenos*, 1-334, Santiago.

Segerstrom, K. (1967): Geology and ore deposits of central Atacama Province, Chile. *Geol. Soc. Amer. Bull.*, 78, 305-318.

Segerstrom, K. and Ruiz, C. (1962): Cuadrángulo Copiapó, Provincia de Atacama, Escala 1:50,000. *Instituto de Investigaciones Geológicas, Chile, Carta*, 6, 1-115.

Segerstrom, K., Thomas, H. and Tilling, R.I. (1963): Cuadrángulo Pintadas. Provincia de Atacama, Escala 1:50,000. *Instituto de Investigaciones Geológicas, Chile*, 12, 1-52.

Sillitoe, R., McKee, E.H. and Vila, T. (1991): Reconnaissance K-Ar geochronology of the Maricunga gold-silver belt, Northern Chile. *Econ. Geol.*, 86, 1261-1270.

Steger, R.H. and Jäger, E. (1977): Subcommission on geochronology: Convention on the use of decay constant in geo- and cosmo-chronology. *Earth Planet. Sci. Letters*, 36, 359-362.

Sugaki, A. and Shimada, N. (1992): K-Ar dating on rocks and minerals related to ore deposits in Chile (1). *Sci. Rep., Econ. Geol. Research Project, Univ. Concepción, No. 2*, 49-55.

Sugaki, A., Shimada, N., Frutos, J. and Alfaro, G. (1983): *Preliminary Investigation on Geology of Hydrothermal Ore Deposits in Andes Area of Chile*. Rep. Overseas Sci. Survey, 1-61, Sendai, Japan.

Vila, T., Sillitoe, R.H., Betzhold, J. and Viteri, E. (1991): The porphyry gold deposit at Marte, Northern Chile, *Econ. Geol.*, 86, 1271-1286.

Wellmer, F.W., Reeve, E.J., Wentzlau, E. and Westenberger, H. (1983): Geology and ore deposits of the Toqui district, Aysen, Chile. *Econ. Geol.*, 78, 1119-1143.

Wellmer, F.W. and Reeve, E.J. (1990): The Toqui zinc-copper-silver deposits, Aysen Province, Chile. In *Stratabound Ore Deposits in the Andes*, Fontobé, L. *et al.*, eds., 473-484, Springer-V., Heidelberg.

OPTICAL AND X-RAY POWDER DIFFRACTION DATA FOR SULFIDE MINERALS SYNTHESIZED HYDROTHERMALLY

Asahiko Sugaki*, Shoji Kojima** and Arashi Kitakaze***
*Kadan 4-30-503, Aoba, Sendai 980, Japan. **Yagiyama Hon-Cho I-24-II, Taihaku, Sendai 982, Japan. ***Faculty of Science, Tohoku University, Aramaki-Aoba, Sendai 980, Japan.

Abstract

Some sulfide and sulfosalt minerals have been synthesized by thermal gradient transport method using powdered minerals as nutrient material. Nutrient sulfide were synthesized previously by evacuated silica glass tube method. The synthetic experiments were performed under the hydrothermal conditions of temperature; 300 and 350°C, and pressure; 300 kgf, employing aqueous solution of 5m ammonium chloride. Then, some sulfide and sulfosalt minerals such as pyrrhotite, covellite, stibnite, sphalerite, galena, greenockite, alabandite, chalcopyrite, bornite, nukundamite, proustite, pyrargyrite, famatinite and enargite were synthesized.

Optical proporties for synthetic minerals were observed under ore microscope. The X-ray powder diffraction data for hydrotermally synthesized products were measured using a Guinier camera. Their cell parameters were obtained by the least squares calculation using all diffraction data.

1. Introduction

Sulfide and sulfosalt minerals are important minerals in the ore deposits. They were usually formed under hydrothermal conditions. Then, hydrothermal experiments are important to make clear the ore forming process and conditions which will be estimated by the studies on the mineral paragenesis and assemblages in ore deposits. In this time, identification of minerals is important. The data of microscopic properties and X-ray powder diffraction for the minerals are very

useful for mineral identification. Therefore, these data were examined and measured using ore microscope and X-ray powder diffraction camera.

In this paper, optical properties, X-ray powder diffraction data and its cell parameters for hydrothermally synthesized sulfide and sulfosalt minerals will be described.

2. Experiment methods

Hydrothermal synthesis of sulfide and sulfosalt minerals were performed using thermal gradient transporting method described by Scott & Barnes (1971), Sugaki *et al.* (1975, 1977, 1984) and Vaughan & Craig (1978). As nutrient materials, powdered sulfide minerals synthesized previously using evacuated glass tube method (Kullerud. 1971; Scott, 1974; Vaughan & Craig, 1978; Sugaki, 1992) were used. Aqueous solution of 5m ammonium chloride was used as transporting solvent. A gold tube of 3.5 mm in outside diameter with 0.15 mm thickness, and about 50 mm in length was employed as a reaction vessel. Synthetic experiments were carried out under hydrothermal conditions of temperature; 300 to 350°C and pressure; 300 kgf.

The synthetic products were occurred as euhedral crystals, and identified to the nutrient minerals. Sulfide and sulfosalt minerals such as pyrrhotite, pyrite, chalcocite, covellite, stibnite, sphalerite, galena, greenockite, alabandite, chalcopyrite, bornite, nukundamite, proustite, pyrargyrite, famatinite, enargite and tennantite were successfully synthesized. The experimental results are shown in Table 1.

Optical properties such as color, pleochroism, anisotropism, internal reflection and cleavage for hydrothermally synthesized minerals were observed under ore microscope.

X-ray powder diffraction data for the minerals synthesized hydrothermally were obtained at 25°C by a Guinier camera using $CuK\alpha_1$ radiation monochromatized by curved quartz crystal. Pure silicon was used as an internal standard except for sphalerite. In the case of sphalerite, synthetic fluorite was used. The intensities and angles (positions) of reflections on a Guinier film were measured by a microphotometer controlled by personal computer in the same method described by Kitakaze (1992). Their cell parameters were also obtained by a least squares calculation using all reflection data.

3. Experimental Results

Pyrrhotite, $Fe_{1-x}S$
Pyrrhotite synthesized hydrothermally at 350°C, 300 kgf (H008) is found as

82

Table 1. Experimental results of hydrothermal synthesis

Run No.	Nutrient materials	Period (days)	Products
350° C, 300 kgr			
H008	FeS	4	Pyrrhotite
H004	CuS	4	Covellite
H002	Sb_2S_3	4	Stibnite
H054	ZnS	5	Sphalerite
H031	$Zn_{0.5}Fe_{0.2}S$	5	Sphalerite
H001	PbS	5	Galena
H047	PbS	7	Galena
H027	CdS	7	Greenockite
H024	CdS	5	Greenockite
H055	MnS	5	Alabandite
H003	Cu_2FeS_2	4	Chalcopyrite
H005	$CuFeS_2$	4	Chalcopyrite
H026	Cu_5FeS_4	6	Bornite
H034	$Cu_{3.39}Fe_{0.61}S_4$	5	Nukundamite
H038	$Cu_{3.39}Fe_{0.61}S_4$	5	Nukundamite
H036	Ag_3AsS_3	4	Proustite
H029	Ag_3SbS_3	7	Pyrargyrite
H045	Cu_3SbS_4	7	Famatinite
H046	Cu_3AsS_4	7	Enargite
300° C. 300 Kgf			
H015	FeS	4	Pyrrhotite
H021	CuS	5	Covellite
H052	CuS	5	Sphalerite
H020	$Zn_{0.5}Fe_{0.2}S$	5	Sphalerite
H043	PbS	8	Galena
H053	MnS	5	Alabandite
H049	Cu_5FeS_4	5	Bornite
H048	$CuFeS_2 + Cu_5FeS_4$	6	Bornite and chalcopyrite
H042	Ag_3AsS_3	8	Proustite
H040	Ag_3SbS_3	4	Pyrargyrite
H044	Cu_3SbS_4	8	Famatinite

hexagonal platy crystals. Under ore microscope, it shows weak pleochroism from creamy brown to creamy brown with pinkish tint in color and has moderate anisotropism changing its interference color from violet dark gray to gray under crossed nicols. No internal reflection is observed. Cleavage can not be found.

The X-ray powder diffraction data for pyrrhotite (H008) synthesized hydrothermally were measured by a Guinier camera using $CuK\alpha_1$ radiation. Their results are given in Table 2. Its cell parameters were calculated by least squares method using all reflection data, and are a=3.4506(1) and c=5.7557(8) Å as hexagonal 1C type structure of pyrrhotite. Observed and calculated d-values are in good agreement with each other as seen in the table.

Table 2. X-ray powder diffraction data for hydrothermally synthesized pyrrhotite (H008)

I	h	k	l	d(obs)	d(calc)	Δ d
51.9	1	0	0	2.9889	2.9883	0.0006
52.7	1	0	1	2.6524	2.6522	0.0003
100.0	1	0	2	2.0733	2.0729	0.0004
35.7	1	1	0	1.7253	1.7253	-0.0000
10.9	1	0	3	1.6144	1.6145	-0.0001
12.7	2	0	2	1.3261	1.3261	-0.0000

CELL PARAMETERS
   a= 3.4506 (1) Å   c= 5.7557 (6) Å

Covellite, CuS

Covellite (H004) synthesized hydrothermally at 350°C, 300 kgf appears as hexagonal platy crystals. Under ore microscope, it has strong pleochroism from bluish white to blue with violet tint in color and strong anisotropism changing its interference color from dark brown to orange brown under crossed nicols. No internal reflection is observed. Cleavage in parallel to (001) face is sometimes visible.

X-ray powder diffraction data of hydrothermally synthetic covellite (H004)

Table 3. The data of X-ray powder diffraction for hydrothermally synthesized covellite (H004)

I	h	k	l	d(obs)	d(calc)	Δ d
6.9	0	0	2	8.1432	8.1726	-0.0295
12.6	1	0	0	3.2865	3.2832	0.0032
27.6	1	0	1	3.2166	3.2189	-0.0023
72.5	1	0	2	3.0490	3.0466	0.0024
96.7	1	0	3	2.8147	2.8121	0.0026
82.9	0	0	6	2.7261	2.7242	0.0019
6.5	1	0	5	2.3179	2.3166	0.0013
9.0	0	0	8	2.0431	2.0432	-0.0001
100.0	1	1	0	1.8955	1.8956	-0.0001
20.6	1	0	8	1.7350	1.7347	0.0003
6.9	0	0	10	1.6343	1.6345	-0.0003
6.4	2	0	2	1.6096	1.6095	0.0001
9.2	2	0	3	1.5715	1.5718	-0.0003
22.7	1	1	6	1.5555	1.5560	-0.0005
3.9	1	1	8	1.3899	1.3896	0.0002
5.3	1	0	11	1.3537	1.3537	-0.0001

CELL PARAMETERS
   a= 3.7911 (3) Å   c= 16.3452 (20) Å

obtained by a Guinier camera are given in Table 3. Its cell parameters refined by a least squares calculation using all reflection data are hexagonal, a=3.7911 (3) and c=16.3452 (19) Å. The calculated and observed d-values in the table are in good accordance with each other. Cell parameters of hydrothermally synthesized covellite are in good agreement with a=3.792 and c=16.344 Å for synthetic covellite reported by JCPDS card (6-464).

Stibnite, Sb_2S_3

Stibnite (H002) synthesized hydrothermally is found as prismatic crystals elongated to c-axis. Under ore microscope, it shows strong pleochroism from light grayish white to grayish white with greenish tint, and strong anisotropism changing its interference color from dark brown to orange brown under crossed nicols. Internal reflection is not observed. Cleave in parallel to c-axis is sometimes visible.

The data of X-ray powder diffraction for synthetic stibnite (H002) were obtained using a Guinier camera and their results are shown in Table 4. Its cell parameters were calculated using all reflection data, and are orthorhombic, a=11.2285(4), b=11.3113(7) and c=3.8373(2) Å. These values are in good agreement with a=11.229, b=11.310, and c=3.839Å for synthetic stibnite given in JCPDS card (6-474).

Sphalerite, ZnS

Synthetic sphalerite (H052) obtained hydrothermally is observed as polyhedral crystals. Under ore microscope, it shows gray in color, and its pleochroism and anisotropism are not observed. It has very extensive internal reflection color from white to yellowish white. Cleavage can not be visible.

X-ray powder diffraction data of hydrothermally synthesized sphalerite (H054) were measured by a Guinier camera, and their results are given in Table 5. Cell parameter refined by least squares calculation is cubic, a=5.4108(2) Å. This value is slightly longer than a=5.4060 Å for synthetic sphalerite given in JCPDS card (5-568).

Galena, PbS

Galena (H047) synthesized hydrothermally appears as cubic or cubo-octahedral forms. Under ore microscope, it shows white with creamy tint, and pleochroiem and anisotropism are not observed. No internal reflection is found. Cleavage along three dimensions often observed in some crystals, and typical triangle pits observed usually in naturally occurring galena (Uytenbogaadt & Burke, 1971) are found.

The data of X-ray powder diffraction for synthetic galena (H001) measured by a Guinier camera are shown in Table 8. Its cell parameter calculated all diffraction data is a=5.9365(2) Å with cubic symmetry. This value is in good agreement with a=5.4060 Å of synthetic galena given in JCPDS card (5-592).

Table 4. The data of X-ray powder diffraction for stibnite (H002) synthesized hydrothermally

I	h	k	l	d(obs)	d(calc)	Δd
6.6	1	1	0	7.9768	7.9688	0.0080
23.8	0	2	0	5.6560	5.6556	0.0003
7.9	2	0	0	5.6156	5.6142	0.0013
41.8	1	2	0	5.0522	5.0511	0.0011
25.6	2	2	0	3.9839	3.9844	-0.0006
21.3	1	0	1	3.6311	3.6311	0.0000
46.2	1	3	0	3.5746	3.5743	0.0003
73.7	3	1	0	3.5536	3.5533	0.0003
27.0	1	1	1	3.4570	3.4574	-0.0003
5.7	0	2	1	3.1757	3.1754	0.0003
100.0	2	1	1	3.0512	3.0506	0.0006
86.6	2	2	1	2.7645	2.7639	0.0006
8.2	1	4	0	2.7414	2.7422	-0.0008
3.9	4	1	0	2.7247	2.7245	0.0003
52.3	3	0	1	2.6799	2.6794	0.0005
33.4	2	4	0	2.5257	2.5255	0.0001
14.3	4	2	0	2.5149	2.5144	0.0005
15.4	2	3	1	2.4258	2.4255	0.0003
14.4	0	4	1	2.2764	2.2765	-0.0001
6.0	4	3	0	2.2521	2.2516	0.0005
18.7	1	4	1	2.2312	2.2311	0.0001
12.0	4	1	1	2.2216	2.2215	0.0001
4.9	5	1	0	2.2028	2.2027	0.0001
16.9	4	2	1	2.1033	2.1031	0.0002
11.9	2	5	0	2.0987	2.0983	0.0004
11.8	5	2	0	2.0871	2.0872	-0.0000
5.2	4	4	0	1.9919	1.9922	-0.0003
3.9	0	6	0	1.8856	1.8852	0.0003
7.2	6	0	0	1.8713	1.8714	-0.0001
8.7	6	1	0	1.8467	1.8463	0.0004
5.9	1	2	2	1.7936	1.7936	-0.0001
4.7	6	2	0	1.7770	1.7767	0.0004
4.4	5	4	0	1.7584	1.7586	-0.0002
17.0	3	5	1	1.7285	1.7285	-0.0000
11.3	5	3	1	1.7238	1.7238	0.0000
20.0	0	6	1	1.6917	1.6920	-0.0003
20.9	3	1	2	1.6886	1.6883	0.0003
4.8	3	6	0	1.6834	1.6837	-0.0003
3.2	1	4	2	1.5722	1.5721	0.0002
12.7	7	2	0	1.5431	1.5432	-0.0001
12.6	2	4	2	1.5276	1.5278	-0.0002
4.4	5	1	2	1.4465	1.4468	-0.0003
9.3	7	2	1	1.4316	1.4318	-0.0001
5.0	2	5	2	1.4162	1.4160	0.0002
5.3	5	2	2	1.4124	1.4125	-0.0001
4.0	8	0	0	1.4036	1.4036	0.0000

CELL PARAMETERS
   a= 11.2885 (4) Å, b= 11.3113 (7) Å, c= 3.8374 (2) Å

Greenockite, CdS
   Hydrothermally synthesized greenockite (H024) appears as polyhedral forms. Under ore microscope, it shows grayish white with greenish tint in color, and

Table 5. X-ray powder diffraction data for sphalerite (H054) obtained by
       hydrothermal synthesis

I	h	k	l	d(obs)	d(calc)	Δd
100.0	1	1	1	3.1225	3.1239	-0.0014
3.9	2	0	0	2.7056	2.7054	0.0003
70.4	2	2	0	1.9136	1.9130	0.0006
31.8	3	1	1	1.6313	1.6314	-0.0001
10.9	2	2	2	1.5618	1.5620	-0.0002
8.2	4	0	0	1.3528	1.3527	0.0001
7.7	3	3	1	1.2413	1.2413	-0.0000
11.6	4	2	2	1.1045	1.1045	-0.0000

CELL PARAMETERS
    a= 5.4108 (2) Å

pleochroism and anisotropism are not observed. It has extensive internal reflection
from orange to dark brown in color. Cleavage is not observed.

X-ray powder diffraction data of synthetic greenockite (H024) obtained by
a Guinier method are given in Table 7. Refined cell parameters using these data
are a=4.1360(1) and c=6.7147(4) Å with hexagonal cell. These values are in good
accordance with a=4.136, and c=6.713 Å for synthetic greenockite shown in
JCPDS card (6-314).

Alabandite, MnS

Alabandite (H055) synthesized hydrothermally is found as prismatic crystal.
It shows light gray in color, and pleochroism and anisotropism are not observed

Table 6. X-ray powder diffraction data for hydrothermally synthesized galena
       (H001)

I	h	k	l	d(obs)	d(calc)	Δd
78.6	1	1	1	3.4288	3.4274	0.0013
100.0	2	0	0	2.9694	2.9682	0.0012
54.3	2	2	0	2.0995	2.0989	0.0006
39.2	3	1	1	1.7901	1.7899	0.0002
19.3	2	2	2	1.7138	1.7137	0.0001
17.8	4	0	0	1.4839	1.4841	-0.0002
12.4	3	3	1	1.3619	1.3619	-0.0000
25.3	4	2	0	1.3275	1.3274	0.0001
16.2	4	2	2	1.2119	1.2118	0.0002
12.6	3	3	3	1.1424	1.1425	-0.0001
-	5	1	1	-	1.1425	-0.0001

CELL PARAMETERS
    a= 5.9365 (2) Å

87

Table 7. The data of X-ray powder diffraction for greenockite (H034) synthesized hydrothermally

I	h	k	l	d(obs)	d(calc)	Δd
74.7	1	0	0	3.5824	3.5819	0.0006
78.5	0	0	2	3.3570	3.3573	-0.0004
100.0	1	0	1	3.1598	3.1603	-0.0006
39.5	1	0	2	2.4487	2.4495	-0.0008
58.8	1	1	0	2.0679	2.0680	-0.0001
66.3	1	0	3	1.8980	1.8981	-0.0001
10.5	2	0	0	1.7906	1.7909	-0.0003
43.8	1	1	2	1.7605	1.7608	-0.0003
20.2	2	0	1	1.7306	1.7305	0.0001
7.1	0	0	4	1.6787	1.6787	0.0000
7.7	2	0	2	1.5801	1.5802	-0.0000
4.1	1	0	4	1.5197	1.5200	-0.0003
16.0	2	0	3	1.3983	1.3984	-0.0001
6.8	2	1	0	1.3538	1.3538	-0.0000
13.5	2	1	1	1.3271	1.3271	0.0000
6.7	1	1	4	1.3033	1.3033	-0.0000
17.2	1	0	5	1.2576	1.2575	0.0001
6.6	2	1	2	1.2554	1.2556	-0.0002
6.2	3	0	0	1.1940	1.1940	0.0000
13.9	2	1	3	1.1586	1.1584	0.0002
7.4	3	0	2	1.1250	1.1249	0.0000

CELL PARAMETERS

   a= 4.1360 (1) Å   c= 6.7147 (4) Å

under ore microscope. It presents extensive internal reflection from orange to greenish yellow in color. No cleavage is observed.

The data of X-ray powder diffraction for hydrothermally synthetic alabandite (H053) obtained by the Guinier method are shown in Table 8. Its cell parameter obtained by least squares calculation using the data is a=5.2241(9) Å as cubic cell. This value is in very good agreement with a=5.224 Å for synthetic alabandite given in JCPDS card (6-518). Although alabandite is normally considered to have cubic symmetry, alabandite synthesized hydrothermally shows hexagonal crystals of short prismatic form, and some unindexed reflection peaks as cubic cell were observed. Therefore, its symmetry can be thought to have another symmetry such as rhombic or hexagonal. Then, investigation on X-ray single crystal study for this crystal is necessary.

Chalcopyrite, CuFeS$_2$

Hydrothermally synthesized chalcopyrite (H005) is found as pyramidal forms. Under ore microscope, it shows orange yellow with very weak pleochroism

Table 8. The data of X-ray powder diffraction for alabandite (H053) synthesized
hydrothermally

I	h	k	l	d(obs)	d(calc)	Δd
12.9	1	1	1	3.0176	3.0162	0.0014
100.0	2	0	0	2.6124	2.6121	0.0004
45.1	2	2	0	1.8471	1.8470	0.0001
9.2	2	2	2	1.5070	1.5081	-0.0011
4.9	4	0	0	1.3059	1.3060	-0.0001
14.7	4	2	0	1.1685	1.1682	0.0004

CELL PARAMETERS
a= 5.2241 (9) Å

and has week but distinct anisotropism changing its interference color from brownish dark gray to bluish gray. Internal reflection and cleavage are not observed.

The X-ray powder diffraction data of synthetic chalcopyrite (H003) were measured by a Guinier camera, and their results are given in Table 9. Cell parameters refined using least squares calculation are tetragonal, a=5.2901(2) and c=10.4216(6) Å. These values are in good accordance with a=5.2893 and c=10.423 Å of natural chalcopyrite given in JCPDS card (35-752). In the table, calculated d-values using cell parameters are in comparison with of observed values, and both data are in good agrement with each other.

Table 9. The X-ray powder diffraction data for synthetic chalcopyrite (H003)
obtained by hydrothermal synthesis

I	h	k	l	d(obs)	d(calc)	Δd
100.0	1	1	2	3.0399	3.0387	0.0012
3.8	2	0	0	2.6469	2.6450	0.0018
2.7	0	0	4	2.6050	2.6054	-0.0004
50.1	2	2	0	1.8708	1.8703	0.0005
39.8	2	0	4	1.8562	1.8562	0.0000
18.6	3	1	2	1.5927	1.5928	-0.0001
10.7	1	1	6	1.5754	1.5754	0.0000
5.6	4	0	0	1.3225	1.3225	-0.0000
3.1	0	0	8	1.3027	1.3027	0.0000
3.8	3	3	2	1.2126	1.2127	-0.0000
7.6	3	1	6	1.2049	1.2049	-0.0001

CELL PARAMETERS
a= 5.2901 (2) Å, c= 10.4216 (6) Å

Bornite, Cu_5FeS_4

Bornite (H048) synthesized hydrothermally is found as polyhedral forms. Under ore microscope, it shows pinkish brown with violet or orange tint in color, and pleochroism and anisotropism are not observed. No internal reflection and cleavage are also found.

The X-ray powder data for synthetic bornite (H026) were obtained by the Guinier method. Their results are shown in Table 10. Its cell parameter calculated by least squares method using the data is a=10.9544(9) Å as cubic 2A type structure of bornite, but true cell is thought to be orthorhombic (Koto & Morimoto, 1975). Therefore, more detailed investigation of powder pattern of bornite obtained hydrothermal synthesis is necessary.

Table 10. The X-ray powder diffraction data for bornite (H026) obtained by hydrothermal synthesis

I	h	k	l	d(obs)	d(calc)	Δd
36.6	3	1	1	3.3033	3.3029	0.0004
45.6	2	2	2	3.1616	3.1623	-0.0007
35.1	4	0	0	2.7399	2.7386	0.0013
20.4	3	3	1	2.5128	2.5131	-0.0003
6.2	3	3	3	2.1076	2.1082	-0.0006
-	5	1	1	-	2.1082	-0.0006
100.0	4	4	0	1.9359	1.9365	-0.0006
12.2	6	2	2	1.6523	1.6514	0.0008
9.1	8	4	4	1.1180	1.1180	-0.0000

CELL PARAMETERS
    a= 10.9544(9) Å

Nukundamite, $Cu_{3.39}Fe_{0.61}S_4$

Synthetic nukundamite (H034) obtained hydrothermally appears as platy form. Under ore microscope, it shows strong plechroism from light gray with violet tint to brownish orange in color, and has strong anisotropism changing its interference color from light gray, light brown to dark brown. Internal reflection is not observed. Cleavage in parallel to platy plane (001) is sometimes visible.

The data of X-ray powder diffraction of synthetic nukundamite (H038) were measured by the Guinier method, and are given in Table 11. Its cell parameters refined by least squares calculation using all reflection data are hexagonal, a=3.7826(4) and c=11.1919(12) Å. These values are in good accordance with a=3.782 and c=11.187 A for natural nukundamite by Rice *et al.* (1979) and a=3.7820(2) and c=11.1950(8) Å for hydrothermally synthesized sample by Sugaki *et al.* (1981).

Table 11. The data of X-ray powder diffraction for nukundamite (H038)
synthesized hydrothermally

I	h	k	l	d(obs)	d(calc)	Δ d
12. 0	0	0	3	3. 7299	3. 7306	-0. 0007
40. 3	1	0	0	3. 2766	3. 2758	0. 0007
100. 0	1	0	1	3. 1470	3. 1439	0. 0031
79. 6	1	0	2	2. 8274	2. 8271	0. 0003
53. 8	0	0	4	2. 7978	2. 7980	-0. 0001
77. 3	1	1	0	1. 8910	1. 8913	-0. 0003
36. 0	1	0	5	1. 8482	1. 8481	0. 0001
9. 1	0	0	7	1. 5988	1. 5988	-0. 0000

CELL PARAMETERS   (REFINED DATA)

a= 3.7826 (4) Å   c= 11.1918 (12) Å

Proustite, Ag$_3$AsS$_3$

Proustite (H042) synthesized hydrothermally is found as hexagonal polyhedral forms. It shows moderate pleochroism from bluish white to white with bluish tint. It has strong anisotropiam, but its interference color cannot be observed because of its strong internal reflection. Extensive internal reflections from ruby red to orange in color are found. No cleavage is observed.

The X-ray powder diffraction data for hydrothermally synthesized proustite (H042) obtained by the Guinier method are given in Table 12. Its cell parameters calculated by least squares method using the data are hexagonal (rhombic), a=10.8180(4) and c=8.6867(9) Å. These values are similar to a=10.714 and c=8.760 Å for natural proustite given in JCPDS card (11-470), and 10.793(1) A, and 8.676(1) Å for synthetic proustite by Sugaki *et al.* (1978).

Pyrargyrite, Ag$_3$SbS$_3$

Synthetic pyrargyrite (H040) obtained hydrothermally appears as granular polyhedral form. Under ore microscope, it shows moderate pleochroism from bluish gray to grayish white in color. It has strong anisotropism, but interference colors cannot be completely observed because of its extensive internal reflection which is from pinkish orange to ruby red in color. Cleavage is not observed.

The data of X-ray powder diffraction for hydrothermally synthesized pyrargyrite (H040) measured by Guinier method are shown in Table 13. Its cell parameters refined by least squares calculation using the data are hexagonal (rhombic), a=11.0500(3) and c=8.7271(13) Å. These values are slightly longer than a=11.047 and c=8.719 A for synthetic sample given in JCPDS card (21-1173), and a=11.030 (1) and c=8.705 (1) Å for synthetic specimen by Sugaki *et al.* (1978).

Table 12. The data of X-ray powder diffraction for synthetic proustite (H042) obtained by hydrothermal synthesis

I	h	k	l	d(obs)	d(calc)	Δd
17.1	1	1	0	5.4103	5.4090	0.0013
72.8	2	1	1	3.2800	3.2796	0.0004
62.4	2	0	2	3.1882	3.1869	0.0013
62.6	3	0	0	3.1232	3.1229	0.0003
66.1	1	2	2	2.7475	2.7458	0.0017
6.9	2	2	0	2.7062	2.7045	0.0017
47.8	1	1	3	2.5565	2.5551	0.0015
100.0	1	3	1	2.4912	2.4897	0.0016
22.1	3	1	2	2.2309	2.2305	0.0004
16.6	3	2	1	2.0867	2.0865	0.0002
7.2	4	1	0	2.0445	2.0444	0.0001
6.8	0	2	4	1.9723	1.9721	0.0002
33.1	2	3	2	1.9270	1.9268	0.0002
9.2	2	1	4	1.8536	1.8528	0.0008
7.2	3	3	0	1.8023	1.8030	-0.0007
15.1	2	4	1	1.7348	1.7349	-0.0002
16.4	5	0	2	1.7211	1.7208	0.0003
12.8	1	3	4	1.6676	1.6675	0.0002
23.3	4	0	4	1.5932	1.5935	-0.0003
11.0	6	0	0	1.5612	1.5615	-0.0002
–	1	2	5	–	1.5612	0.0000
6.7	4	3	1	1.5169	1.5166	0.0003
11.1	5	2	0	1.5003	1.5002	0.0001
7.2	7	1	3	1.1407	1.1408	-0.0001
4.8	3	3	6	1.1295	1.1297	-0.0002

CELL PARAMETERS
   a= 10.8180 (4) Å   c= 8.6997 (9) Å

Famatinite, Cu₃SbS₄

   Famatinite (H045) synthesized hydrothermally is found as granular aggregates of polyhedral crystals. Under ore microscope, it shows strong pleochroism from pale purplish pink to pinkish gray in color and strong anisotropism changing its interference color from bluish dark gray to yellowish brown. Synthetic famatinite has polysynthetic twinning similar to natural famatinite (Uytenbogaadt & Burke, 1971; Picot & Johan, 1982). Internal reflections and cleavage are not observed.

   The X-ray powder diffraction data for hydrothermally synthesized famatinite (H045) were obtained by the Guinier method, and their results are given in Table 14. Its cell parameters calculated least squares method using the data are tetragonal, a=5.3860 (2) and c=10.7517 (6) Å. These values are in good agreement with a=5.3853 (1) and c=10.7483 (4) Å for synthetic famatinite by Sugaki *et al.* (1982), and those or natural specimen by Berry & Thompson (1962).

Table 13. The X-ray powder diffraction data for pyrargyrite (H040) synthesized
hydrothermally

I	h	k	l	d(obs)	d(calc)	Δ d
74.7	1	0	0	3.5824	3.5819	0.0006
78.5	0	0	2	3.3570	3.3573	-0.0004
100.0	1	0	1	3.1598	3.1603	-0.0006
39.5	1	0	2	2.4487	2.4495	-0.0008
58.8	1	1	0	2.0679	2.0680	-0.0001
66.3	1	0	3	1.8980	1.8981	-0.0001
10.5	2	0	0	1.7906	1.7909	-0.0003
43.8	1	1	2	1.7605	1.7608	-0.0003
20.2	2	0	1	1.7306	1.7305	0.0001
7.1	0	0	4	1.6787	1.6787	0.0000
7.7	2	0	2	1.5801	1.5802	-0.0000
4.1	1	0	4	1.5197	1.5200	-0.0003
16.0	2	0	3	1.3983	1.3984	-0.0001
6.8	2	1	0	1.3538	1.3538	-0.0000
13.5	2	1	1	1.3271	1.3271	0.0000
6.7	1	1	4	1.3033	1.3033	-0.0000
17.2	1	0	5	1.2576	1.2575	0.0001
6.6	2	1	2	1.2554	1.2556	-0.0002
6.2	3	0	0	1.1940	1.1940	0.0000
13.9	2	1	3	1.1586	1.1584	0.0002
7.4	3	0	2	1.1250	1.1249	0.0000

CELL PARAMETERS
a= 11.0500 (3) Å   c= 8.7271 (13) Å

Enargite, Cu₃AsS₄

$Enargite, Cu_3AsS_4$

Synthetic enargite (H046) obtained hydrothermally appears as long prismatic
forms. Under ore microscope, it shows distinct pleochroism pinkish gray to light
gray with pinkish tint in color, and strong anisotropism changing its interference
color from light brown to pale bluish gray. Internal reflection is not observed.
Sometimes, cleavage is found parallel to elongation.

The data of X-ray powder diffraction for enargite (H046) synthesized
hydrothermally were measured by the Guinier method. Their results are given in
Table 15, and its cell parameters calculated using the data are orthorhombic,
a=6.4325 (5), b=7.4042 (8) and c=6.1499 (4) Å. These values are also in good
accordance with a=6.41, b=7.42 and c=6.15 Å for natural enargite by Berry and
Thompson (1962), and a=6.4313 (3), b=7.4017 (3), and c=6.1487 (3) Å for
synthetic enargite by Sugaki *et al.* (1982).

Table 14. The X-ray powder diffraction data for synthetic famatinite (H045)
obtained by hydrothermal synthesis

I	h	k	l	d(obs)	d(calc)	Δd
8.9	1	0	1	4.8181	4.8155	0.0026
2.3	1	1	0	3.8071	3.8084	-0.0013
100.0	1	1	2	3.1087	3.1076	0.0011
5.7	1	0	3	2.9823	2.9837	-0.0015
29.5	2	0	0	2.6938	2.6930	0.0008
2.3	2	0	2	2.4084	2.4078	0.0007
5.8	2	1	1	2.3506	2.3504	0.0002
42.6	2	0	4	1.9027	1.9024	0.0002
24.3	3	1	2	1.6238	1.6237	0.0002
15.4	1	1	6	1.6214	1.6214	-0.0001
4.7	2	2	4	1.5538	1.5538	-0.0000
10.9	4	0	0	1.3463	1.3465	-0.0002
4.1	0	0	8	1.3440	1.3440	0.0000
5.7	3	3	2	1.2356	1.2355	0.0001
15.0	3	1	6	1.2345	1.2345	-0.0000
2.6	4	2	0	1.2043	1.2043	-0.0000

CELL PARAMETERS
    a= 5.3860 (2) Å   c= 10.7517 (6) Å

4. Conclusion

Some sulfide and sulfosalt minerals, such as pyrrhotite, covellite, stibnite, sphalerite, galena, greenockite, alabandite, chalcopyrite, bornite, nukundamite, proustite, pyrargyrite, famatinite and enargite were synthesized hydrothermally ant 350° and 300°C of temperature, and 300 kgf of pressure.

Optical properties such as reflection color, pleochroism, anisotropism, internal reflection and cleavage for synthetic products were observed under ore microscope.

X-ray powder diffraction data for hydrothermally synthesized sulfide and sulfosalt minerals were measured using a Guinier camera. The intensities and positions for each reflection were obtained using a microphotometer. Their cell parameters for the synthetic minerals refined by least squares calculation using all reflection data are following.

pyrrhotite ($Fe_{1-x}S$): hexagonal, a=3.4506(6), c=5.7557(6) Å,
covellite (CuS): hexagonal, a=3.7911(3), c=16.3452(19) Å,
stibnite (Sb_2S_3): orthorhombic, a=11.2285(4), b=11.3113(7), c=3.8373(2) Å,
sphalerite (ZnS): cubic, a=5.4108(2) Å
galena (PbS): cubic, a=5.9365(2) Å,

Table 15. The data for X-ray powder diffraction for enargite (H046) synthesized
hydrothermally

I	h	k	l	d(obs)	d(calc)	Δd
50.6	2	0	0	3.2153	3.2163	-0.0009
67.6	1	2	0	3.2074	3.2086	-0.0012
100.0	0	0	2	3.0744	3.0750	-0.0006
46.9	2	0	1	2.8493	2.8500	-0.0008
93.8	1	2	1	2.8437	2.8447	-0.0010
13.3	2	0	2	2.2220	2.2226	-0.0006
25.4	1	2	2	2.2194	2.2201	-0.0006
4.9	1	0	3	1.9535	1.9532	0.0003
35.3	3	2	0	1.8550	1.8554	-0.0004
24.2	0	4	0	1.8505	1.8511	-0.0006
3.6	1	3	2	1.8437	1.8440	-0.0003
2.8	3	0	2	1.7586	1.7588	-0.0003
77.0	2	0	3	1.7282	1.7287	-0.0005
-	1	2	3	-	1.7275	0.0007
3.3	4	0	0	1.6082	1.6081	0.0001
7.8	2	4	0	1.6048	1.6043	0.0005
20.6	0	4	2	1.5863	1.5859	0.0005
9.3	4	0	1	1.5559	1.5558	0.0001
5.3	2	4	1	1.5522	1.5524	-0.0002
3.2	2	1	4	1.3633	1.3634	-0.0001
17.1	4	0	3	1.2654	1.2653	0.0002
18.2	2	4	3	1.2634	1.2634	0.0000
11.6	1	1	5	1.1923	1.1923	-0.0001
-	5	2	1	-	1.1922	0.0001
25.3	2	0	5	1.1487	1.1488	-0.0001
-	1	2	5	-	1.1485	0.0002
2.2	4	4	2	1.1290	1.1292	-0.0001

CELL PARAMETERS
 a= 6.4325 (5) Å   b= 7.4042 (8) Å   c= 6.1499 (4) Å

greenockite (CdS): hexagonal, a=4.1360(1), c=6.7147(4) Å,
alabandite (MnS): cubic, a=5.2241(9) Å,
chalcopyrite (CuFeS$_2$): tetragonal, a=5.2901(2), c=10.4216(6) Å,
bornite (Cu$_5$FeS$_4$): cubic, a=10.9544(40 Å,
nukundamite (Cu$_{3.39}$Fe$_{0.61}$S$_4$): hexagonal, a=3.7826(40, c=11.1918(12) Å,
proustite (Ag$_3$AsS$_3$): hexagonal, a=10.8180(4), c=8.6867(9) Å,
pyrargyrite (Ag$_3$SbS$_3$): hexagonal, a=11.0500(3), c=8.7271(13) Å,
famatinite (Cu$_3$SbS$_4$): tetragonal, a=5.3860(2), c=10.7517(6) Å,
enargite (Cu$_3$AsS$_4$): orthorhombic, a=6.4325(5), b=7.4042(8), c=6.1499(4) Å.

Acknowledgment

The authors wish to express their thanks to Dr. Marcos Pincheira, Sr. Osvaldo Rabbia, Dra. Ursula Kelm and Sra. Vilma Sanhueza in the GEA, University of Concepcion for their help in the hydrothermal experiment works.

References

Berry, L.G. & Thompson, R.M. (1962) X-ray powder data for ore minerals. Geol. Soc. Amer., Mem., 78, 85.

JCPDS (1986) Mineral Diffraction File, Data Book. Int. Nat. Center for Diffraction Data, Swarthmore, Pa., U.S.A.

Koto, K. & Morimoto, N. (1975) Superstructure investigation of bornite, Cu_5FeS_4 by the modified partial Patterson function. *Acta Cryst.*, B31, 2268-2273.

Kitakaze, A. (1992) Guinier film reading and calculation system. In T*extbook for Instrumental Analyses on Economic Geology and Related Sciences,* ed. A. Sugaki No. 2, JICA, pp. 47-72.

Kullerud, G. (1971) Experimental techniques in dry sulfide research. In *Research Techniques for High Pressure and High Temperature,* ed. G.C. Ulmer, Springer-Verlag, New York, 288-315.

Picot, P. & Johan, Z. (1982) Atlas of Ore Minerals. Elsevier Sci. Pub. Co., p. 180 (Famatinite).

Rice, C.M., Atkin, D., Bowles, J.F.W. & Criddle, A.J. (1979) Nukundamite a new mineral, and idaite. *Miner. Mag.,* 43, 193-200.

Scott, S.D. (1974) Experimental methods in sulfide synthesis. In *Sulfide Mineralogy* ed. P.H. Ribbe, Miner, Soc. Amer. Short Course Notes, 1,S1-S38.

Scott, S.D. & Barnes, H.L. (1971) Sphalerite geothermometry and geobarometry. *Econ. Geol.,* 66, 653-669.

Sugaki, A. (1992) Synthetic method of sulfide minerals -evacuated glass- tube method. In *Textbook for Instrumental Analyses on Economic Geology and Related Sciences,* ed. A. Sugaki, JICA, N° 2, 73-105.

Sugaki, A., Shima, H. Kitakaze, A. & Harada, H. (1975) Isothermal phase relations in the system Cu-Fe-S under hydrothermal conditions at 350° and 300°C. *Econ. Geol.,* 70, 806-823.

Sugaki A., Shima, H., Kitakaze, A. & Fukuoka, M. (1977) Hydrothermal synthesis of pyrrhotite and their phase relation at low temperature. *Sci. Rept. Tohoku Univ.,* Ser III, 13, 165-182.

Sugaki, A., Shima, H. & Kitakaze, A. (1978) Synthesized silver antimony and silver arsenic sulfosalt minerals. *Sci. Rept. Tohoku Univ.,* Ser. III, 14, 53-65.

Sugaki, A., Shima, H., Kitakaze, A. & Mizota, T. (1981) Hydrothermal synthesis of nukundamite and its crystal structure. *Amer. Miner.,* 66, 398-402.

Sugaki, A. Kitakaze, A. & Shimizu, Y. (1982) Phase relations in the Cu_3AsS_4-Cu_3SbS_4 join. *Sci. Rept. Tohoku Univ.,* Ser. III, 15, 257-271.

Sugaki, A., Kitakaze, A., & Hayashi, K. (1984) Hydrothermal synthesis and phase relations of the polymetallic sulfide system, especially on the Cu-Fe-Bi-S systems. In *Material Science of the Earths Interior,* ed. I. Sunagawa, Terra Pub. Co., Tokyo, 545-583.

Uytenbogaadt, W. & Burke, E.A.J. (1971) Tables for Microscopic Identification of ore Minerals, Dover Pub Inc., New York, pp. 64-65 (Galena), pp. 110-111 (Famatinite).

EXAMINATIONS FOR SULFIDE MINERALS SYNTHESIZED HYDROTHERMALLY BY SCANNING ELECTRON MICROSCOPE

Asahiko Sugaki*, Arashi Kitakaze** and Morihiro Aoki***
*Kadan 4-30-503, Aoba, Sendai 980, Japan. **Faculty of Science, Tohoku University, Aramaki-Aoba, Sendai 980, Japan. ***Miyagi University of Education, Aramaki-Aoba, Sendai 980, Japan.

Abstract

Some sulfide and sulfosalt minerals have been synthesized using thermal gradient transport method. Sulfide minerals synthesized previously using an evacuated silica glass tube method are employed as nutrient material. The synthetic experiments were carried out under the hydrothermal conditions of temperature 300-350°C and pressure 300 kgf, using aqueous solution of 5m ammonium chlorite as solvent. Then, sulfide and sulfosalt minerals such as pyrrohotite, pyrite, chalcocite, covellite, stibnite, bismuthinite, sphalerite, galena, greenockite, alabandite, chalcopyrite, bornite, nukundamite, proustite, pyrargyrite, famatinite, enargite and tennantite were synthesized as euhedral crystals.

Morphological observations under a scanning electron microscope were carried out for hydrothermally synthesized sulfide minerals. Morphological characteristics for crystal forms, appeared face and twinning etc. are explained.

1. Introduction

Sulfide and sulfosalt minerals are main constituents in ore deposits. They were usually deposited from hydrothermal ore solution. Then, hydrothermal synthesis is one of important experiments to make clear the ore forming environment. Some information of ore forming conditions can be obtained in comparison with morphological characteristic between synthetic and natural minerals.

Hydrothermal synthesis of sulfide and sulfosalt minerals were performed using thermal gradient transporting method described by Scott & Barnes (1971), Scott (1974), Sugaki et al. (1975, 1977, 1984) and Vaughan & Craig (1978). As nutrient material, powdered sulfide minerals synthesized previously by means of an evacuated silica glass method (Kullerud, 1971; Scott, 1974, Sugaki, 1992) were used. Aqueous solution of 5m ammonium chloride was used as solvent. As reaction vessel, a gold tube of 3.5 mm in outside diameter with 0.15 mm thickness, and about 50 mm in length was employed. Hydrothermal synthesis was performed under hydrothermal conditions of 300 to 350°C of temperature and 300 kgf of pressure. The synthetic products were found as crystal aggregates of euhedral form as same minerals as nutrient materials. Sulfide and sulfosalt minerals such as pyrrhotite, pyrite, chalcocite, covellite, stibnite, bismuthinite, sphalerite, galena, greenockite, alabandite, chalcopyrite, bornite, nukundamite, proustite, pyrargyrite, famatinite, enargite and tennantite were successfully synthesized.

Morphological characteristics of synthetic minerals were observed under a scanning electron microscope (SEM) of JEOL type JSM-5300. Mineral samples were not coated by any metals, because of obseved minerals having electro conductivity. Accelerating voltage of SEM was normally 20 to 30 kV. At high magnification, pictures can be obtained at high accelerating voltage (normally 30 kV).

Observation results of morphology, appearing faces, twinning and growth feature for SEM photomicrographs of the minerals synthesized hydrothermally will be described below.
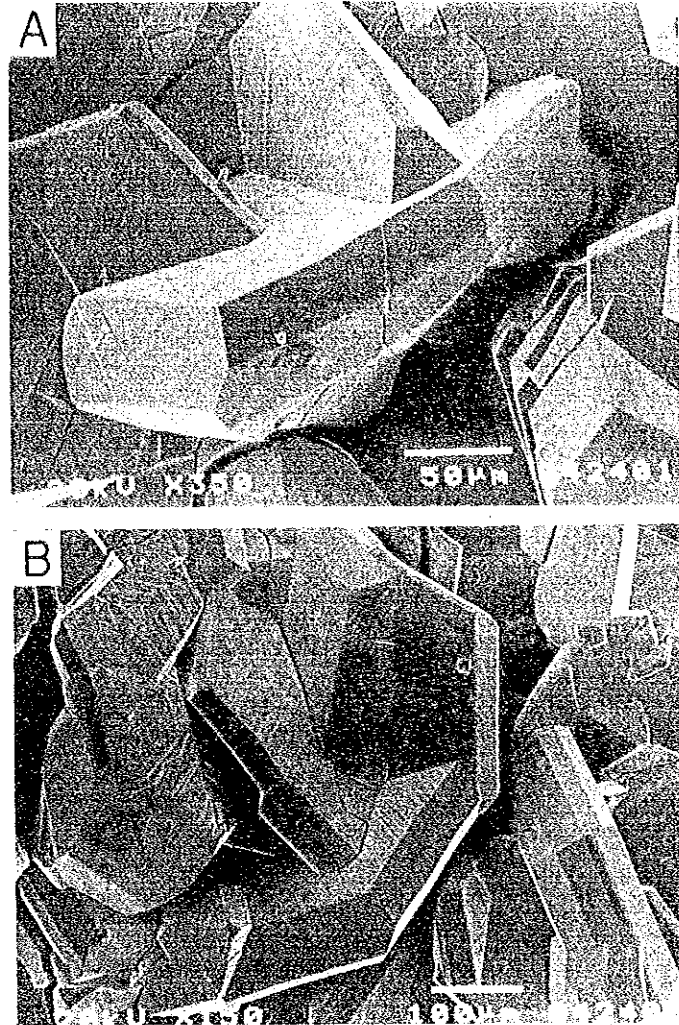
Fig. 1. Secondary electron micrographs of pyrrhotite synthesized
        hydrothermally at 300°C, 300 kgf (H015).
        A, B: Hexagonal platy crystals of pyrrhotite.

2. Observation Results

Pyrrhotite

Pyrrhotite appears as aggregates of well-formed hexagonal tabular to platy crystal (Fig. 1 A, B) as seen in Sugaki *et al.* (1977, 1984). Basal (001) face, hexagonal (102) pyramid and hexagonal (100) prism are usually found in synthetic crystals. Hexagonal (201) pyramid is sometimes observed as seen in Fig. 1B. The spiral growth steps are commonly found on the surface of basal (001) plan.

99
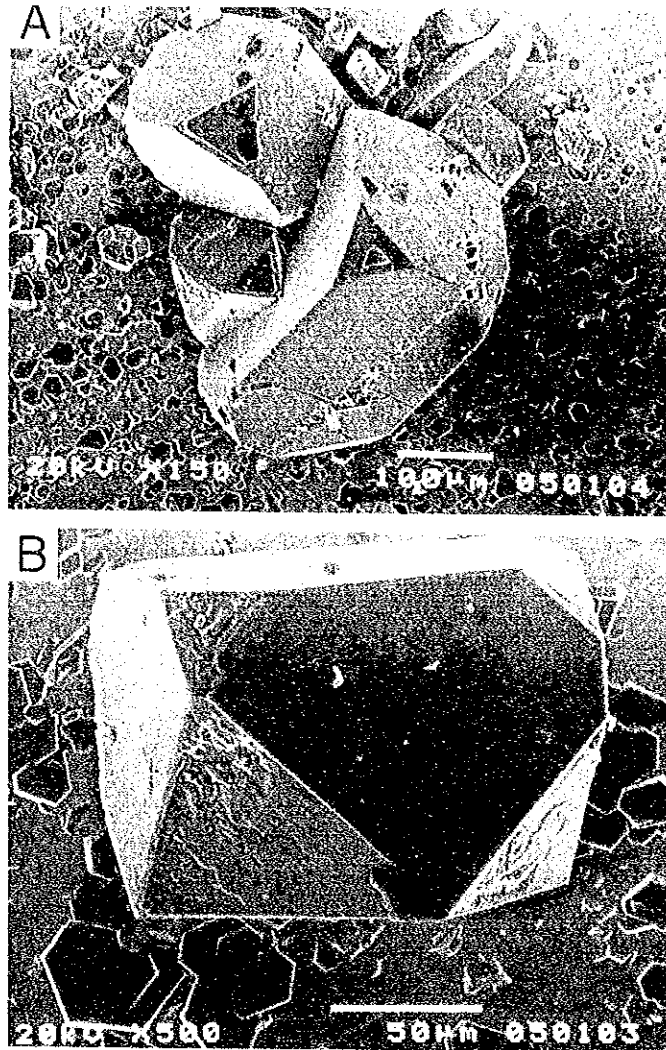
Fig. 2. Secondary electro micrographs of pyrite synthesized
hydrothermally at 350° C, 300 kgf (H017).
A, B: Cubo-octahedral crystals of pyrite.

Pyrite

Pyrite is found as cubo-octahedral forms and its aggregates (Fig. 2 A, B) as
same as reported by Sugaki *et al.* (1977, 1984). Two planes of basal (100), and
cubic pyramid (111) are usually appeared. Normally, basal (100) face develops
lather than (111) face (Fig. 2A). But, both faces are sometimes found as about
similar size (Fig. 2B). Growth steps are normally observed on the (111) face.
Parallel striations commonly found in natural pyrite (Palache *et al.*, 1949) can not
be occurred.
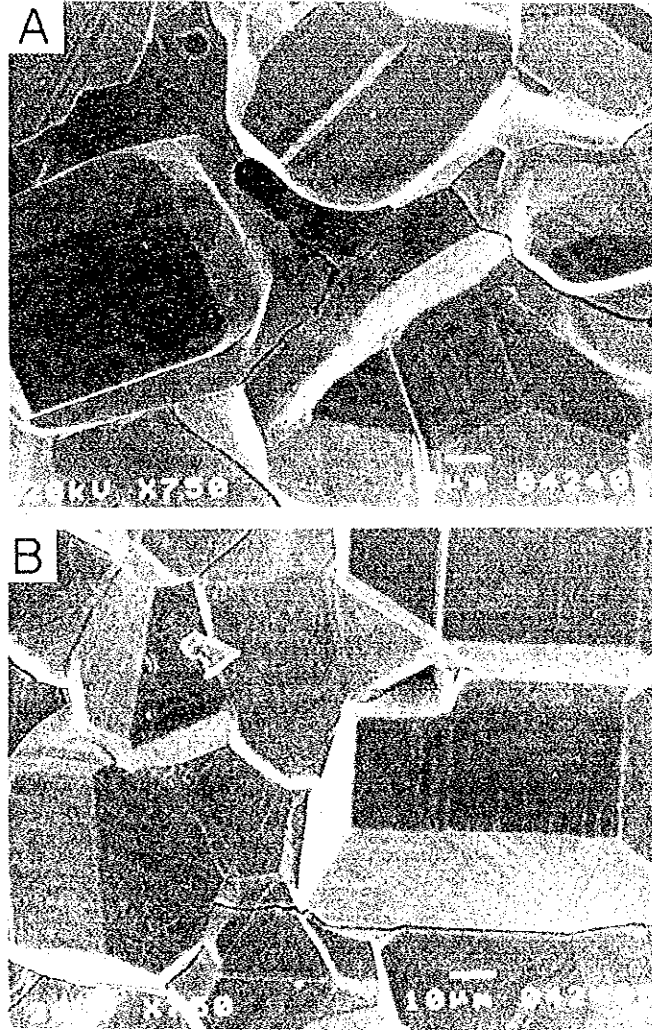
Fig. 3. SEM micrographs of chalcocite synthesized at 300°C,
300 kgf (H014).
A, B: Polyhedral crystals of chalcocite.

Chalcocite

Chalcocite is found as aggregates of polyhedral short prismatic or thick tabular crystals (Fig. 3A, B). Basal (001) face and pyramids of (101) and (011) normally appear. Sometimes prism faces of (100) and (010) are found as small size. Striation or exsolution lamellae are observed on the surface of (110), (101) and (001) faces (Fig. 3B).
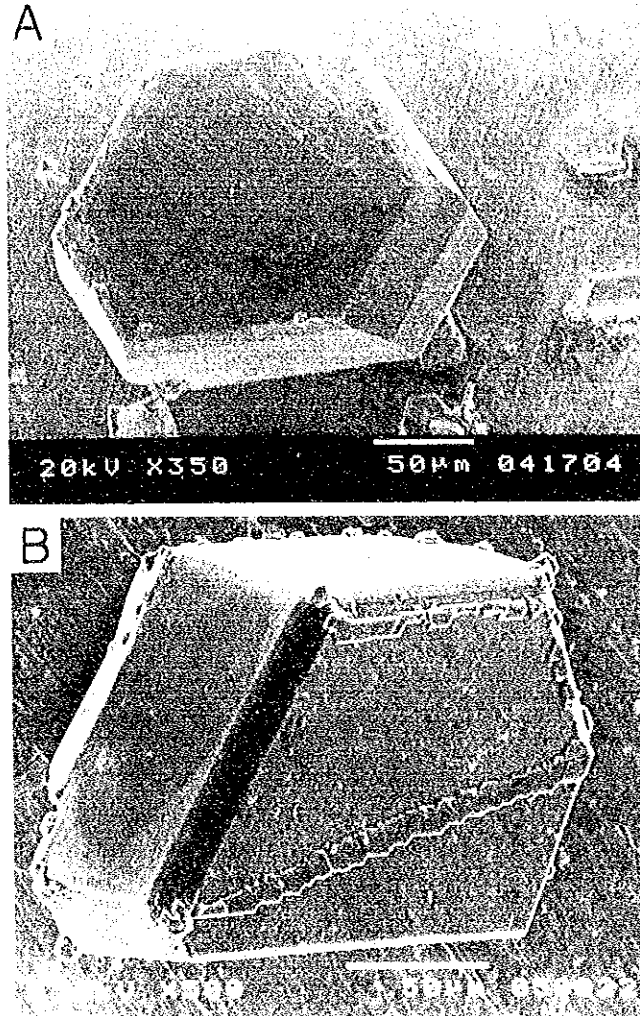
Fig. 4. SEM micrographs of covellite synthesized hydrothermally.
A: Hexagonal platy crystal (H004, 350°C, 300 kgf).
B: Hexagonal tabular crystal (H021, 300°C, 300 kgf).

Covellite

Covellite appears as hexagonal tabular to platy form as seen in Fig. 4A, B. Basal pinacoid (001) and hexagonal prism (100) appear usually as well developed face. Hexagonal (101) prism face is also found in almost crystal. Growth step of hexagonal form is observed on basal (001) pinacoid face.

102
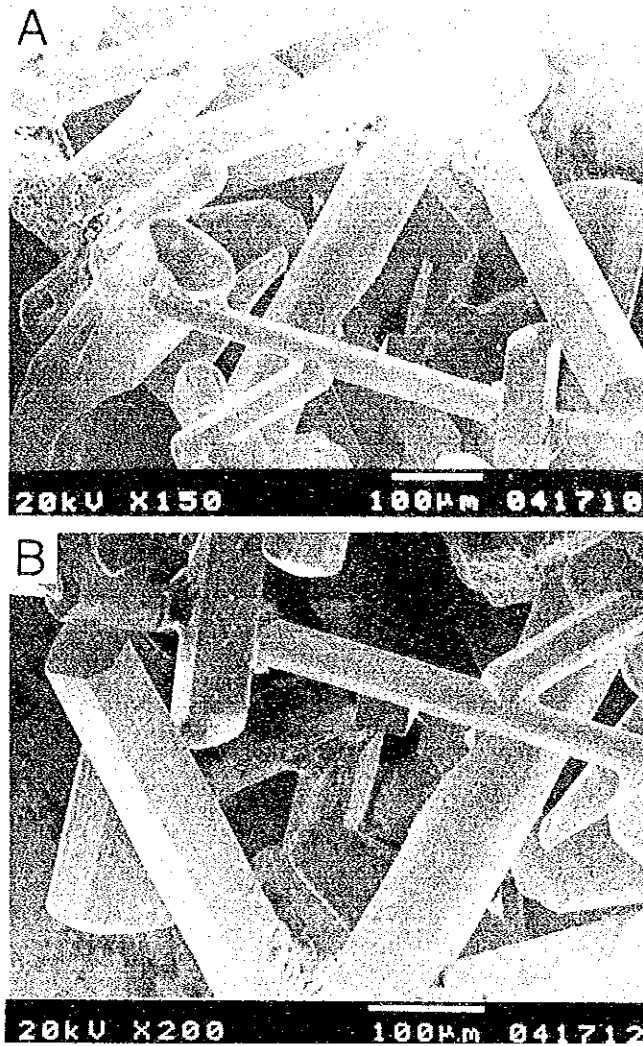
Fig. 5. SEM micrographs of stibnite synthesized hydrothermally at 350°C, 300 kgf (H002).
A, B: Long prismatic crystals of stibnite.

Stibnite

Stibnite is found as irregular aggregates of prismatic crystal elongated to c-axis (Fig. 5A, B). Prism faces of (110), (010) and (210) are usually observed. Top of prismatic crystal is rounded, and then clear face is not seen. But rhombic prism (111) is rarely found in some crystals.
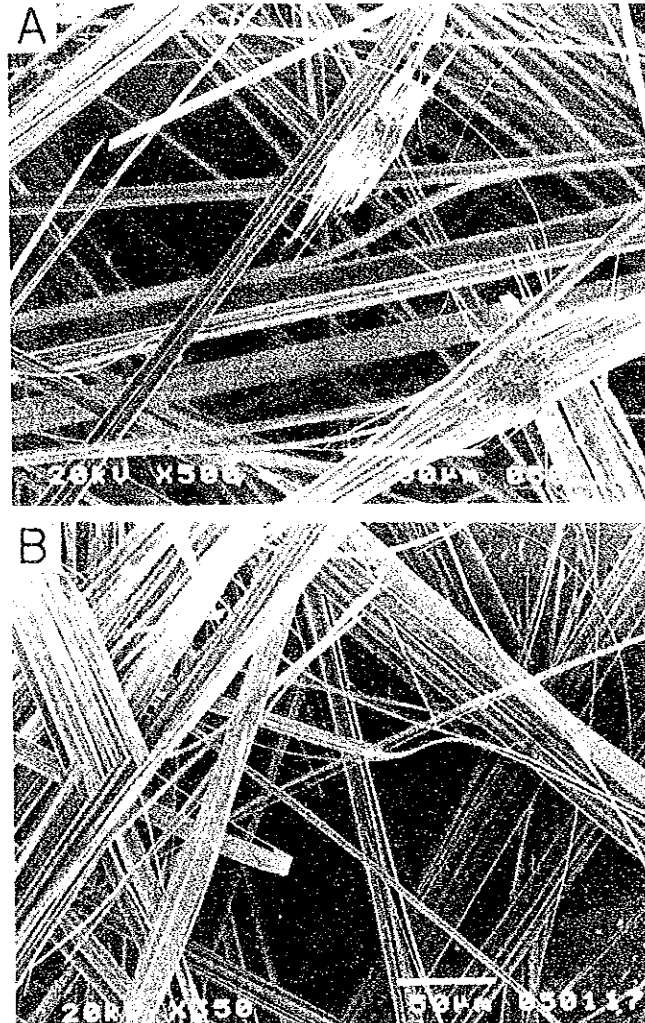
Fig. 6. SEM micrographs of bismuthinite synthesized
hydrothermally at 350°C, 300 kgf (H016).
A, B: Acicular crystals of bismuthinite.

Bismuthinite

Bismuthinite shows parallel aggregates of acicular to fibrous crystal elongated
to c-axis as seen in Fig. 6A, B. It is sometimes foliated. Striations in parallel to c-
axis are observed usually.

104
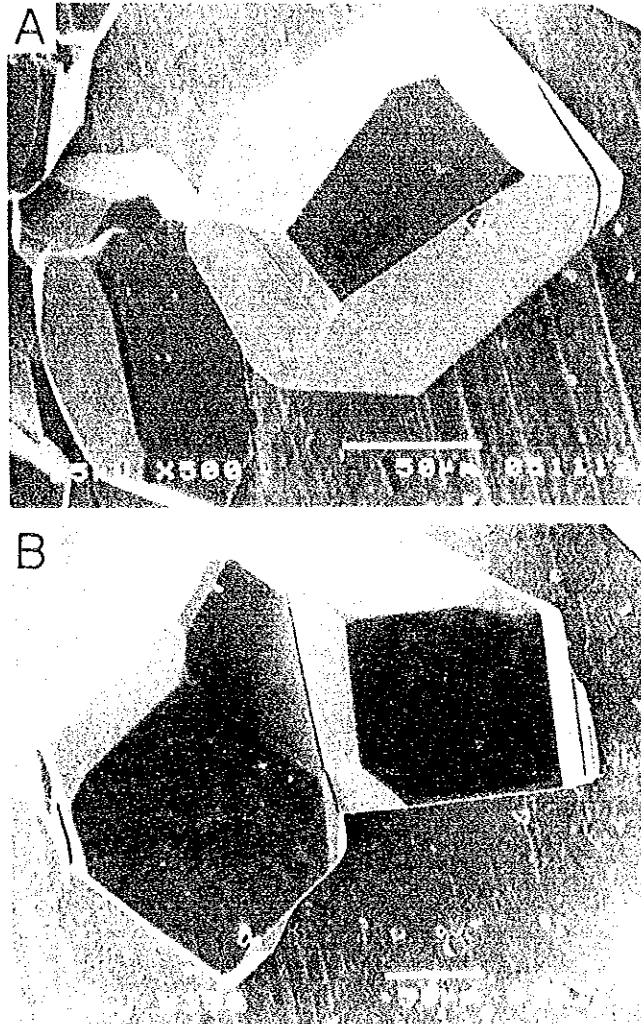
Fig. 7. SEM micrographs of sphalerite synthesized
hydrothermally at 350°C, 300 kgf.
A, B: Polyhedral crystals of sphalerite.

Sphalerite

Sphalerite is observed as cubic polyhedral crystals (Fig. 7A, B). It is normally found as basal pinacoid (100) and prism (110) planes. Although naturally occurring sphalerite develops cubic pyramid (111) as seen in textbook by Palache *et al.* (1949), this face is found as small plane in hydrothermally synthetic sphalerite. Crystal surface is very clear, then growth step or striation can not be observed.
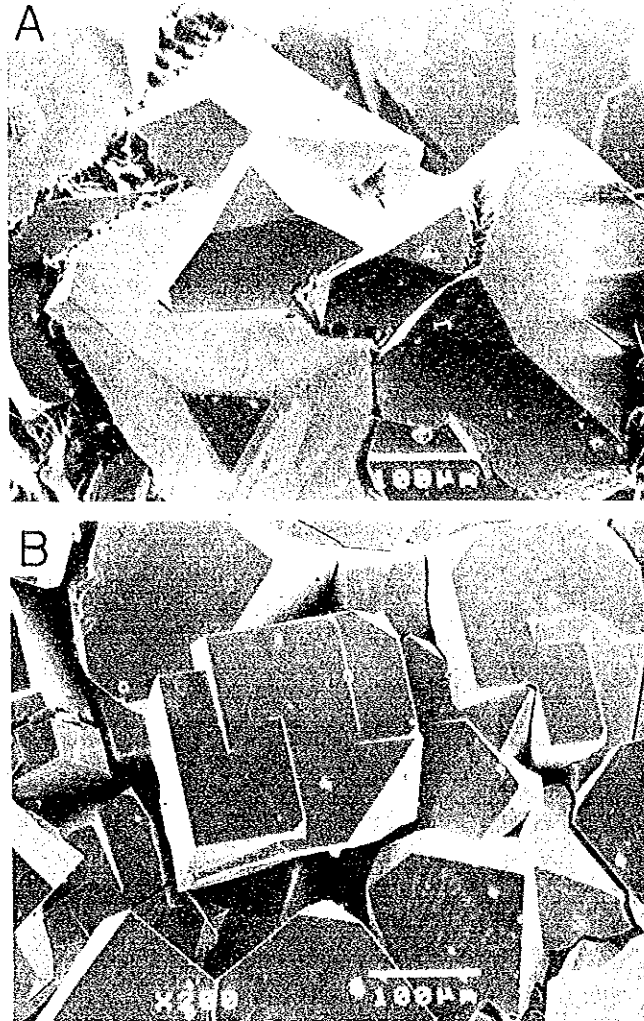
Fig. 8. SEM micrographs of galena synthesized hydrothermally.
A: Cubo-octahedral crystals of galena (H043, 300°C, 300 kgf).
B: Cubic crystal of galena (H047, 350°C, 300 kgf).

Galena

Galena appears as crystal aggregates of cubic or cubo-octahedral form (Fig. 8A, B), similar to naturally occurring form (Palache *et al.*, 1949). Cubic face (100) is commonly dominant plane. Cubic prism (111) face is observed in almost crystal, but some crystal is lack this face (Fig. 8B). Spiral growth step is sometimes found on (100) face.
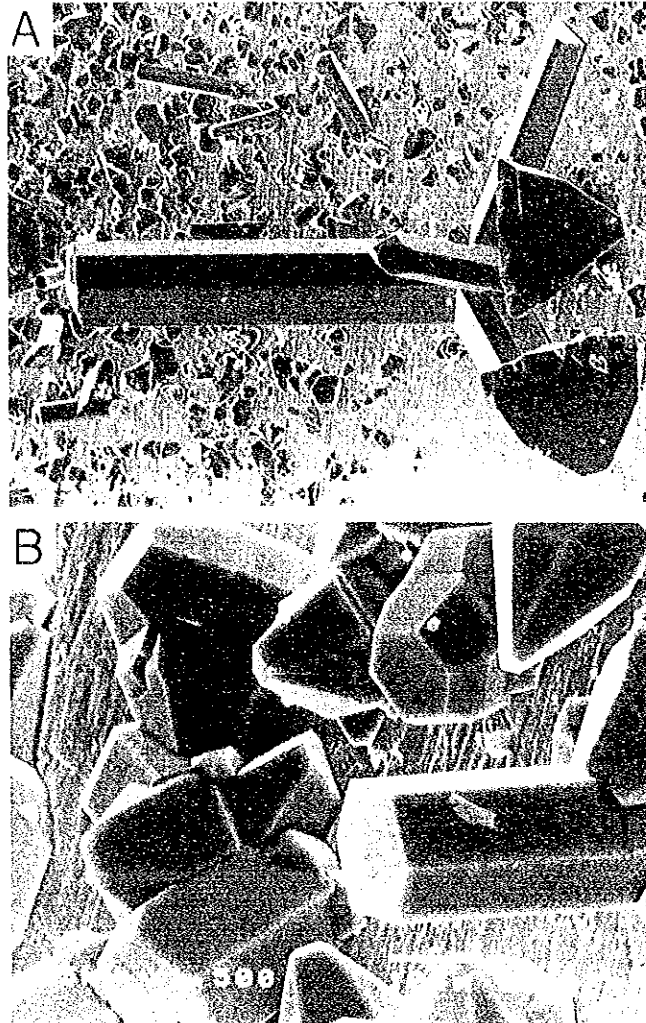
Fig. 9. SEM micrographs of greenockite synthesized
hydrothermally at 350°C, 300 kgf (H027).
A: Long prismatic crystals of greenockite.
B: Hexagonal short prismatic and hemimorphic twinned
crystals of greenockite.

Greenockite

Greenockite appears as hexagonal prismatic to hemimorphic pyramidal crystal (Fig. 9A, B). Basal (001) and (100) prism faces are commonly observed in hexagonal prismatic crystals. Prism face (503), and growth twinning on (102) plane showing L letter shape is sometimes observed as seen in Fig. 9A. Hexagonal prism (503) face often develops, and crystal shows hexagonal hemimorphic form (Fig. 9B) as seen in natural crystal (Palache *et al.*, 1949, Ahlfeld & Muñoz, 1955). Twinned crystals on (112) are often found as seen in Fig. 9B. It is similar to natural twinning from the Llallgua mine, Bolivia (Ahlfeld & Muñoz, 1955).
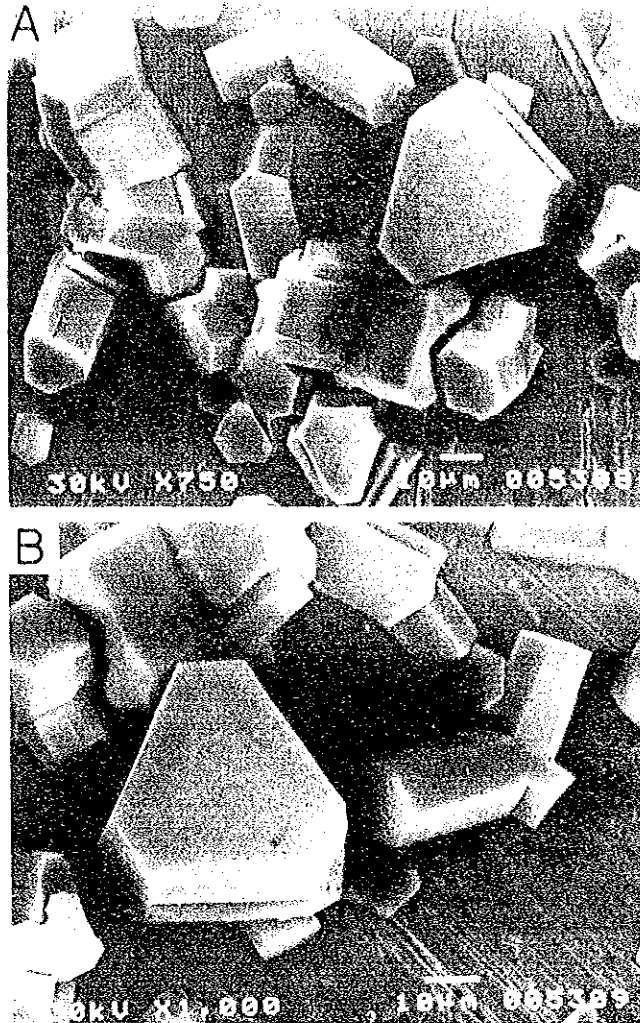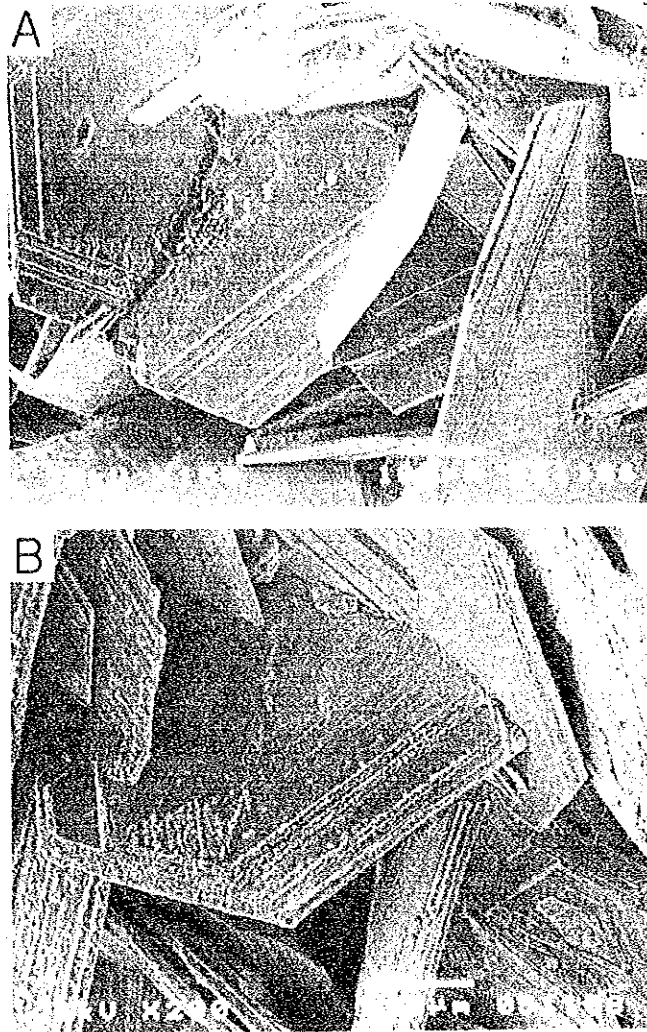
Fig. 10. SEM micrographs of alabandite synthesized
hydrothermally at 350°C, 300 kgf (H053).
A, B: Hexagonal prismatic crystals of alabandite.

Alabandite

Alabandite is belonging to cubic crystal system, but synthetic alabandite is
found as hexagonal prismatic form (Fig. 10 A, B). Basal plane of prismatic crystal
is thought to be cubic (111) pyramid face. Meanwhile, prism planes of prismatic
crystal are assumed corresponding to cubic (100) and (111). Twinning on (111)
as L letter shape is often observed. Hexagonal prismatic crystal is thought to
appear as very thin platy aggregate of polysynthetic lamellar twinning on (111)
plane (Palacheh *et al.*, 1949).

Fig. 11. SEM micrographs of chalcopyrite synthesized
hydrothermally at 350°C, 300 kgf (H003).
A, B: Tetrahedral crystals of chalcopyrite showing
striation.

Chalcopyrite

Chalcopyrite is found as crystal aggregates of tetrahedral form as seen in Fig.
11A, B. Tetragonal (112) pyramid with spheroidal form usually appears as most
development face with rough surface, and has many striations in parallel to (110)
direction. Small (001) and (101) are observed in Fig. 11B. Growth twinning on
(112) is sometimes found in some crystals. Triangular or trapezoidal growth steps
are found on (001) face.

109
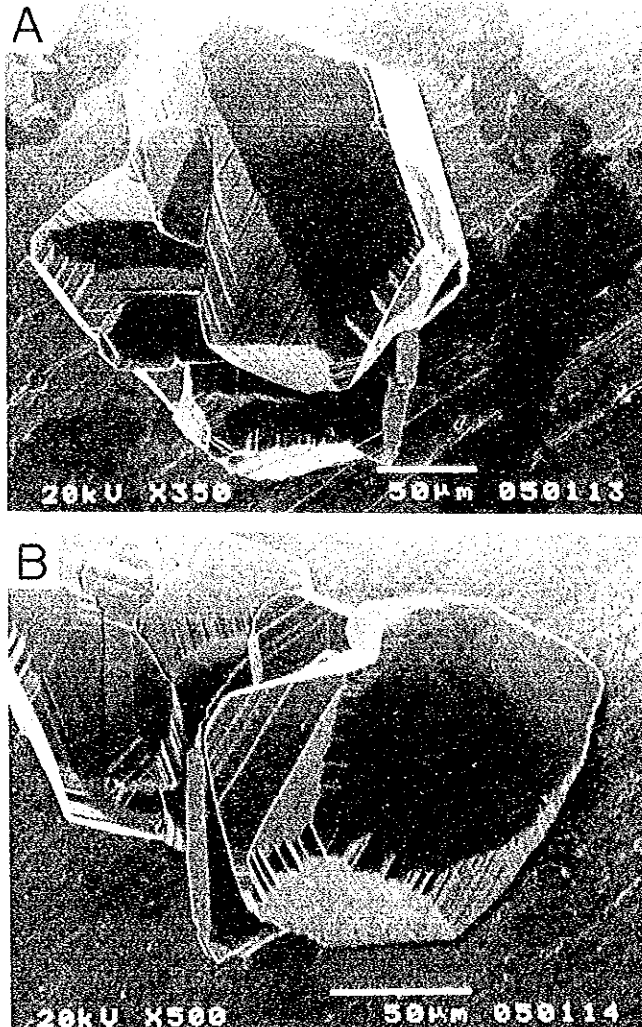
Fig. 12. SEM micrographs of bornite synthesized hydrothermally at 300°C, 300 kgf.
A, B: Cubo-octahedral crystals of bornite.

Bornite

Bornite is found as crystal aggregate of cubo-octahedral form (Fig. 12 A, B). It principally consists of (100) face accompanied with (111) face. On the (111) face, triangular growth steps are usually observed. Like rough (110) face was found characteristically in bornite crystal, and consists of growth steps composed with (110) and (111) faces.

Fig. 13. SEM micrographs of nukundamite synthesized
hydrothermally at 350°C, 300 kgf (H034).
A, B: Hexagonal platy crystals of nukundamite.

Nukundamite

Nukundamite appears as crystal aggregates of hexagonal platy form (Fig. 13
A, B) as same as reported by Sugaki *et al.* (1981, 1984). Basal (001) is well
development, and thin (100) prism is found. Hexagonal or trapezoidal growth
steps are usually observed on (001) plane.

111
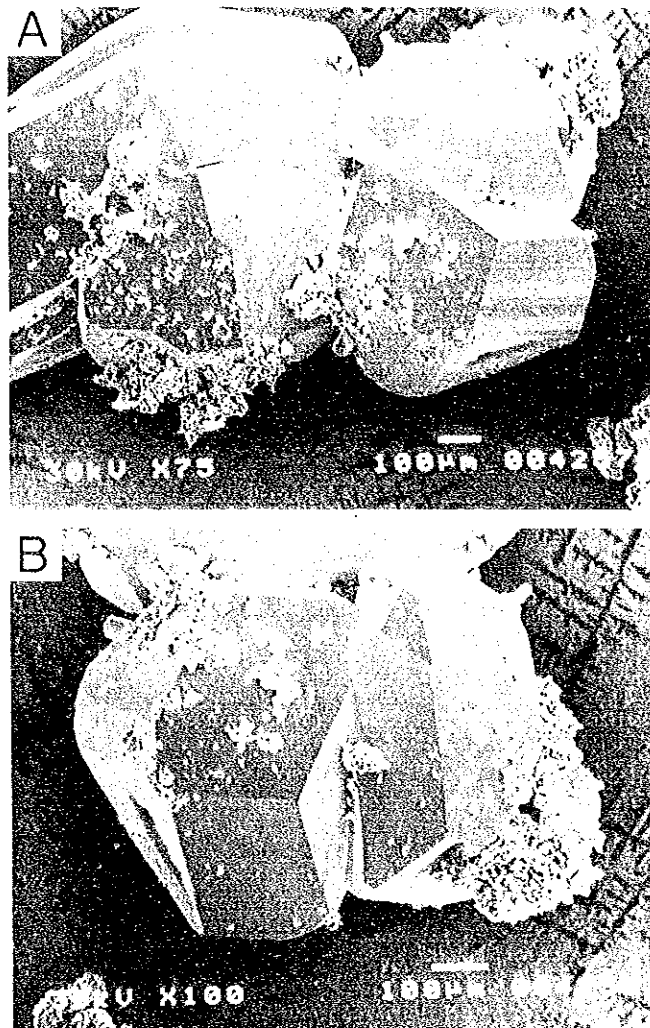
Fig. 14. SEM micrographs of proustite synthesized
hydrothermally at 300°C, 300 kgf (H042).
A, B: Polyhedral crystals of proustite

Proustite

Proustite is found as aggregates of polyhedral crystals (Fig. 14). Striation is
observed on some faces (Fig. 14 A).
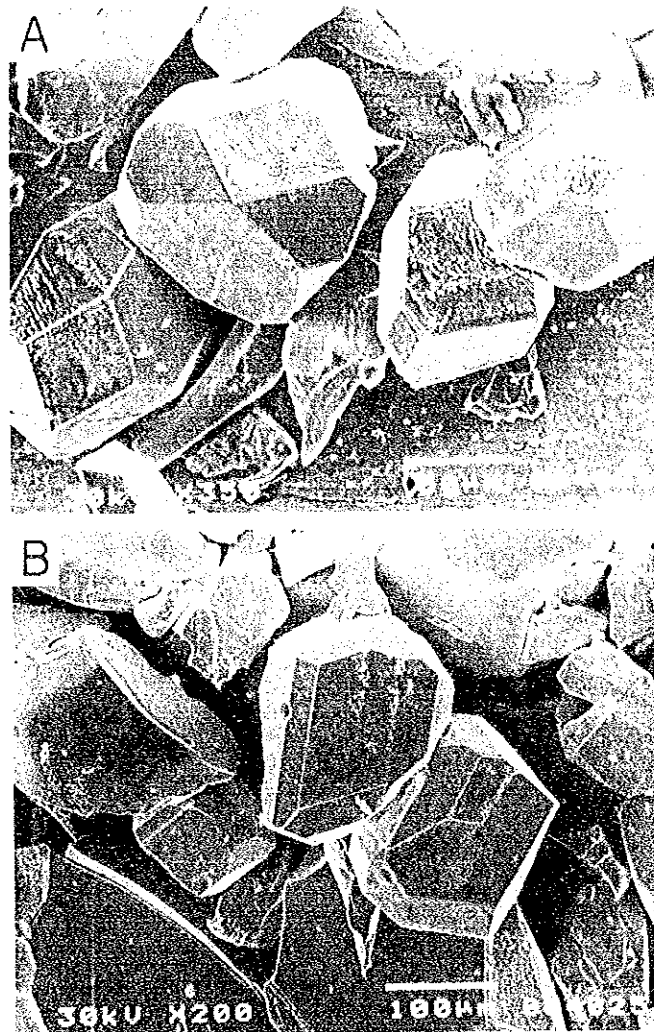
Fig. 15. SEM micrographs of pyrargyrite synthesized
hydrothermally at 300°C, 300 kgf (H040).
A, B: Polyhedral crystals of pyrargyrite.

Pyrargyrite

Pyrargyrite appears as granular polyhedral crystals composed with trigonal
pyramid and prism faces which can not be indexed (Fig. 15 A, B). Some prism
faces have rough surface.
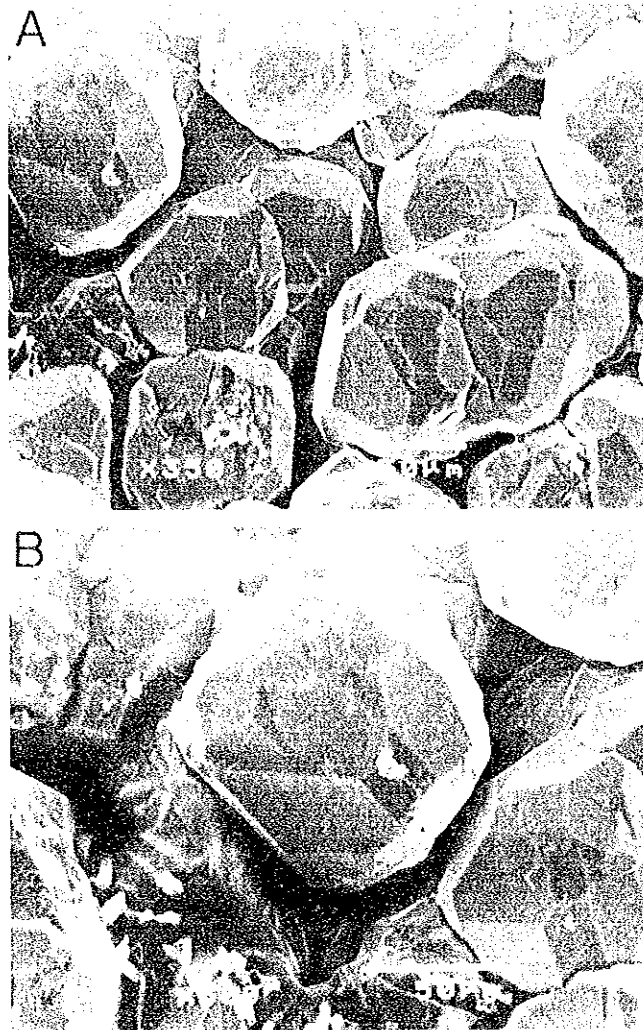
Fig. 16. SEM micrographs of famatinite synthesized
hydrothermally at 300°C, 300 kgf (H044).
A, B: Aggregates of polyhedral crystals of famatinite.

Famatinite

Famatinite is found as granular aggregates of polyhedral crystals composed
with rhombic prism and pyramid faces (Fig. 16 A, B). This form is more
complicate then natural one (Paleche *et al.*, 1949).
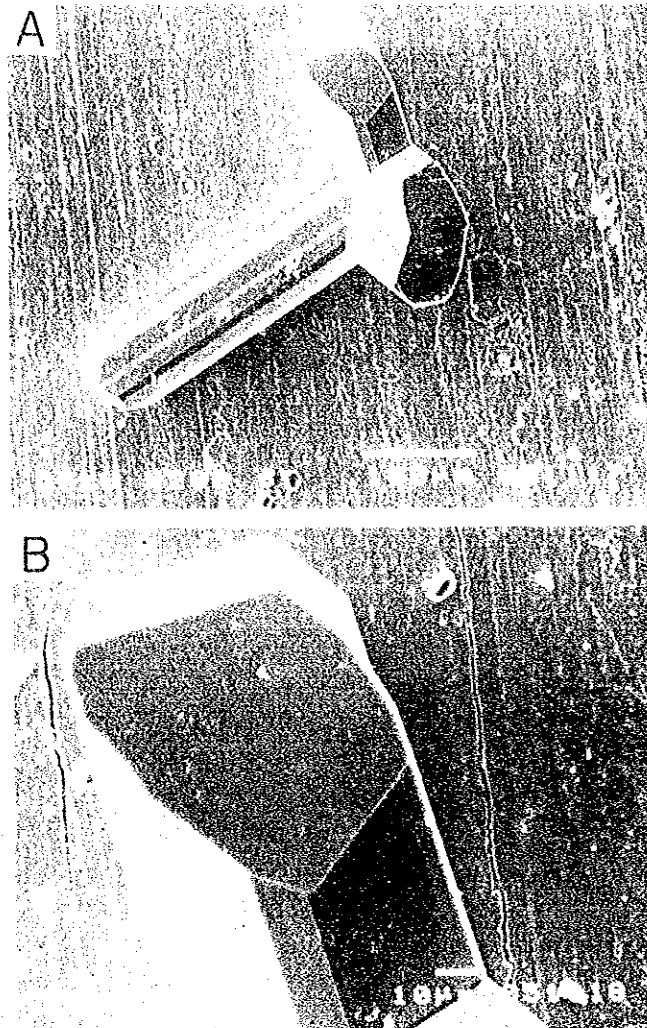
Fig. 17. SEM micrographs of enargite synthesized
hydrothermally at 300°C, 300 kgf (H033).
A: Long prismatic twinned crystals of enargite.
B: Growth twinning of enargite.

Enargite

Enargite appears as long prismatic form and usually twinned crystals on (320) as seen in Fig. 17 A, B. It consists of (110), (100) and (120) prisms, and (101) pyramid face.
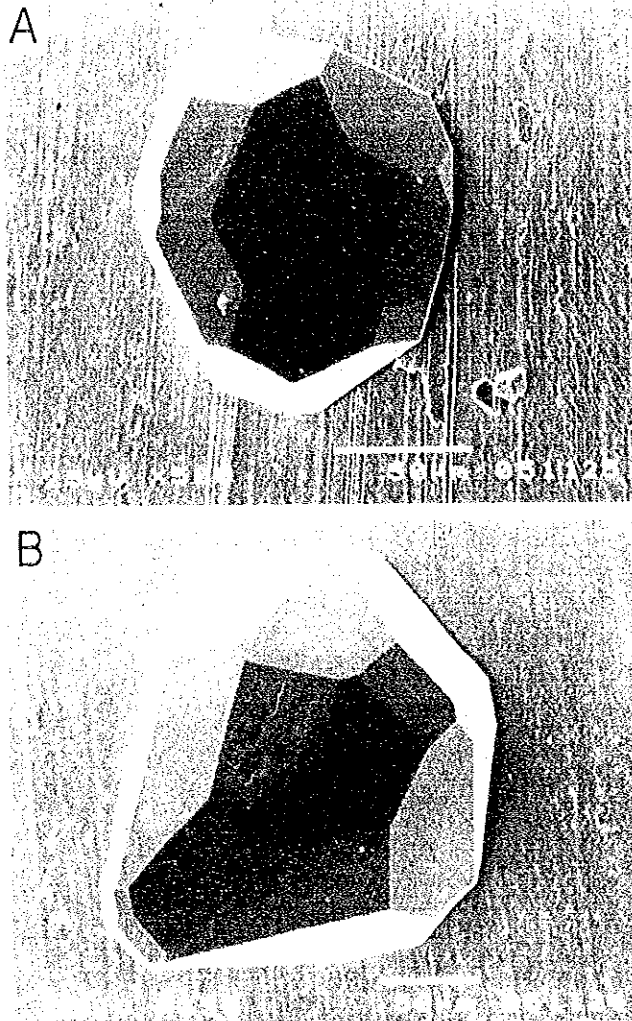
Fig. 18. SEM micrographs of tennantite synthesized
hydrothermally at 300°C, 300 kgf (H033).
A, B: Polyhedral crystals of tennantite.

Tennantite

Tennantite is found polyhedral single crystal composed with (100), (112), (111), (110) and (221) faces (Fig. 18).

3. Conclusion

Some sulfide and sulfosalt minerals such as pyrrhotite, pyrite, chalcocite, covellite, stibnite, bismuthinite, sphalerite, galena, greenockite, alabandite, chalcopyrite, bornite, nukundamite, proustite, pyrargyrite, famatinite, enargite and tennantite were synthesized hydrothermally at 350° and 300°C, 300 kgf.

Products observed under a scanning electron microscope are usually found as euhedral crystals and their aggregates. Growth twinning is commonly observed in crystals of greenockite, alabandite and enargite. Growth steps on basal face of pyrrhotite and nukundamite are usually found. Characteristic striations appear in chalcopyrite and bornite crystals. Although alabandite belongs in cubic system, its crystal shows hexagonal prismatic form and more detailed crystallographic study is necessary.
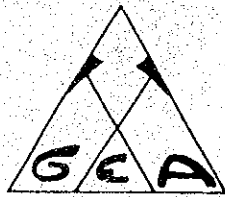
Acknowledgment

References

Ahlfeld, F. & Muñoz J. (1955) Las Especies Minerales de Bolivia. Banco Minero de Bolivia. pp. 29.

Kullerud, G. (1971) Experimental techniques in dry sulfide research. In *Research Techniques for High Pressure and High Temperature*, ed. G. C. Ulmer, Springer-Verlag, New York, 288-315.

Palache, C., Berman, H. & Frondel, C (1949) Dana's System of Mineralogy, Volume 1, 7 ed. John Wiley & Sons.

Scott, S.D. (1974) Experimental methods in sulfide synthesis. In *Sulfide Mineralogy* ed. P.H. Ribbe, Miner. Soc. Amer. Short Course Notes. 1, S1-S38.

Scott, S.D. & Barnes, H. L. (1971) Sphalerite geothermometry and geobarometry. *Econ. Geol.*, 66, 653-669.

Sugaki, A. (1992) Synthetic method of sulfide minerals -evacuated glass-tube method. In *Textbook for Instrumental Analyses on Economic Geology and Related Sciences*. ed. A. Sugaki, JICA, N° 2, 73-105.

Sugaki, A., Kitakaze, A., & Hayashi, K. (1984) Hydrothermal synthesis and phase relations of the polymetallic sulfide system, especially on the Cu-Fe-Bi-S systems. In *Material Science of the Earths Interior*, ed. I. Sunagawa, Terra Pub. Co., Tokyo, 545-583.

Sugaki, A., Shima, H., Kitakaze, A. & Harada, H. (1975). Isothermal phase relations in the system Cu-Fe-S under hydrothermal conditions at 350° and 300°C. *Econ. Geol.*, 70. 806-823.

Sugaki A., Shima, H., Kitakaze, A. & Fukuoka, M. (1977). Hydrothermal synthesis of pyrrhotite and their phase relation at low temperature. *Sci. Rept. Tohoku Univ.*, Ser. III, 13, 165-182.

Sugaki, A., Shima, H., Kitakaze, A. & Mizota, T. (1981). Hydrothermal synthesis of nukundamite and its crystal structure. *Amer. Miner.*, 66, 398-402.

Vaughan, D. J. & Craig, J. R. (1978) Mineral chemistry of metal sulfides, Cambridge Univ. Press, Cambridge, 264-272.